Dissertation zur Erlangung des Doktorgrades

an der Fakultät für Chemie und Pharmazie

der Ludwig-Maximilians-Universität München

Investigation on the bioactivities of natural products with the focus on phyllobilins, a novel substance class of bioactive phytochemicals – isolation, characterization, and bioactivity testing to probe the influence on early steps of atherosclerosis

Patricia Frei

aus Marktoberdorf, Deutschland

2023

Erklärung

Diese Dissertation wurde im Sinne von §7 der Promotionsordnung vom 28. November 2011 von Frau Prof. Dr. Angelika M. Vollmar betreut.

Eidesstattliche Versicherung

Diese Dissertation wurde eigenständig und ohne fremde Hilfe erarbeitet.

München, den 14.09.2023

Patricia Frei

(Patricia Frei)

Dissertation eingereicht am: 18.09.2023

1. Gutachter: Prof. Dr. Angelika M. Vollmar

2. Gutachter: Prof. Dr. Simone Moser

Mündliche Prüfung am: 31.10.2023

Meiner Familie

Table of contents

1 Summary 1

2 Introduction 6

2.1 Natural products – contemporary guideposts for medicines 6

2.2 Phyllobilins - a novel class of natural and bioactive products 6

2.3 Aims of the study 10

3 Materials and Methods 13

3.1 Materials 13

3.1.1 Compounds 13

3.1.2 Reagents: Biochemicals, kits and cell culture reagents 13

3.1.3 Antibodies 15

3.1.4 Technical equipment 16

3.1.5 Software 17

3.1.6 Consumables 18

3.1.7 Plant material 18

3.2 Analytical methods 19

3.2.1 Analytical HPLC 19

3.2.2 Semi-preparative HPLC 19

3.2.3 LC-MS 20

3.2.4 Spectroscopy 20

3.2.5 Spectroscopic data of isolated compounds 20

3.3 Isolation of phyllobilins 23

3.3.1 Isolation of phyllobilins of *Echinacea purpurea* and *Tropaeolum majus* 23

3.3.2 Isolation of *Pp*-DPxB (*Vv*-DPxB) of *Parrotia persica* 24

3.3.3 Isolation of phyllobilins of *Cercidiphyllum japonicum* 24

3.3.4 Partial synthesis of *Cj*-PxB by solid-phase oxidation of *Cj*-PleB or *Po*-PleB 25

3.3.5 Concentration determination of DMSO stocks of isolated compounds 25

3.4 Characterization of phyllobilins of *Tropaeolum majus* and *Humulus lupulus* ... 25
3.4.1 Chemoprofiling ... 25
3.4.2 Comparison of retention times ... 26
3.4.3 Leaf spray ... 26
3.4.4 Stability of *Tm*-PxB-1 in extraction solvents ... 26
3.5 Cell culture ... 26
3.5.1 Cell culture buffers and solutions ... 26
3.5.2 Cell lines and culture media ... 27
3.5.3 Passaging ... 27
3.5.4 Thawing ... 28
3.6 Stability assay ... 28
3.7 FRAP assay ... 28
3.8 DPPH assay ... 29
3.9 ORAC assay ... 29
3.10 COX Inhibition assay ... 29
3.11 Cell proliferation assay ... 30
3.12 Intracellular ROS assay ... 30
3.13 Lucigenin-enhanced NADPH oxidase activity assay ... 30
3.14 Protein expression by Flow cytometry ... 31
3.15 Quantitative real-time PCR analysis ... 32
3.16 Western Blot analysis ... 33
3.17 Collagen IV staining by confocal imaging ... 35
3.18 *In-vitro* MMP-9 activity assay ... 36
3.19 Migration of THP-1 cells by Boyden Chamber assay ... 37
3.20 Transendothelial Migration of THP-1 cells by Boyden Chamber assay ... 37
3.21 Statistical analysis ... 38
4 Part I: Phyllobilins - a bioactive natural product class contributing medicinal plants activity ... 40

4.1 Introduction 40
4.2 Results 44
4.2.1 Influence of phyllobilins on properties of phytopharmaceuticals 44
4.2.2 Characterization of novel phyllobilins of *Humulus lupulus* 48
4.2.3 Structural characterization, anti-oxidative-, and anti-inflammatory activities of phylloxanthobilins in *Tropaeolum majus* L., a plant with relevance in phytomedicine 51
4.3 Discussion 59
5. Part II: Comparison of the anti-atherosclerotic potential of phyllobilins and bilirubin on early stages of atherosclerosis 65
5.1 Introduction 65
5.2 Results 70
5.2.1 Isolation and characterization of *Pp*-DPxB (*Vv*-DPxB), *Cj*-PxB and *Cj*-PleB 70
5.2.2 Effects of PBs on endothelial cell proliferation 71
5.2.3 Anti-oxidative potential of phyllobilins in the context of atherosclerosis 72
5.2.4 PBs impact NADPH oxidase activity and protein levels 73
5.2.5 PBs and BR effect monocyte migration and endothelial transmigration 75
5.2.6 PBs and BR do not modulate protein and mRNA expression of adhesion proteins 77
5.2.7 Modulation of MMP activity by PBs and BR 80
5.3 Discussion 82
5.3.1 *In-cellulo* anti-oxidative radical scavenger ability of PBs and BR is potentially mediated by the inhibition of NADPH oxidase activity and impacts endothelia function maintenance 82
5.3.2 Effects of PB and BR on diapedesis of monocytes is not mediated by the expression of adhesive proteins 85
5.3.3 Reduced monocyte migration by PBs and BR is potentially related to NOX4 and MMP-9 enzyme activity inhibition 86

5.3.4 Inhibition of MMP-9 by PBs and BR can impact endothelial dysfunction and VSMC migration 88
5.3.5 Potential impact of PBs in next stages of atherosclerosis progression 88
6. Contribution: Redox-Mediated Amination of Pyrogallol-Based Polyphenols 90
6.1 Introduction 90
6.2 Library of pyrogallol-derived polyphenols 91
6.3 Screening of a library of pyrogallol-derived polyphenols for anti-oxidative properties 91
7. References 94
8. Appendix 103
8.1 Supplementary Information 103
8.2 Abbreviations 118
8.3 Index of figures 120
8.4 Index of tables 122
8.5 Acknowledgements 123
8.6 List of publications and conference contributions 125
8.6.1 Research articles 125
8.6.2 Conference contributions 125

SUMMARY

1 Summary

Phyllobilins (PBs) present a young class of natural products that have recently been gaining recognition as relevant phytochemicals. Being highly abundant in senescent vascular plants, they arise by the degradation of chlorophyll, predominantly in autumn, but, e.g., also because of pathogen attacks. They share a tetrapyrrole structure that is similar to the heme degradation product bilirubin (BR), but their molecular structure can be modified by the plant in various manner. Like BR, PBs are strong antioxidants that potentially impact several physiological processes. Furthermore, a yet unpredictable variety of the structures is possible, as mother nature magnificently produces structural diversity. The aim of this thesis was to explore the abundancy of PBs and the implications of their bioactivities.

Based on the strong anti-oxidative potency of PBs, we hypothesized that the natural products impact the properties of phytomedicines. In a first attempt, one PB of *Echinacea purpurea* (*Ep*-PxB-5) was used as model substance. The addition of *Ep*-PxB-5 did not improve the stability of a major ingredient, caftaric acid, but we found that medicinal extracts of *Echinacea purpurea* render more potent in anti-oxidative activity over several days when *Ep*-PxB-5 was added.

Furthermore, in the first part of this thesis, we have uncovered PBs in the medicinal plants *Humulus lupulus* (hops) and *Tropaeolum majus* (nasturtium), in high abundancy. For both plants, novel structures were identified, and their bioactivities were illuminated closer. PBs can be categorized in Type-I and Type-II PBs, which differ in the replacement of an aldehyde function by an oxo-group as a consequence of deformylation. In senescent leaves of hops, two Type-II PBs, *Hl*-DPleB and *Hl*-DPxB, were formed, which we found to contribute to roughly a third of the yellow coloration of the leaves in autumn. Furthermore, *Hl*-DPxB showed stronger *in-vitro* anti-oxidative potential than the potent reference molecule Trolox. *In-cellulo,* both *Hl*-DPleB and *Hl*-DPxB exhibited comparable results in scavenging ROS. Apart from anti-oxidative testing, also anti-proliferative effects on cancer cells were tested, as hops cones are commonly associated with anti-carcinogenic effects. Interestingly, no influence on the proliferation of the cells was visible at the chosen concentration range, which differs from Typ-I PBs. With our results, we aid in understanding the structure activity relationship of PBs.

Moreover, four novel Type-I PBs (*Tm*-PxB-(1-4)) were identified in yellowing leaves of *Tropaeolum majus*, nasturtium, and structurally characterized. Thereby one structure, *Tm*-PxB-2, evoked our interest, as the molecule showed a distinct loss of a carboxyl function at $C8^2$, which indicated the natural presence of a pyro-PB (pyPB). By leaf-spray MS, we firstly verified *Tropaeolum majus* as plant source of a pyPB with a classic phylloxanthobilin (PxB) structure. *Tropaeolum majus* is a traditionally used medicinal plant for the treatments of catarrhs of the upper respiratory tract and urinary tract infections with anti-bacterial and diuretic effects. *In-vitro* and *in-cellulo*-antioxidant studies were conducted to assess the potency of the novel structures, thereby revealing strong effects. Additionally, COX-1 and COX-2 inhibition in the low micromolar range was demonstrated for *Tm*-PxB-1 and *Tm*-PxB-4. Thereby, anti-inflammatory effects as assessed by COX-2 inhibition were comparable to those of isoquercitrin, the active flavonoid of nasturtium plant extracts, and stronger than those of chlorogenic acid, which is also a known polyphenolic ingredient. With our results, we contribute knowledge on the incomplete chemoprofiling of *Tropaeolum majus* leaves and uncover potent ingredients of the plant leaves that contribute pharmacologically to the medicinal usage of the plant (**Figure 1**).

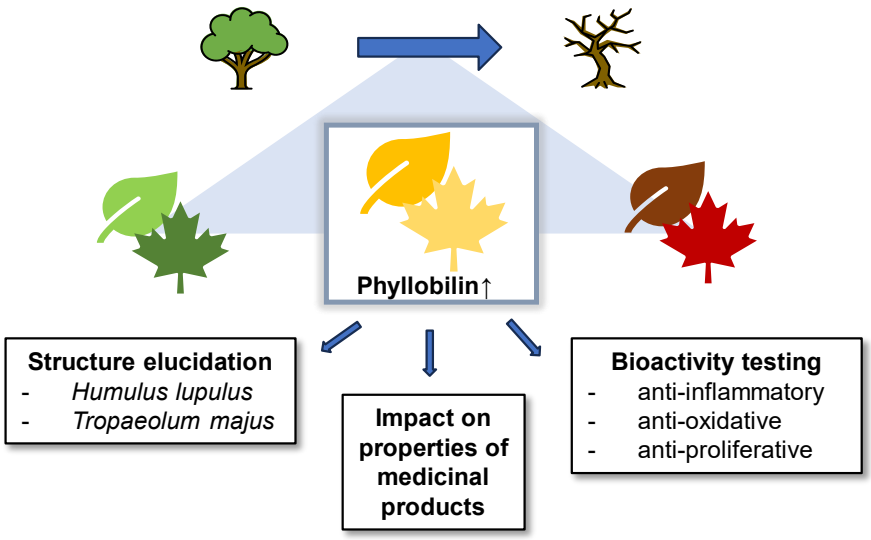

Figure 1 Graphical abstract on phyllobilin sources and focus on Part I of the thesis.

In the second part of this thesis, we investigated the influence of BR and PBs on early stages of atherosclerosis progression. Since oxidative stress is a major driver of atherosclerosis, and bilins are known anti-oxidative compounds, we probed the effects of PBs compared to its heme-derived counterpart, BR, on atherosclerosis related parameters. First, we confirmed the anti-oxidative potency of PBs and BR *in-vitro* by FRAP

and DPPH assays and showed the anti-oxidative effects *in-cellulo* with experiments using the endothelial cell line HUVEC. We found strong potential of PBs and BR on scavenging reactive oxygen species (ROS) in endothelial cells. Moreover, we provide first evidence on the ability of PBs to inhibit NADPH oxidases (NOXs) activity. NOX enzymes are the major producers of ROS in cells. Highly elevated ROS levels lead to endothelial damage and endothelial dysfunction, which is related to atherosclerotic plaque formation. Combining the suppressive effects of “bilins” on ROS production via NOX inhibition and the radical scavenging effects, we conclude that PBs might impact the progression of endothelial dysfunction during early atherosclerosis formation. In addition, we firstly revealed a direct inhibition of PBs and BR on MMP-9 activity *in-vitro*, which we could also prove in HUVEC cells. MMP-9 is a matrix metalloprotease that is involved in monocyte transmigration by degrading extracellular matrix (ECM) and is connected to all stages of atherosclerosis by aggrieving the pathogenesis from plaque formation to plaque rupture. In transwell migration experiments, we found that PBs and BR inhibited monocyte migration as well as monocyte transendothelial migration without affecting expression levels of the adhesive proteins VCAM-1, ICAM-1 and E-selectin. Based on current evidence from literature, we suggest that NOX and MMP-9 inhibition are responsible for the suppressive effects on transendothelial migration of monocytes by bilins. Furthermore, based on our results, we speculate that bilins could interfere with VCAM-1 mediated signaling by scavenging ROS, thereby inhibiting NOX and MMP-9 activation. In summary, PBs are natural products that influence monocyte transmigration and are compounds with promising bioactivities to counter atherosclerosis progression (**Figure 2**).

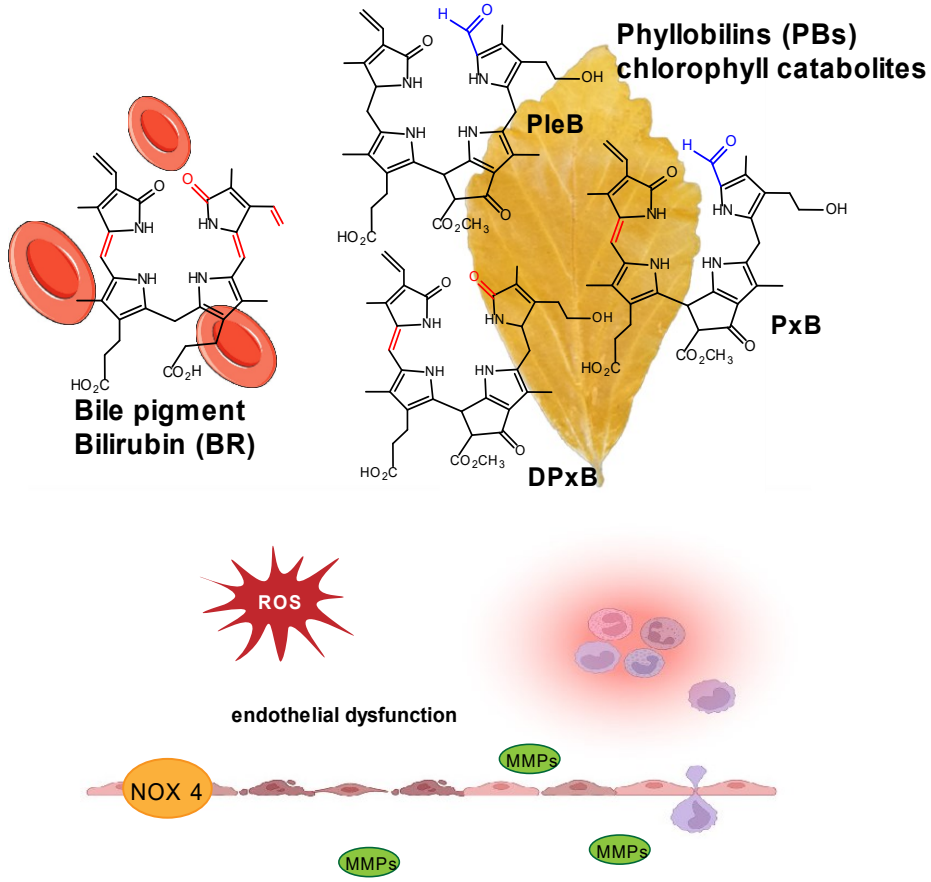

Figure 2 Schematic overview on chemical structures of BR and PB candidates and influences on early stages of atherosclerosis progression as found in Part II in this work.

Taken together, part I and part II of this thesis clearly emphasize that PBs are natural compounds with promising anti-oxidative, anti-inflammatory, and anti-migratory bioactivities, abundant in leaves of medicinal plants. Additionally, these bioactivities were shown to impact mechanisms of atherosclerosis progression.

INTRODUCTION

2 Introduction

2.1 Natural products – contemporary guideposts for medicines

Natural products (NPs) have impacted drug discovery from the past until now and they remain irreplaceable to date for pharmacotherapy. For example, the discovery and isolation of the natural products paclitaxel, salicin, digitoxin from plants and penicillin from fungi have revolutionized the treatment of life-threatening diseases, including cancer, cardiovascular or infectious diseases.[1] Especially in the field of small molecules of low molecular weight, the diversity of natural compounds is tremendous. Combining the chemical structures of NPs with combinatorial standard medicinal chemistry, enhances markedly the pharmacological potency of agents.[2] Serving as drug leads, NPs are of marked value for developing pharmaceuticals to treat cardiovascular and metabolic disorders for instance.[3] Historically, the exploration of anti-choleretic properties of statins, as lovastatin isolated from *Aspergillus terreus,* induced the development of multiple synthetic and semi-synthetic statis, which present the first-line pharmacotherapy to lower blood lipids worldwide to date.[4] Although the anti-glycemic NP, galegine from *Galega officinalis*, did not pass clinical trials because of its toxicity, its chemical structure founded the discovery of metformin, an important drug to treat diabetes mellitus type 2.[5] Consequently, NPs inherit a tremendous potential to impact medicinal product research in the future, which remains to be fully exploited.

2.2 Phyllobilins - a novel class of natural and bioactive products

Phyllobilins are more than just waste products! The phyllobilins (PBs) are a group of natural products that are currently being established as promising bioactive group among phytochemicals.[6] Derived from plant pigment chlorophyll (Chl), they are linear open-chain tetrapyrroles with strong similarities to the heme degradation substance bilirubin (BR). Based on this structural feature, the novel group of phytochemicals was named phyllobilins.[7] During senescence in autumn or initiated by external stimuli like pathogen attacks[8], a programmed systematic degradation pathway of Chl called PAO/phyllobilin pathway is started in various chlorophyll-rich plants. The need for the degradation of Chl arises from its cytotoxicity. During breakdown, Chl is released from its binding proteins, thereby becoming toxic to the plant cells.[9]

To detoxify Chl, free Chl molecules are converted to PBs at the thylakoid membrane within the chloroplast (**Figure 3**). Not yet fully deciphered, the biosynthesis of PBs follows

multiple enzymatic and non-enzymatic steps, thereby eventually forming different types of PBs: Chl *b* is enzymatically converted by two reductional steps via non-yellow coloring 1 (NYC1), NYC1-like (NOL) and hydroxymethyl Chl a reductase (HCAR) to Chl *a*, then the central Mg^{2+} ion from Chl *a* is released by the stay-green Mg-dechelatase (SGR) resulting in the formation of pheophytin *a* (Phein *a*) (**Figure 3**).[10] Those enzymes are Chl *a* specific and consequently, Chl *b* can only be degraded after conversion into Chl *a*.[11] The phytyl-residue of Phein *a* enzymatically gets removed by pheophytinase (PPH) to form Pheide *a* (**Figure 3**).[12] Both, Phein *a* and Pheide *a* are still phytotoxic for the cells and subsequently had to be degraded further by opening of the macrocycle. This is accomplished by two independent, but physically interacting, enzymes.[13] The first enzyme, PAO (pheophorbide *a* oxygenase), opens the porphyrin ring under production of the first linear tetrapyrrole PB metabolite RCC ('red' Chl-catabolite) (**Figure 3**).[14] As first metabolite in the pathway so far, RCC can pass the chloroplast membrane.[13, 15] Located in the chloroplast stroma, the second enzyme RCCR (RCC reductase) reduces RCC at the C15/C16 double bond to primary phyllolumibilins (*p*PluBs), firstly named *p*FCCs, primary fluorescent Chl catabolites (**Figure 3**). The reduction introduces a stereocenter at C16. Whether an 'n' or 'epi' configuration is present, is favored by the RCCR isotype present in the respective plant. By the conversion to *p*PluB, the phototoxicity of Chl is believed to be removed.[13, 15-16] The last step in the PAO/pathway that is attributed to take place in the chloroplast is the hydroxylation via TIC55, an oxygenase, at the terminal carbon $C3^2$ to hydroxy-*p*PluB (Hydroxy-*p*FCC) (**Figure 3**). It was found that hydroxy-*p*PluB, also considered "secondary" PluB (*s*FCC), is the precursor of all hydroxylated PBs in senescent leaves of *Arabidopsis*.[17]

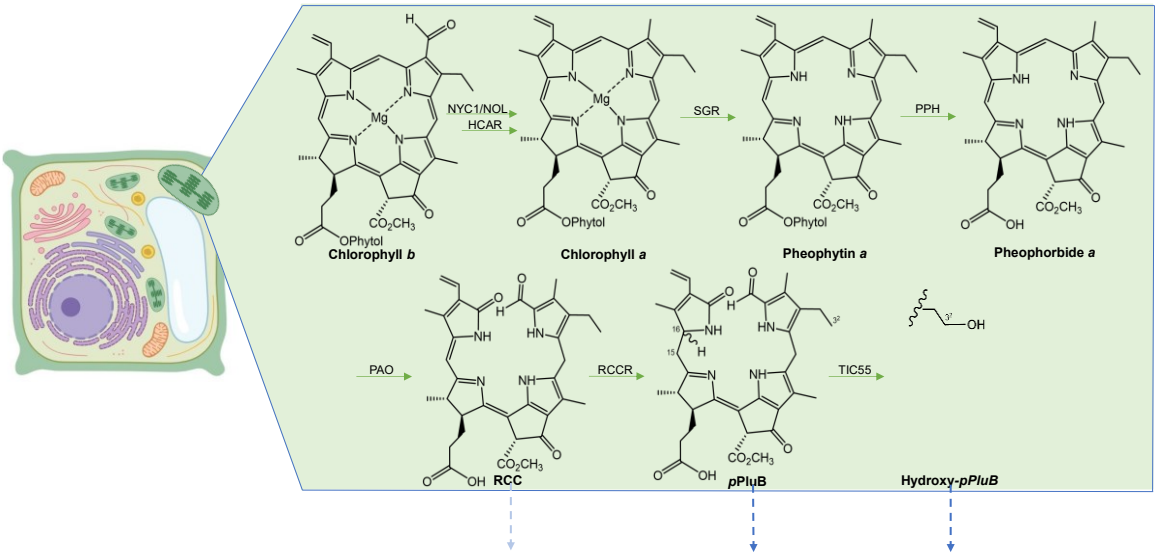

Figure 3 Schematic overview of the first part of the PAO/pathway of chlorophyll breakdown in senescent leaves. Enzymatic degradation of phototoxic Chl to non-toxic *p*Plubs occurs in the chloroplast. RCC, *p*PluB and Hydroxy-*p*Plub are excreted into the cytosol by unknown transporters. The figure was adapted from Kuai et al.[10a]

Contrary to the well understood first part of the PAO/pathway, the subsequent modification reactions that occur in the cytosol are highly species-specific and still bear some mysteries (**Figure 4**). $O3^3$ -glucosylation, $O3^3$ -malonylation and C18 vinyl group dihydroxylation is believed to take place in the cytosol.[13] The enzymes, which are involved in the side chain modifying reactions have not been fully characterized yet. For example, *p*PluB can by hydroxylated to hydroxylated-*p*PluB by TIC55, which can be further glycosylated and/or malonylated by yet undetermined cytosolic enzymes. However, three enzymes were found in *Arabidopsis* to modify side chains so far, CYP89A9[18], methylesterase 16 (MES26)[19] and TIC55[17]. Apart from modifications like esterification at the propionyl group, further deformylation at C1 can appear. CYP89A9, located in the ER, possesses oxidative deformylation activity and converts PluBs in the cytosol to their dioxobilin-type analogon, DPluBs (DFCC) (**Figure 4**).[18] At this stage, the biosynthesis of PBs branches in two paths. All PBs that did not undergo deformylation carry an aldehyde function and are classified as Type-I PBs, whereas the dioxo counterplayer are named Type-II PBs (**Figure 4**).[20] The demethylation at $C8^2$ can be catalyzed by MES16, a hydrolase, in *Arabidopsis*.[19]

PluBs are likely to spontaneously isomerize to PleBs, phylloleucobilins, or firstly named NCCs, while entering the acid environment in the vacuole.[21] Similarly, DPluBs are converted to DPleBs, dioxo-phylloleucobilins (**Figure 4**).[22] Acid tautomerization in the vacuole requires active transport of PluBs and DPluBs into the vacuole. Again, the

underlying transporters are missing. Consequently, these colorless metabolites are also the first ones in the biosynthesis of PBs that are known to accumulate in the vacuoles. PleBs and DPleBs potentially oxidize with exposure to air or day light to phylloxanthobilins (PxBs) or dioxo-phylloxanthobilins (DPxBs) (**Figure 4**). Firstly, they were named as YCC, yellow-colored Chl catabolite and DYCC, dioxo-yellow-colored Chl catabolite, respectively.[20, 23] In accordance with this nomenclature, a change in coloration to yellow appears, which can be explained by the oxidative insertion of an extensive π-conjugated electron system. Undergoing further oxidation processes, colors shift to red by introducing a double bond at C10, thereby forming phylloroseobilins, PrBs (eponymous PiCC, pink chlorophyll catabolite) (**Figure 4**).[23a]

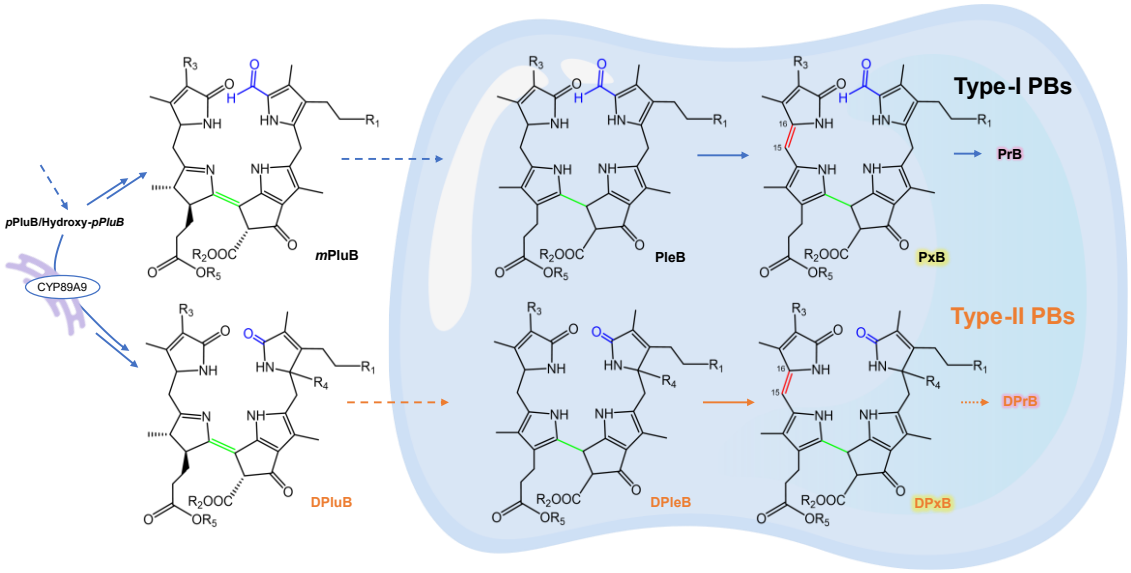

Figure 4 Second part of PAO/phallobilin pathway occurs in the cytosol and vacuoles and leads to the formation of Type-I and Type-II phyllobilins. After the release via unknown transporters of *p*PluB/Hydroxy-*p*PluB from the chloroplast several modifications can appear in the cytosol as demethylation by MES16 enzyme. Modified PluBs (*m*PluBs) are formed. By CYP89A9 mediated deformylation, branching of the pathway into Typ-II PBs is initiated. *m*PluBs and DPluBs are taken up by the vacuole in an undeciphered way whereby a spontaneous acid triggered formation to PleBs and DPleBs follows. PleB and DPleBs can be oxidized in two steps to PxB and DPxB and further to PrB and theoretically DPrB, respectively.[13]

Recently, PBs with a uniquely rearranged carbon skeleton were found in fern by Erhart et al. Additionally, those special PBs, named *i*PB miss the typical chain at C8^2, technically classifying them as pyro-PBs.[24] How and at which stage of PAO/pathway this conversion of carbon backbone and decarboxylation of the carbon side chain at C8^2 happens, is still an open question and it might be limited to the special evolutionary stage of lower plants and gymnosperms in general. To date, this feature of decarboxylation is seen to be lost during the evolution of angiosperms.[13, 24]

By reiterating the statement “Phyllobilins are more than just waste products!”, our work underlines that PBs are more than just by-products produced by plants. The fundamental basis was provided earlier by our group (Prof. Simone Moser), which firstly started investigations on the bioactive potential of PBs.[25] It was found that medicinal plants contain a remarkable diversity in PB content. The deciphering of five different strong anti-oxidative PxBs in *Echinaceae purpurea* opened the field of systematic research on the contribution of PBs on the bioactive effects of pharmaceutically used plants.[26] More PxBs were found in *Urtica dioica* later with strong anti-inflammatory potency by inhibition of COX-1 and COX-2 in low micromolar ranges and downregulation of COX-2 expression levels in macrophages. This work also revealed the so far overlooked presence of PBs in pharmaceutical products.[27] In addition to anti-oxidative, which besides was also reported for Type-II PBs of savoy cabbage[28], and anti-inflammatory potential, also strong anti-cancer effects in human cancer cells by inhibiting proliferation, inducing apoptosis with G2/M cell cycle arrest, were demonstrated for Type-I PBs.[25] Firstly, actin, was identified as a target of PBs. Thereby, targeting the actin cytoskeleton of cells inhibited actin dynamics, impacted cell migration and cell shape.[29] Moreover, recent investigations extent the information on the anti-inflammatory and immunoregulatory effects of PBs by demonstrating suppressive impact on immunoregulatory metabolic pathways of tryptophan breakdown in human blood peripheral mononuclear cells (PBMCs).[30] These structures have the potential to influence many other physiological functions. In summary, there is still a lack of knowledge about this ubiquitous structural class, even though its formation can be uniquely observed visually especially during autumn.

PBs, strong antioxidants, are part of human daily nutrition[8a, 28, 31] and cover a yet unknown potential to interfere with a variety of severe oxidative stress mediated diseases like cardiovascular, neurological, respiratory, rheumatoid arthritis, several kidney diseases, and cancer.[32] Apart from other NPs like flavonoids, the physiological relevance of PBs on those illnesses is unknown and remains to be explored.

2.3 Aims of the study

Natural products are of fundamental importance for developing novel drugs to conquer diseases. PBs are a young class of phytochemicals which expand the diversity of bioactive substances, and they might serve as model structures for medicinal chemists or as health contributing substances of daily nutrition in the future. This thesis wants to contribute to two parts of the process of establishing PBs as relevant phytochemicals.

Our first goal was to identify PBs in various medicinal plants and to elucidate their structures, yielding new PB candidates with potential bioactivity. In this context, we elucidated novel PB structures in senescent leaves of *Humulus lupulus* and *Tropaeolum majus*.

Secondly, we aimed to investigate the bioactivities of the PBs with special regard on their anti-oxidative potential. Thereby we classified the isolated PBs of *Humulus lupulus* and *Tropaeolum majus* and investigated the impact of a PB, as antioxidant, on the properties of a phytomedicine. Further we examined the potential of PBs to counter an oxidative stress induced disease, atherosclerosis, thereby comparing the phytochemicals with the antioxidant BR and elucidating potential mechanisms of action.

In this thesis, the above objectives were pursued in two parts:

Part I: Phyllobilins - a bioactive natural product class contributing medicinal plants activity

1. Studies on the impact of a PxB, as antioxidant, on the properties of a phytomedicine
2. Testing of bioactivities of novel Dioxo-PBs in yellow leaves of *Humulus lupulus* (hops)
3. Structure elucidation of four PxBs of senescent *Tropaeolum majus* (nasturtium) leaves and biological characterization of the isolated substances

Part II: Comparison of the anti-atherosclerotic potential of phyllobilins and bilirubin on early stages of atherosclerosis

1. Characterization of the anti-oxidative potency of three different PB candidates and BR in *in-vitro* and *in-cellulo* approaches
2. Determination of oxidative mechanisms during atherosclerosis that PBs potentially interfere with
3. Assessment of potential effects of PBs and BR on transendothelial-/ migration of monocytes
4. Studies on mechanisms or targets responsible for the inhibition of transendothelial-/ migration of monocytes by PBs and BR

MATERIALS AND METHODS

3 Materials and Methods

3.1 Materials

3.1.1 Compounds

Compound	Producer/source
Hl-DPxB	Christian Nadegger (Prof. Müller, University of Innsbruck, Austria)
Hl-DPleB	Christian Nadegger (Prof. Müller, University of Innsbruck, Austria)
Po-PleB	Dr. Willmar Schwabe GmbH & Co. KG (Karlsruhe, Germany)
Polyphenol compounds	Salavat Ashirbaev (Prof. Zipse, LMU Munich, Germany)

Table 1 Compounds

3.1.2 Reagents: Biochemicals, kits and cell culture reagents

Reagent	Company
2,2'-azobis(2-methyl-propionamidine) dihydrochloride (AAPH)	Merck, Darmstadt, Germany
Acetic acid (AcOH)	VWR International GmbH, Ismaning, Germany
Amphotericin B	PAN Biotech, Aidenbach, Germany
Bilirubin (BR)	Sigma-Aldrich, Taufkirchen, Germany
Bovine serum albumin (BSA)	Carl Roth, Karlsruhe, Germany
Bradford reagent Roti® Quant	Bio-Rad, Munich, Germany
Brij 35	Sigma-Aldrich, Steinheim, Germany
Calcein-AM	Biomol GmbH, Hamburg, Germany
Calcium chloride ($CaCl_2$)	AppliChem GmbH, Darmstadt, Germany
Collagen IV (#5022)	Advanced Biomatrix, Carlsbad, CA
Collagen G	Biochrom AG, Berlin, Germany
Complete®	Roche Diagnostics, Penzberg, Germany
Cayman Chemicals COX Fluorescent Inhibitor Screening kit	Cayman Chemicals, Ann Arbor, USA
Crystal violet	Carl Roth, Karlsruhe, Germany
2´,7´-dichlorodihydrofluoroscein diacetate (H_2DCF-DA)	Thermo Fisher (Waltham, MA, USA)
Dimethylsulfoxide (DMSO)	Sigma-Aldrich, Taufkirchen, Germany
Diphenyleniodoniumchlorid (DPI)	Sigma-Aldrich, Taufkirchen, Germany
2,2-diphenyl-1-picrylhydrazyl (DPPH)	Merk, Darmstadt, Germany
Disodiumhydrogenphosphate dihydrate (Na_2HPO_4 x 2 H_2O)	Merck, Darmstadt, Germany

Dithiothreitol (DTT)	Sigma-Aldrich, Taufkirchen, Germany
Dulbecco's Modified Eagle Medium (DMEM)	PAA Laboratories, Pasching, Austria
Echinacea-ratiopharm® Liquid	Ratiopharm GmbH, Ulm, Germany
Endothelial Cell Growth Medium (ECGM) kit enhanced	Pelobiotech GmbH, Martinsried, Germany
Ethanol (EtOH)	VWR International GmbH, Ismaning, Germany
Erastin	Cayman Chemicals, Ann Arbor, USA
Ethylendiaminetetraacetic acid (EDTA)	Sigma-Aldrich, Taufkirchen, Germany
Fetal calf serum (FCS)	Biochrom AG, Berlin, Germany
Fluoresceinisothiocyanat(FITC)-Dextran M_w 70,000 Da	Sigma-Aldrich, Taufkirchen, Germany
FluorSave™ Reagent	Merck Millipore, Darmstadt, Germany
Fluorescein sodium	Merck, Darmstadt, Germany
D(+)-Glucose, anhydrous	Carl Roth, Karlsruhe, Germany
N-(2-Hydroxyethyl)piperazine-N'-ethanesulfonic acid (HEPES)	Carl Roth, Karlsruhe, Germany
NNGH	Sigma Aldrich, St. Louis, MO, USA
Hoechst 33342	Sigma Aldrich, St. Louis, MO, USA
High-Capacity cDNA Reverse Transcription Kit	Applied Biosystems, Waltham, USA
Hoechst 33342	Sigma Aldrich, Taufkirchen, Germany
Hydrochloric acid (HCl)	VWR International GmbH, Ismaning, Germany
Hydrogen peroxide (30%)	Bernd Kraft, Duisburg, Germany
Iron(III) chloride ($FeCl_3$)	Merck, Darmstadt, Germany
Lucigenin	Sigma Aldrich, Taufkirchen, Germany
Magnesium sulfate heptahydrate ($MgSO_4$ x 7 H_2O)	Grüssing GmbH, Filsum, Germany
Recombinant Human MCP-1 (CCL2)	Peprotech, Rocky Hill, NJ, USA
Recombinant human active MMP-9	Merck, Darmstadt, Germany
Fluorogenic substrate peptide MMP-9	Merck, Darmstadt, Germany
NADPH	Biomol GmbH, Hamburg, Germany
NNGH	Sigma-Aldrich, Steinheim, Germany
Page Ruler™ Prestained Protein Ladder	Fermentas, St. Leon-Rot, Germany
Palmitic acid (PA)	Sigma Aldrich, Taufkirchen, Germany
Paraformaldehyde (PFA)	Thermo Fisher Scientific, Waltham, MA
Recombinant Human TNF-α	Peprotech, Rocky Hill, NJ, USA
Penicillin/Streptomycin 100x	PAA Laboratories, Paching, Austria
Phenymethylsulfonyl fluoride (PMSF)	Sigma-Aldrich, Taufkirchen, Germany
Potassium chloride (KCl)	AppliChem GmbH, Darmstadt, Germany
Potassium dihydrogen phosphate (KH_2PO_4)	Merck, Darmstadt, Germany
PowerUp™ SYBR® Green Master Mix	Applied Biosystems, Waltham, USA
Primers	Metabion, Planegg, Germany

Quercetin	Merck, Darmstadt, Germany
RNeasy® Mini Kit (250)	QIAGEN, Hilden, Germany
RPMI 1640	PAN Biotech, Aidenbach, Germany
Silica gel, 0.035-0.070 mm, 60 A	Thermo Scientific, Waltham, MA, USA
Sodium acetate	Merck, Darmstadt, Germany
Sodium chloride (NaCl)	Carl Roth, Karlsruhe, Germany
Sodiumdihydrogenphosphate dihydrate (NaH_2PO_4 x H_2O)	Merck, Darmstadt, Germany
Sodium fluoride (NaF)	Merck, Darmstadt, Germany
Sodium hydrogencarbonate ($NaHCO_3$)	Merck, Darmstadt, Germany
Sodium orthovanadate (Na3VO4)	ICN, Biomedicals, Aurora, OH, USA
Sodiumdodecylsulfate (SDS)	Carl Roth, Karlsruhe, Germany
2,4,6-Tri(2-pyridyl)-s-triazine (TPTZ)	Merck, Darmstadt, Germany
Tris buffer, 1.0 M, pH 8.0	Merck, Darmstadt, Germany
Trisodium citrate	Sigma-Aldrich, Taufkirchen, Germany
Trolox	Enzo Life Sciences GmbH, Lörrach, Germany
Trypsin	PAN Biotech, Aidenbach, Germany

Table 2 Reagents

3.1.3 Antibodies

Name	Species	Catalogue	Manufacturer	Dilution
Anti-collagen antibody, Type IV	rabbit	AB756P	Chemicon, Limburg an der Lahn, Germany	**1:200**
HO-1	rabbit	PC340	Oncogene, San Diego, CA, USA	**1:200**
MMP-2	rabbit	4022	Cell signaling, Danvers, MA, USA	**1:1000**
MMP-9	rabbit	M5177	Sigma-Aldrich, Taufkirchen, Germany	**1:1000**
NOX4	goat	Sc-21860	Santa Cruz Biotechnology, Dallas, TX, USA	**1:200**

Table 3 Primary antibodies

Name	Label	Species	Catalogue	Manufacturer	Dilution
ICAM1/CD54 [1H4]	FITC	mouse IgG_{2b}	GTX80290	Genetex, Irvine, CA, USA	**1:10**
CD106	RPE	mouse IgG_1	orb435267	Biorybt, Cambridge, UK	**1:25**
VCAM-1 (E-10)	FITC	mouse IgG_1	Sc-13160 FITC	Santa Cruz Biotechnology, Dallas, TX, USA	**1:50**
Mouse IgG1 Isotype Control	PE	mouse IgG_1	orb195302	Biorybt, Cambridge, UK	**1:25**
Mouse IgG2b isotype control [MPC-11]	FITC	mouse IgG_{2b}	GTX01519-06	Genetex, Irvine, CA, USA	**1:500**
normal mouse IgG1	FITC	mouse IgG_1	Sc-2855	Santa Cruz Biotechnology, Dallas, TX, USA	**1:50**

Table 4 Conjugated primary antibodies

Name	Species	Catalogue	Manufacturer	Dilution
Alexa Fluor 488 IgG (H+L)	goat anti-rabbit	A-11008	Thermo Fisher Scientific, Waltham, MA	**1:400**
HRP conjugate	donkey-anti-goat IgG	Ab97120	Abcam, Cambridge, UK	**1:5000**
HRP conjugate	Goat-anti-rabbit IgG	7074	Cell signaling, Danvers, MA, USA	**1:2000**

Table 5 Secondary antibodies

3.1.4 Technical equipment

Device	Company
Agilent 1260 Infinity II LC system	Agilent Technologies Germany GmbH & Co. KG, Waldbronn, Germany

BD FACS Canto II	BD Biosciences, San Jose, CA, USA
Büchi Pure C-830	BÜCHI Labortechnik GmbH, Essen, Germany
ChemiDoc™ Touch Imaging System	Bio-Rad Laboratories GmbH, Munich, Germany
Christ RVC 2-18 CD plus rotary vacuum concentrator, Christ CT 02-50	Martin Christ Gefriertrocknungsanlagen GmbH, Osterode am Harz, Germany
IKA® RV 3 eco rotary evaporator combined with IKA® HB ECO 5099 water bath	IKA®-Werke GmbH & CO. KG, Staufen, Germany
DW-10N freeze dryer	Darwell, Chongqing, China
Lamina flow Heraeus, Herasafe	Thermo Scientific, Waltham, MA, USA
Leica DMi1 microscope + camera Leica MC120HD	Leica Microsystems, Wetzlar, Germany
Leica TCS SP8 confocal laser scanning microscope	Leica Microsystems, Wetzlar, Germany
Millipore Express® PLUS membrane filter	Merck Millipore, Darmstadt, Germany
Mikro 22R centrifuge	Hettich, Tuttlingen, Germany
MultiQuick 5 Vario Stabmixer MQ 5200 WH	De'Longhi Braun Household GmbH, Neu-Isenburg, Germany
Nanodrop® 1000 spectrophotometer	PEQLAB Biotechnologie GmbH, Erlangen, Germany
Orion II microplate Luminometer	Berthold Detection Systems GmbH, Bad Wildbad, Germany
Primus 25 advanced® Thermocycler	PEQLAB Biotechnologie GmbH, Erlangen, Germany
QuantStudio™ 3 Real-Time PCR System	Applied Biosystems, Waltham, MA, USA
SpectraFluor Plus™	Tecan, Crailsheim, Germany
Tecan Spark 10M multimode microplate reader	Tecan, Crailsheim, Germany
Thermo Spectronic Genesys 5 (336001) UV-Visible spectrophotometer	Thermo Scientific, Waltham, MA, USA
Vi-Cell™ XR cell counter	Beckman Coulter, Brea, CA, USA
Water bath Haake W19	Thermo Scientific, Waltham, MA, USA

Table 6 Technical devices and lab equipment

3.1.5 Software

Software	Company
Agilent ChemStation® software Rev. B04.02, Agilent software OpenLab CDS	Agilent Technologies, Santa Cruz, CA, USA
BioRender.com	BioRender, Toronto, Canada
Büchi Pure software 1.5	Büchi Labortechnik AG, Flawil, Schweiz
ChemDraw 20.0.0.41	PerkinElmer, Waltham, MA, USA
FlowJo 7.6	BD Biosciences, Arshland, OR, USA

GraphPad Prism 9.5.1	GraphPad Software, San Diego, CA, USA
Image J	National Institutes of Health, Behtesda, MD, USA
Image Lab™	Bio-Rad, Munich, Germany
LAS X Core Software	Leica Microsystems, Wetzlar, Germany
Microsoft Office Standard 2016	Microsoft, Redmond, WA, USA
MestreNova 14.1.1	Mestrelab Research S.L., Santiago de Compostela, A Coruña, Spanien
Xcalibur 4.1	Thermo Scientific, Waltham, MA, USA

Table 7 Software

3.1.6 Consumables

Product	Company
Costar Transwell®, 6.5 mm Insert, 24 well, 8.0 µm polycarbonate membrane, tissue culture treated	Corning Incorporated, corning, NY, USA
Cell culture flasks: 25 cm^2, 75 cm^2	Sarstedt, Nürnberg, Germany
Chimney well, black, 96 well plates	Greiner Bio-one, Frickenhausen, Germany
Disposable pipettes: 5 ml, 10 ml, 25 ml	Sarstedt, Nürnberg, Germany
Falcon tubes: 15 ml, 50 ml	Sarstedt, Nürnberg, Germany
Glass beads, acid washed, 425-600 µM	Sigma Aldrich, Taufkirchen, Germany
MicroAmp® Fast Optical 96-Well Reaction Plate, 0.1 ml	Applied Biosystems, Waltham, USA
Microliter plates: 6 well, 12 well, 24 well, 96 well	Sarstedt, Nürnberg, Germany
Petri dishes: 100 mm	Sarstedt, Nürnberg, Germany
Pipette tips: 10 µl, 100 µl, 1000 µl	Sarstedt, Nürnberg, Germany
SafeSeal tubes: 0.5 ml, 1.5 ml, 2 ml	Sarstedt, Nürnberg, Germany
Sep-Pak-C18 catridge 5 g	Waters Associates, Milford, USA
µ-slide 8 well ibiTreat, uncoated	ibidi, Martinsried, Germany

Table 8 Consumables

3.1.7 Plant material

Senescent leaves of katsura trees (*Cercidiphyllum japonicum*), nasturtium (*Tropaeolum majus L.*) and ironwood tree (*Parrotia persica*) were collected in the botanical garden Munich. Senescent leaves of *Echinaceae purpurea L.* were harvested in the medicinal garden at the department of pharmacy of the Ludwig-Maximilian's University and the identity of the plant was determined by Prof. Susanne S. Renner (Department of Systematic Botany and Mycology, Faculty of Biology, University of Munich) as already published (voucher specimen: acronym M; Moser & Karg 1).[26] Spinach (*Spinacia*

oleracea) was purchased in a local supermarket and senescent hops leaves (*Humulus lupulus*) were obtained from the Hopfenforschungszentrum Hüll 5 1/3, Wolnzach.

3.2 Analytical methods

3.2.1 Analytical HPLC

Analytical HPLC analysis was performed with an Agilent 1260 Infinity II LC system with a 1260 Infinity Degasser, a 1100 Series quaternary pump and 1100 Series diode array detector connected to an Agilent Poroshell column 120EC-C18 4 µm 4.6 × 150 mm with Phenomenex ODS 4 × 3 mm i.d. pre-column. Injection volume for all experiments was 100 µl. Depending on the experiment and the samples to be tested, an appropriate method was used. All methods are listed in **Table 9**. Method Nr. 1 was used routinely as standard method for pure samples or intermediate checkup.

Nr.	Solvent A	Solvent B	Solvent composition	Flow (ml/min)
1	Ammonium acetate buffer 10 mM pH 7	ACN	0-2 min 5% B, 2-17 min 5% to 100% B, 17-20 min 100% B, 20-22 min 100% to 5% B	0.5
2	Ammonium acetate buffer 10 mM pH 7	ACN	0-2 min 5% B, 2-27 min 5% to 95% B, 27-31 min 95% to 100% B, 31-34 min 100% to 5% B	0.5
3	Ammonium acetate buffer 10 mM pH 7	ACN	0-5 min 5% B, 5-45 min 5% to 60% B, 45-51 min 60% to 100% B, 51-53 min 100% B, 53-55 min 100% to 5% B	0.5
4	TFA 0.1%	ACN	0-2 min 2% B, 2-17 min 2% to 45% B, 17-19 min 45% to 100% B, 22-24 min 100% to 2% B, 24-25 min 2% B	1.0
5	TFA 0.1%	ACN	0-5 min 2% B, 5-45 min 2% to 45% B, 45-50 min 45% to 100% B, 50-52 min 100% B, 2-56 min 100% to 2% B, 56-58 min 2% B	1.0

Table 9 analytical HPLC methods

3.2.2 Semi-preparative HPLC

Semi-preparative HPLC was carried out using a Büchi Pure C-830 with prep HPLC pump 300 bar, fraction collector, and prep sample injection valve and diode array detector. The column was a Luna® C18, 5 µm, 250 mm x 21.2 mm, with a Phenomenex pre-column

C18 15 x 21.2 mm and the method comprised mobile phase A = Phosphate buffer 0.02 M, pH 7, B = MeOH, flow 18 ml/min with solvent composition: 0-5 min 15% B, 5-10 min 15% to 30% B, 10-40 min 30% to 55% B, 40-42 min 55% to 100% B.

3.2.3 LC-MS

Low resolution LC-MS was conducted using an Agilent 1100 SL system (G1313A ALS, G1316A COLCOM, G1316A VWD, G1312A Bin Pump) coupled to a Bruker Daltonik HCTultra PTM Discovery system (ESI mode). As column an Agilent Poroshell column 120EC-C18 4 µm 4.6 × 150 mm with connected Phenomenex ODS 4 × 3 mm i.d. pre-column; was used, solvents were degassed in an ultrasonic bath and samples filtered by a PTFE syringe filter (Ø 0.45 µm). Gradient consisted of A = Water + 0.1% FA, B = ACN + 0.1% FA, flow 0.5 ml/min with solvent composition 0-2 min 5% B, 2-17 min 5% to 100% B.

3.2.4 Spectroscopy

NMR spectra were recorded on an Avance III HD 500 MHz NMR spectrometer from Bruker BioSpin equipped with a CryoProbe™ Prodigy broadband probe using d6-DMSO as solvent. Data were processed using MestreNova 14.1.1. ESI-MS and MS/MS: High Resolution-Mass Spectra were measured in the LMU Department of Chemistry MS facility; data were processed with Xcalibur. MS^2 fragmentations and leaf spray mass spectrometry were measured using a Thermo Scientific Q Exactive mass spectrometer and generated with Xcalibur and mMass.[33]

3.2.5 Spectroscopic data of isolated compounds

Atom numbering of the following characterized PxBs is presented **Supplementary Figure 20** and follows the rules of established PB molecule nomenclature.[7]

Ep-PxB-5

R_t = 11,5 min. UV/Vis (HPLC trace, HPLC Method Nr. 1), λ_{max}, nm (relative ε) 218 (0.75), 246 (0.55), 312 (0.69), 424 (1.00). HR-ESI-MS: m/z_{found} = 805.32831 $[M-H]^-$; $m/z_{calculated}$ ($C_{41}H_{49}O_{13}N_4$) = 805.32179 (Δ = 8.096 ppm)

Tm-PxB-1

R_t = 9,9 min. UV/Vis (HPLC trace, HPLC Method Nr. 1), λ_{max}, nm (relative ε) 210 (0.71), 242 (0.60), 314 (0.72), 418 (1.00). HR-ESI-MS: m/z_{found} = 661.25238 $[M-H]^-$; $m/z_{calculated}$ ($C_{34}H_{37}N_4O_{10}$) = 661.251517 (Δ = 1.306 ppm); MS/MS (hcd10): m/z (%) = 663.27 (5, $[M+H]^+$, $C_{34}H_{39}O_{10}N_4^+$); 645.25 (75, $[M+H-H_2O]^+$); 627.24 (32, $[M+H-H_2O-H_2O]^+$); 601.26 (100, $[M+H-H_2O-CO_2]^+$); ^{1}H-NMR (500 MHz, DMSO-D_6, 25°): *δ*[ppm] = 2.00 (*s*, 3H, H_3C-7^1); 2.01 (*s*, 2H, H_2C-12^2); 2.04 (*s*, 3H, H_3C-13^1); 2.15 (*s*, 3H, H_3C-17^1); 2.16 (*s*, 3H, H_3C-2^1); 2.50 (*m*, 2H, H_2C-3^1) superimposed by DMSO; 2.62 (*m*, 2H, H_2C-12^1); 3.30 (*m*, 2H, H_2C-3^2) superimposed by water; 3.50 (*s*, H, H_AC-18^2); 3.67 (*m*, H, HC-8^2); 3.67 (*m*, H, H_BC-18^2); 3.70 (broad *d*, *J*=16.0 Hz, H, H_AC-5); 3.80 (broad *d*, *J*=16.0 Hz, H, H_BC-5); 4.46 (*s*, H, HC-18^1); 4.87 (*d*, *J*=2.5 Hz H, HC-10); 5.96 (*s*, H, HC-15); ^{13}C-NMR (500 MHz, DMSO-D_6, 25°): *δ*[ppm] = 9.2 (7^1); 9.3 (13^1); 9.6 (17^1); 9.6 (2^1); 21.1 (12^1); 22.0 (5); 34.7 (12^2); 36.4 (10); 48.5 (3^1); 61.0 (3^2); 67.1 (18^1); 69.3 (8^2); 69.4 (18^2); 98.9 (15); 108.2 (7); 119.4 (3); 121.1 (12); 123.4 (14); 124.5 (8); 126.4 (13); 127.7 (1); 127.8 (16); 131.5 (6); 133.5 (11); 136.0 (4); 143.7 (17); 158.7 (9); 171.9 (8^3); 174.7 (12^3); 194.5 (8^1).

Tm-PxB-2

R_t = 10,6 min. UV/Vis (HPLC trace, HPLC method Nr. 1), λ_{max}, nm (relative ε) 210 (0.71), 240 (0.61), 314 (0.73), 418 (1.00). HR-ESI-MS: m/z_{found} = 617.26333 $[M-H]^-$; $m/z_{calculated}$ ($C_{33}H_{37}N_4O_8$) = 617.261688 (Δ = 2.660 ppm). MS/MS (hcd14): m/z (%) = 619.26 (2, $[M+H]^+$, $C_{33}H_{39}O_8N_4^+$); 601.27 (100, $[M+H-H_2O]^+$); 583.26 (4, $[M+H-H_2O-H_2O]^+$)

Tm-PxB-3

R_t = 11,0 min. UV/Vis (HPLC trace, HPLC method Nr. 1), λ_{max}, nm (relative ε) 218 (0.43), 244 (0.52), 316 (0.70), 418 (1.00). HR-ESI-MS: m/z_{found} = 645.25606 $[M-H]^-$; $m/z_{calculated}$ ($C_{34}H_{38}N_4O_9$) = 645.256602 (Δ = -0.840 ppm). MS/MS (hcd10): m/z (%) = 647.27 (5, $[M+H]^+$, $C_{34}H_{39}O_9N_4^+$); 629.26 (56, $[M+H-H_2O]^+$); 611.25 (34, $[M+H-H_2O-H_2O]^+$); 585.27 (100, $[M+H-H_2O-CO_2]^+$)

Tm-PxB-4

R_t = 11,6 min. UV/Vis (HPLC trace, HPLC method Nr. 1, 100 mM aq. ammonium acetate buffer pH 7/ACN), λ_{max}, nm (relative ε) 212 (0.94), 244 (0.50), 314 (0.67), 430 (1.00). HR-ESI-MS: m/z_{found} = 627.24784 $[M-H]^-$; $m/z_{calculated}$ ($C_{34}H_{35}N_4O_8$) = 627.246038 (Δ = 2.873 ppm). MS/MS (hcd10): m/z (%) = 629.26 (71, $[M+H]^+$, $C_{34}H_{37}O_8N_4^+$); 611.25 (62, $[M+H-H_2O]^+$); 585.27 (100, $[M+H-CO_2]^+$); ^{1}H-NMR (500 MHz, DMSO-D_6, 25°): *δ*[ppm] = 2.00 (*s*, 2H, H_2C-12^2); 2.01 (*s*, 3H, H_3C-7^1); 2.06 (*s*, 3H, H_3C-13^1); 2.13 (*s*, 3H, H_3C-17^1); 2.16 (*s*,

3H, H_3C-2^1); 2.50 (*m*, 2H, H_2C-3^1) superimposed by DMSO; 2.60 (*m*, 2H, H_2C-12^1); 3.30 (*m*, 2H, H_2C-3^2) superimposed by water; 3.69 (*m*, H, H_AC-5); 3.71 (*m*, H, HC-8^2); 3.81 (*m*, H, H_BC-5); 4.90 (*d*, *J*=2.5 Hz H, HC-10); 5.26 (*dd*, *J*=2.8/17.6 Hz H, H_AC-18^2); 6.04 (*s*, H, HC-15); 6.21 (*dd*, *J*=2.8/17.6 Hz H, H_BC-18^2); 6.59 (*dd*, *J*=17.6 Hz H, HC-18^1); ^{13}C-NMR (500 MHz, DMSO-D_6, 25°): δ[ppm] = 9.0 (17^1); 9.0 (2^1); 9.2 (7^1); 9.2 (13^1); 21.9 (5); 25.4 (12^1); 34.6 (12^2); 36.4 (10); 60.9 (3^2); 69.6 (8^2); 100.0 (15); 108.2 (7); 116.3 (18^2); 119.0 (3); 120.9 (12); 122.2 (18); 122.9 (14); 123.9 (8); 124.6 (13); 127.0 (18^1); 127.9 (16); 128.3 (1); 131.9 (6); 133.5 (11); 136.1 (4); 141.7 (17); 158.5 (9); 170.3 (19); 171.6 (8^3); 174.0 (12^3); 194.0 (8^1).

assignment	*Tm*-PxB-1 Δ(^{1}H) / ppm	*Tm*-PxB-1 Δ(^{13}C) / ppm	*Tm*-PxB-4 Δ(^{1}H) / ppm	*Tm*-PxB-4 Δ(^{13}C) / ppm
C 1		127.7		128.3
C 2		-		-
C 2^1	2.16	9.6	2.16	9.0
C 3		119.4		119.0
C 3^1	2.50	48.5	2.50	-
C 3^2	3.30	61.0	3.30	60.9
C 4		136.0		136.1
C 5	3.70 / 3.80	22.0	3.69 / 3.81	21.9
C 6		131.5		131.9
C 7		108.2		108.9
C 7^1	2.00	9.2	2.01	9.2
C 8		124.5		123.9
C 8^1		194.5		194.0
C 8^2	3.67	69.3	3.71	69.6
C 8^3		171.9		171.6
O 8^4				
C 8^5				
C 9		158.7		158.5
C 10	4.87	36.4	4.90	36.4
C 11		133.5		133.5
C 12		121.1		120.9
C 12^1	2.62	21.1	2.60	25.4
C 12^2	2.01	34.7	2.00	34.6
C 12^3		174.7		174.0
C 13		126.4		124.6
C 13^1	2.04	9.3	2.06	9.2
C 14		123.4		122.9
C 15	5.96	98.9	6.04	100.0
C 16		127.8		127.9
C 17		143.7		141.7

C 17[1]	2.15	9.6	2.13	9.0
C 18		-		122.2
C 18[1]	4.46	67.1	6.59	127.0
C 18[2]	3.50 / 3.67	69.4	5.26 / 6.21	116.3
C 19		-		170.3
C 20	-	-	-	-

Table 10 Assignment of ^{1}H-signals from 500 MHz ^{1}H-NMR spectra in DMSO-D_6; ^{13}C assignment HMQC und HMBC spectra.

Pp-DPxB (*Vv*-DPxB)

R_t = 10,5 min. UV/Vis (HPLC trace, Method Nr.1, 100 mM aq. ammonium acetate buffer pH 7/ACN), λ_{max}, nm (relative ε) 212 (1.00), 244 (0.53), 426 (0.88). HR-ESI-MS: m/z_{found} = 629.26221 $[M-H]^-$; $m/z_{calculated}$ ($C_{34}H_{35}N_4O_8$) = 629.26896 (Δ = -10.727 ppm).

^{1}H-NMR (500 MHz, DMSO-D_6, 25°): *δ*[ppm] = 1.56 (*s*, 3H, H_3C-2[1]); 2.07 (*s*, 3H, H_3C-7[1]); 2.01 (*s*, 3H, H_3C-13[1]); 2.15 (*s*, 3H, H_3C-17[1]); 2.36/2.58 (*m*, 2H, H_2C-3[1]) superimposed by DMSO; 2.93 (*d*, H, H_2C-5) superimposed by water; 3.51 (*m*, H, H_AC-5); 4.82 (*d*, *J*=4.8 Hz H, HC-10); 5.28 (*dd*, *J*=2.8/19.20 Hz H, H_AC-18[2]); 6.07 (*s*, H, HC-15); 6.16 (*dd*, *J*=2.8/18.02 Hz H, H_BC-18[2]); 6.57 (*dd*, *J*=17.6 Hz H, HC-18[1])

Cj-PleB

R_t = 12,5 min. UV/Vis (HPLC trace, Method Nr.1, 100 mM aq. ammonium acetate buffer pH 7/ACN), λ_{max}, nm (relative ε) 216 (1.00), 314 (0.62). HR-ESI-MS: m/z_{found} = 645.29105 $[M-H]^+$; $m/z_{calculated}$ ($C_{35}H_{41}N_4O_8$) = 645.28461 (Δ = 9.98 ppm).

Cj-PxB

R_t = 13,0 min. UV/Vis (HPLC trace, Method Nr.1, 100 mM aq. ammonium acetate buffer pH 7/ACN), λ_{max}, nm (relative ε) 214 (0.94), 244 (0.57), 314 (0.73), 426 (1.00). HR-ESI-MS: m/z_{found} = 643.27506 $[M-H]^+$; $m/z_{calculated}$ ($C_{35}H_{39}N_4O_8$) = 642.26896 (Δ = 9.48 ppm).

3.3 Isolation of phyllobilins

3.3.1 Isolation of phyllobilins of *Echinacea purpurea* and *Tropaeolum majus*

Phyllobilins were isolated as described earlier according Karg et al.[26] with minor adjustments. In brief, 100 g of frozen senescent leaves were ground with 250 ml of extraction mixture consisting of 60% MeOH, 40% PBS 50 mM pH 5.2 using a Braun hand blender Model MR 5000 in a 1000 ml beaker. The mixture was incubated at RT in the dark for 1h, then filtered through a pleated filter paper with a Ø of 400 mm. The solid residue was washed twice with 200 ml of solvent mixture and filtered again. By addition of 50%

AcOH, the solution was acidified to pH 3.5 and stirred at RT in the dark overnight. Before further purification with semipreparative HPLC, the extract was concentrated to 20 ml, centrifuged, and filtered or lyophilized using a DW-10N freeze dryer (Darwell, Chongqing, China). The procedure was repeated for another 100 g of leaves. Fractions containing phyllobilins were combined and re-purified by semi-preparative HPLC after evaporating and re-dissolving in 20/80 MeOH/PBS 100 mM pH 7. The purity of isolated PB was confirmed by analytical HPLC, then compounds were dissolved in ACN/potassium phosphate buffer (pH 2.5) 20/80 and stirred overnight. Using SPE (Sep-Pak-C18 cartridge 5g), pure PB were eluted with ACN and lyophilized. The stability of the purified compound after acidifying was controlled by HPLC. For further use, DMSO stocks were prepared and stored at -20 °C.

3.3.2 Isolation of *Pp*-DPxB (*Vv*-DPxB) of *Parrotia persica*

100 g of frozen leaves of Ironwood tree (*Parrotia persica*) were pre-crushed by hand using liquid nitrogen, then ground using a hand blender MultiQuick 5 Vario Stabmixer MQ 5200 WH (De'Longhi Braun Household GmbH, Neu-Isenburg, Germany). 200 ml MeOH was added and after homogenization with the hand blender, the solution was filtered through a cotton cloth. The procedure was repeated twice with the residue, fractions were combined and evaporated by a rotary evaporator to a final volume of 50 ml. To obtain a dry load for subsequent flash chromatography, silica gel 60 A was added, and the mixture was carefully dried under vacuum. 6 - 8 g of dry load was applied to a silica column (40 mm diameter, 300 mm length, 100 g silica gel 60 A), that was washed with DCM. DPxB was eluted with increasing MeOH (DCM/MeOH, 85:15, 70:30, 55:45). The different fractions were analyzed by analytical HPLC. DPxB containing fractions were combined, evaporated, and redissolved in MeOH/PBS 20:80 and purified by semi-preparative HPLC.

3.3.3 Isolation of phyllobilins of *Cercidiphyllum japonicum*

Large Scale isolation of *Cj*-PleB and *Cj*-PxB of senescent Katsura tree leaves (*Cercidiphyllum japonicum*) was implemented according to the published protocol of Karg et al.[25] with minor modifications. Briefly, 300 g of frozen leaves were crushed using a hand blender and 1200 ml of hot water 1200 ml was added in a stainless-steel beaker. Having filtered through a cotton cloth and washing of the residue with 500 ml of hot water, the solution was cooled to RT. The aqueous solution was extracted three times with 200 ml of DCM. DCM fractions were combined and evaporated using a rotary evaporator (IKA®

RV 3 eco, IKA®-Werke GmbH & CO. KG, Staufen, Germany). The residue was dissolved in 20% MeOH in PBS and purified by semi-preparative HPLC.

3.3.4 Partial synthesis of *Cj*-PxB by solid-phase oxidation of *Cj*-PleB or *Po*-PleB

7 g of silica was added to a solution of 10 mg of *Cj*-PleB or *Po*-PleB in 6 ml of DCM/MeOH 5:1 and carefully dried by evaporation on a rotary evaporator. The dry powder was stirred overnight under constant lightening by a tungsten light bulb. The oxidation process and eventually complete formation of *Cj*-PxB was monitored by analytical HPLC. Crude product was then eluted by EtOH, filtered through a paper filter, evaporated, and purified by semi-preparative HPLC. Pure fractions of *Cj*-PxB were pooled, evaporated again, and redissolved in ACN/PBS (pH 2.5). The solution was stirred overnight and by using SPE (Sep-Pak-C18 catridge 5 g), pure *Cj*-PxB was eluted with ACN. The final product of *Cj*-PxB was lyophilized using a Christ RVC 2-18 CD plus rotary vacuum concentrator (Martin Christ Gefriertrocknungsanlagen GmbH, Osterode am Harz, Germany). Solid *Cj*-PxB was stored at – 80 °C. DMSO stocks were prepared and stored at – 80 °C for long term storage or – 20 °C for short term storage.

3.3.5 Concentration determination of DMSO stocks of isolated compounds

Purity of substances was checked by analytical HPLC, then lyophilized samples were dissolved in DMSO. Concentrations of methanolic dilutions were calculated by UV/VIS spectroscopy with the extinction coefficients (ε) at the indicated wavelengths shown in **Table 11**.

PB type	log ε	Wavelength	Literature
DPleB	4.49	237 nm	[34]
PleB	4.23	312 nm	[35]
PxB, DPxB	4.51	426 nm	[23b]

Table 11 Extinction coefficients of PBs used for concentration determination by UV/VIS spectroscopy

3.4 Characterization of phyllobilins of *Tropaeolum majus* and *Humulus lupulus*

3.4.1 Chemoprofiling

A piece of approximately 1 cm^2 each of four different yellow leaves of *Tropaeolum majus* and *Humulus lupulus* was cut out and ground with 200 µl of MeOH in a mortar, diluted 1:11 with potassium phosphate buffer 100 mM pH 7 (20/80), and centrifuged. A 100 µl

portion of the extract was analyzed by analytical HPLC. PxBs were assigned by their UV/Vis spectra from a diode array detector, and their relative content was assessed by their HPLC peak areas relative to the sum of peak areas at 420 nm.

3.4.2 Comparison of retention times

A fresh spinach leaf was ground with 200 µl of MeOH in a mortar, diluted 1:11 with a potassium phosphate buffer 100 mM pH 7 (20/80), and centrifuged. A DMSO-stock of isolated PleB of *Tropaeolum majus* was diluted in phosphate buffer 100 mM pH 7 (20/80). Samples were analyzed by analytical HPLC.

3.4.3 Leaf spray

Leaf spray analysis of senescent *Tropaeolum majus* leaves was performed according a published protocol with minor modifications using a Thermo Scientific Q Exactive (Thomas Müller, University of Innsbruck).[25] Yellow senescent leaves were freshly collected and cut into triangles using a scissor. The tips of the leaf triangles were mounted in front of the MS inlet. During the measurement, approx. 10 µl of MeOH were dropped onto the leaf triangles several times.

3.4.4 Stability of *Tm*-PxB-1 in extraction solvents

To test the stability of *Tm*-PxB-1 during extraction processes, *Tm*-PxB-1 was dissolved in either PBS of different pH values (pH 7/5.2/2.5), or AcOH (pH 3.5), and peak areas were analyzed by analytical HPLC after 1 h or 24 h of incubation at RT. Relative peak areas were calculated relative to HPLC peak areas of freshly prepared *Tm*-PxB-1 in PBS pH 7 which was immediately injected. PxBs were identified by their UV spectrum and retention times. *Tm*-PxB-1 samples in PBS 2.5 overnight were additionally analyzed by LC-MS.

3.5 Cell culture

3.5.1 Cell culture buffers and solutions

Buffer/solution	Composition
Collagen G	1.25 ml collagen G (0.4%) in 500 ml PBS
Phosphate buffered saline (PBS) pH 7.4	132.2 mM NaCl 10.4 mM Na_2HPO_4 3.2 mM KH_2PO_4

	in H_2O
PBS + Ca^{2+}/Mg^{2+} (PBS^{+}) pH 7.4	137 mM NaCl 2.68 mM KCl 8.1 mM Na_2HPO_4 1.47 mM KH_2PO_4 0.25 mM $MgCl_2$ x 6 H_2O in H_2O
Trypsin/EDTA (T/E)	Trypsin 0.05% (*w/v*) Na_2EDTA x 2 H_2O 0.02% (*w/v*) in PBS

Table 12 Cell culture buffers and solutions

3.5.2 Cell lines and culture media

HeLa cells were obtained from the *Deutsche Sammlung von Mikroorgansimen und Zellkulturen* (DSMZ; Braunschweig, Germany), HUVEC cells were purchased from Promocell and THP-1 cells were a kind gift from the laboratory of Prof. Merkel (LMU). All cells were cultured at 37 °C under 5% CO_2. Hela cells were cultured in DMEM medium supplemented with 10% fetal calf serum (FCS). Human umbilical vein endothelial cells (HUVEC) were used in passage #6 or #7 and were cultivated in ECGM cell culture medium supplemented with the ECGM kit enhanced, 10% FCS, 1% penicillin / streptomycin and 1% amphotericin B. Before seeding HUVECs, all surfaces were precoated with collagen G for a minimum of 30 min. THP-1 cells were cultivated in RPMI 1640 containing 10% FCS.

3.5.3 Passaging

Cells were passaged when reaching confluency. Upon reaching a cell density of 8 x 10^5 cells/ml as determined by cell couting using a ViCell^{TM} XR cell counter, THP-1 cells were used for experiments or split by diluting cells to a final cell concentration of 1 x 10^5 cells/ml in 75 cm^2 culture flasks in growth medium. At all times, overgrowth over more than 10^6 cells/ml was avoided. For passaging HeLa and HUVEC cells, growth medium was removed, and cells were washed twice with pre-warmed PBS and detached by pre-warmed trypsin/ethylenediaminetetraacetic (EDTA) (T/E) solution for 3-5 min at 37 °C. Cells were centrifuged (1000 rpm, 5 min, RT) after the tryptic digestion was stopped by addition of growth medium and resuspended in growth medium. For experiments, cells

were counted and seeded on, in case of HUVECs precoated, plates, flasks or dishes in the appropriate concentrations. Hela cells were split in a 1:10 ratio every 3 to 4 days.

3.5.4 Thawing

Cryovials were thawed by warming up in a water bath at 37 °C for 2 min. After addition of pre-warmed culture medium, DMSO was removed by centrifugation (1000 rpm, 5 min, RT). Then cells were resuspended in culture medium and seeded into 25 cm^2 flasks prior to 75 cm^2 flask after 24 h.

3.6 Stability assay

For stability studies, a standardized Echinacea-ratiopharm® Liquid extract from the company ratiopharm (PZN 07686199) was purchased and diluted 1:10 with 22% EtOH, which is the solvent of the original extract. The dilution was centrifuged at 1000 rpm for 5 min and filtered. In an amber botte with an airtight cap, isolated *Ep*-PxB-5 or DMSO as control was added to the prediluted *Echinacea* extract or to 22% EtOH to a final concentration of 100 µM or 200 µM. Keeping bottles at RT, samples were taken with a cannula at days 0, 1, 3, 6 and 10 to perform subsequent HPLC peak area analysis and FRAP assays. For peak area determination by HPLC analysis, samples were diluted 4:5 with PBS and by running HPLC method 3 (**Table 9**), 100 µl of samples were injected. For FRAP assay, samples were diluted 1:6 to ensure data points are within the calibration curve values and thus the linearity of the read-out, as examined by pre-experiments. The anti-oxidative testing by FRAP assay was performed as described in detail in **3.7**.

3.7 FRAP assay

The FRAP assay was adopted from Karg et al.[26] according to the protocol of Benzie et al.[36] with minor modifications. Briefly, freshly prepared FRAP reagent was added to 100 µM of compounds and different concentrations of Trolox for 5 min at 37 °C in a 96 well plate. The FRAP reagent consisted of 10 vol 300 mM acetate buffer pH 3.6, 1 vol 10 mM TPTZ (2,4,6-Tri(2-pyridyl)-s-triazine) in 40 mM HCl and 1 vol 20 mM iron(III)chloride. Antioxidants reduce the Fe^{3+}-$(TPTZ)_2$-complex to intense blue Fe^{2+}-$(TPTZ)_2$ complex with an absorption maximum at 593 nm. A calibration curve was done by measuring the absorbance of different Trolox concentrations. Antioxidant power of the compounds was calculated as Trolox equivalents.

3.8 DPPH assay

The DPPH assay was performed as described previously.[28] Samples, Trolox and 0.3 mM DPPH solution were prepared fresh in EtOH (75% *v/v*). In a 96 well plate, for sample wells (A1) 25 µl of compound or for control wells (A2) 25 µl of EtOH (75% *v/v*) were added to 50 µl of DPPH solution. Blank wells (A0) consisted of 25 µl compound dilution and 50 µl EtOH (75% *v/v*). After incubation for 60 min at 40 °C, absorbance was measured at 505 nm. Radical scavenging activity was calculated using the formula: (A2+(A0-A1))/A2*100.

3.9 ORAC assay

The oxygen radical absorbance capacity (ORAC) assay was conducted as published earlier by Gostner et al.[37] with minor modifications. In a flat-bottom (chimney well, black) 96 well plate, 25 µl of samples and Trolox dilutions were incubated with 150 µl of an 81,6 nM solution of fluorescein for 10 min at 37 °C. Trolox served as standard and was prepared in different concentrations ranging from 5 – 50 µM in phosphate buffer (75 mM, pH 7.4), and samples were diluted from 5 mM DMSO stocks to 10 µM or 15 µM. After addition of 25 µl ice cold 2,2'-azobis(2-methyl-propionamidine) dihydrochloride (AAPH, 100 mM) solution, fluorescence was measured every two minutes for 80 min at 37 °C using an Infinite F200 Pro Plate reader (480 nm/530 nm). Values relative to initial readings were used to calculate the AUC by using a linear trapezoidal method. After subtraction of the blank, final values were calculated using a Trolox regression linear and were expressed as Trolox equivalents.

3.10 COX Inhibition assay

The COX inhibition assay was performed using Cayman Chemicals COX Fluorescent Inhibitor Screening kit according to the manufacturer's instructions. In this assay, arachidonic acid is converted to hydroperoxyl endoperoxide (PGG2) by a COX component of the bifunctional enzymes COX-1 and COX-2. Followed by the reduction of PGG2 to Prostaglandin H2 by peroxidase component and 10-acetyl-3,7-dihydroxyphenoxazine (ADHP), highly fluorescent resorufin is generated. Its fluorescence can be measured with an extinction wavelength of 535 nm and an emission wavelength of 595 nm. In brief, ovine COX-1 or human recombinant COX-2 enzymes were incubated with *Tm*-PxB-1, *Tm*-PxB-4, CGA, or IQ in different concentrations, or buffer as positive control with 100% initial COX activity, for 5 min. Wells without enzymes served as negative control. The fluorescence intensity was measured 2 min after adding arachidonic acid. After subtracting

the negative control, percentages of initial activities were normalized towards the positive control with 100% initial activity. IC_{50} values were calculated by nonlinear regression using GraphPad Prism 9.5.1 (GraphPad Software).

3.11 Cell proliferation assay

Cell proliferation assay was determined by a crystal violet staining. Adherent cells were seeded at the following cell densities (HeLa: 5 x 10^3, HUVEC: 5x10^3) into wells of a 96 well plate. After letting cells adhere for 24 h, cells were treated as indicated for 72 h and additional untreated wells were stained for day zero value according to the crystal violet procedure. For staining, cells were washed with PBS+, dyed with 0.5% crystal violet solution for 10 min and carefully washed with water. After drying of the plate overnight, crystal violet was solubilized with trisodium citrate buffer for 10 min and absorbance was measured at 550 nm using a SpectraFluor Plus plate reader (Tecan, Crailsheim, Germany). Values were normalized to a DMSO control after subtracting of the day zero value and IC_{50} were calculated by nonlinear regression using GraphPad Prism 9.5.1 (GraphPad Software).

3.12 Intracellular ROS assay

The intracellular ROS assay was conducted according to Yokomizo et al.[38] In short, cells were seeded at the indicated cell densities (Hela: 1 x 10^4, HUVEC: 8 x 10^3) per well in 96 well plates and preincubated for 24 h or until confluency for HUVEC cells. After treatment with compounds in the indicated concentrations or control for 24 h, medium was removed, and H_2DCF-DA (10 µM) was added for 30 min incubation. After washing with PBS, cells were incubated with hydrogen peroxide (1 mM) for 30 min. The formation of a highly fluorescent 2´, 7´-dichlorofluorescein (DCF) by intercellular oxidation of H_2DCF-DA was measured by a Tecan SpectraFluor plus microplate reader (excitation wavelength 485 nm; emission wavelength 530 nm). Data were normalized to the hydrogen peroxide treated control and cell viability was assayed upon treatment with compound by a crystal violet staining as described in **3.11**, measured with a spectrophotometer at 590 nm. The number of viable cells was normalized to a control.

3.13 Lucigenin-enhanced NADPH oxidase activity assay

The NADPH oxidase activity assay is based on a chemiluminescence reaction of lucigenin with superoxide anions that are produced by NAPDH oxidases.[39] HUVECs were seeded

in precoated T-75 flasks and grown until confluence. For harvesting, cells were washed with ice cold PBS and lysed by adding ice cold lysis buffer (20 mM HEPES, 1 mM EDTA, Complete®, 1 mM PMSF) in a minimal volume. Before cell scraping and pooling into a falcon, flasks were kept on ice for 15 min. Additional cell disruption was achieved by glass beading. Thereby glass beads were added and the falcon was vortexed tree times for one minute, each time with one minute pause on ice. The lysate was centrifuged at 4 °C, for 10 min at 800 g. The supernatant was collected and kept on ice for protein determination by Bradford as described in **3.16** and subsequent NADPH oxidase activity assay. The protein determination ensured an equal protein loading for all repeated experiments and the linearity of the chemiluminescence assay, that was titrated before. Lucigenin, compounds, and NADPH were prepared fresh in prewarmed Krebs-HEPES buffer. DPI and PA served as controls and are known inhibitor or inducer of NADPH oxidases. To perform the experiment, 10 µl of lucigenin was pipetted into a white plate and was dark adapted for 10 min. Then 10 µl of compounds and 170 µl of lysates suspension (50-90 µg protein) was added. Background was measured at 37 °C for 10 min, every 2 min in a kinetic mode using an Orion II microplate Luminometer (Berthold Detection Systems). Reaction was initiated by adding 10 µl NADPH and luminescence was recorded for 30 min under same conditions. Lucigenin and compounds reached 20 µM final concentration and NADPH was 100 µM. NADPH oxidase activity was normalized to the NADPH added control and was calculated by subtracting the mean of the values of the 30 min measurement by the mean of values of the background reading.

Krebs-HEPES buffer	
NaCl	99 mM
KCl	4,7 mM
$MgSO_4$ x 7 H_2O	1,2 mM
KH_2PO_4	1 mM
$CaCl_2$	1,9 mM
$NaHCO_3$	25 mM
Glucose	11,1 mM
HEPES	20 mM

Table 13 Composition of the Krebs-HEPES buffer

3.14 Protein expression by Flow cytometry

Protein expression levels were determined by fluorochrome labeled primary antibody staining on a BD FACS Canto II (BD Biosciences). HUVEC cells were seeded at a cell density of 0.04 x 10^6 cells per well in a coated 24 well plate and were grown until

confluence. 30 min prior to the treatment with 10 ng/ml TNF-α for 16 h, cells were stimulated with substances or controls for the indicated concentrations. Cells were washed twice with pre-warmed PBS and detached with 100 µl T/E at 37 °C. Then, cell suspensions were transferred into pre-cooled FACS tubes containing 100 µl 4% formalin and were incubated for 10 min. After dilution with 1000 µl PBS, tubes were centrifuged for 5 min at 1200 rpm. The supernatant was discarded, and antibodies (**Table 4**) were added as specified to the remaining liquor. After dark incubation for 45 min at RT, PBS was added for washing. After additional centrifugation for 5 min at 1200 rpm, cells were resuspended in 200 µl PBS. Directly after, cells were kept in the dark on ice while flow cytometric analysis was conducted. When parallel experiments were performed using two different labeled antibodies for different proteins, before recording cellular probes, compensation was carried out to cleave a spectral overlap using the BD FACS canto II software and BD™ CompBead Plus Anti-Mouse Ig, κ/Negative Control (BSA) Compensation Plus (7.5 µm) particles set (BD Biosciences). Antibodies used for compensation were a Mouse IgG2b isotype control FITC (Genetex #GTX01519-06) and Mouse IgG1 Isotype Control, PE conjugated (Biorbyt #orb195302).

3.15 Quantitative real-time PCR analysis

For the quantification of VCAM-1, ICAM-1, E-selectin mRNA levels, cells were treated with TNF-α for 4 h to induce adhesive protein expression levels as determined in pre-experiments (**Supplementary Figure 31**) and NOX subunit determination was assessed as indicated. After cell lysis, mRNA was isolated using the RNeasy® Mini Kit (250) (QIAGEN, Hilden, Germany) according to the manufacturer's protocol and mRNA concentration was determined with a Nanodrop® Spectrophotometer (PEQLAB Biotechnologie, Erlangen, Germany). mRNA was stored at – 80 °C or transcribed by reverse transcription to cDNA using the High-Capacity cDNA Reverse Transcription Kit (Applied Biosystems, Waltham, USA) as described by the manufacturer. Quantitative real-time polymerase chain reaction (qPCR) was performed using a QuantStudio™ 3 Real-Time PCR System (Applied Biosystems, Waltham, USA). Primers were designed with the ThermoFisher Cloud OligoPerfect tool or the NCBI database and were purchased from metabion (Planegg, Germany). Nucleotide codes are shown in **Table 14**. Per well 100 ng of cDNA, PowerUp™ SYBR® Green Master Mix (Applied Biosystems, Waltham, USA), RNase-free water and 0.025 mols of FW and 0.025 mols of RV primer were pipetted in a ratio of 8:25:15:1:1 into a MicroAmp® Fast Optical 96-Well Reaction Plate, 0.1 mL (Applied Biosystems, Waltham, USA). X-fold change in mRNA was assessed by the $\Delta\Delta C_T$ method

as described earlier[40] and GAPDH was used as housekeeping gene. For each primer pair primer efficiency was analyzed by using 500 ng, 50 ng and 5 ng of cDNA per well.

Target	FW (5'-3')	RV (5'-3')
E-selectin	GGCAGTTCCGGGAAAGATCA	GTGGGAGCTTCACAGGTAGG
GAPDH	ACGGGAAGCTTGTCATCAAT	CATCGCCCCACTTGATTTT
p22phox	GGGGAAGAGGAAGAAGGGCT	CAGCCGCCAGTAGGTAGATG
ICAM-1	GCAGACAGTGACCATCTACAGCTT	CTTCTGAGACTTGTGGCTTCGT
NOX4	CTGTGGTGTTACTATCTGTATTTTCTC	CTTGCTGCATTCAGTTCAACA
VCAM-1	AGGGTCTACCAGCTCCAGAG	GGGATTCACAGCCCATGACA

Table 14 Primers with nucleotide codes used for qPCR analysis

3.16 Western Blot analysis

Western Blot analysis served to investigate protein levels of NOX4, MMP-2 and MMP-9. Therefore, HUVEC were seeded in coated 10 mm dishes at a density of 1.5 x 10^6 cells per dish and were grown until confluence. Cells were treated with BR (20 µM), *Cj*-PxB (5 µM), *Cj*-PleB (20 µM), *Pp*-DPxB (*Vv*-DPxB) (20 µM) for 24 h. For cell lysis, cells were washed twice with ice-cold PBS. 300 µl of radioimmunoprecipitation (RIPA) lysis buffer was added and lysates were transferred into 1.5 ml Eppendorf tubes. Lysates were centrifuged (14 000 rpm, 10 min, 4 °C) to remove cell debris. Protein concentrations were quantified by Bradford assay according to a published protocol.[41] In short, lysate solution was diluted 1:10 with H_2O. In a 96 well plate, 10 µl of protein sample was added to 190 µl of a 1:5 dilution of Bradford reagent Roti® Quant (Bio-Rad) in water. After an incubation time of 5 min, absorbance was determined at 592 nm using a SpectraFluorPlus™ (Tecan). Protein concentrations were quantified by linear regression analysis with bovine serum albumin (BSA) dilutions as protein standards. To adjust protein concentrations, each sample was diluted with 1x SDS (sodium dodecyl sulfate) and 5x sample buffer. Proteins were denatured at 95 °C for 5 min and were separated by sodium dodecyl sulfate polyacrylamide gel electrophoresis (SDS-PAGE) in electrophoresis buffer (100 V, 21 min then 200 V, 43 min) on discontinuous polyacrylamide gels. Gels were combined by a gradient separation gel (4-20%) and a stacking gel. By tank blotting (100 V, 90 min, 4 °C) proteins were transferred to either nitrocellulose or polyvinylidene difluoride (PVDF) membranes, that have been equilibrated before in 1X tank buffer. Afterwards, membranes were blocked with 5% non-flat dry milk powder in PBS (Blotto) for 2 h. Primary antibody was added overnight at 4 °C (**Table 3**). Membranes were washed four times with TBS-T for 5 min each, before the secondary HRP-coupled antibody was added for 2 h (**Table 5**). Four time washing procedure was repeated prior to the incubation with ECL solution and

chemiluminescence detection with a ChemiDoc™ Touch Imaging System (Bio-Rad). By comparison with Page Ruler™ Plus Prestained Protein Ladder (Fermentas), bands were assigned. Protein levels were analyzed by Image Lab™ Software (Bio-Rad) and were normalized to the total protein level.

Buffer/gel	**Composition**	
RIPA lysis buffer	Tris/HCl	50 mM
	NaCl	150 mM
	Nonidet NP-40	1%
	Sodium deoxycholate	0.25%
	SDS	0.10%
	H_2O	
	Added before use:	
	Complete® EDTAfree	4 mM
	PMSF	0.5 mM
	Activated Na_2VO_4	2 mM
5X SDS sample buffer	Tris/HCl pH 6.8	3.125 M
	Glycerol	50%
	SDS	5%
	DTT	2%
	Pryonin Y	0.025%
	H_2O	
Electrophoresis buffer	Tris	4.9 mM
	Glycine	38 mM
	SDS	0.1%
	H_2O	
TBS-T (pH 7.6)	Tris/HCl	50 mM
	NaCl	150 mM
	Tween 20	0.05%
Tank buffer	Tris base	48 mM
	Glycine	39 mM
	Methanol	20%
	H_2O	

Table 15 Composition of buffers and solutions for Western Blot analysis

Ingredient	**Stacking gel**	**4-20% Separation gel**	
		4%	20%
Rotiphorese® Gel 30	13.3%	13.3%	66.7%

Tris-HCl pH 6.8	125 mM	-	-
Tris-Hcl pH 8.8	-	375 mM	375 mM
TCE	-	0.05%	0.05%
SDS	0.1%	0.1%	0.1%
TEMED	0.2%	0.1%	0.1%
APS	0.1%	0.05%	0.05%
in H_2O			

Table 16 Composition of gels for Western Blot analysis

4-20% gradient gel was achieved by mixing both solutions in one pipette. Gradient is formed by ascending air bubbles.

3.17 Collagen IV staining by confocal imaging

Prior to seeding, 8-well µ-slides (ibidi, Martinsried, Germany) were coated with 250 µl collagen IV (5022, Advanced Biomatrix, Carlsbad, CA) solution at a density of 10 µg/cm^2 for 60 min at 37 °C. Therefore, collagen IV solution was prepared fresh by diluting with 0.25% acetic acid according to the manufacturer's instructions. Having removed the collagen solution, HUVEC cells were seeded in a density of 5 x 10^4 cells/well, thereby adding the compounds and inhibitor NNGH (Sigma Aldrich, St. Louis, MO). After having incubated for 24 h at 37 °C, cells were washed with PBS+ and were fixed with 4% PFA (Thermo Fisher Scientific, Waltham, MA) solution in PBS for 10 min at RT. Cells were washed again with PBS. 5% BSA (Roth, Karlsruhe, Germany) in PBS was added for 60 min under constant shaking at RT to block nonspecific binding sites. Anti-collagen antibody, type IV primary antibody (Chemicon, Limburg an der Lahn, Germany) was added overnight at 4 °C. Then, wells were washed three times with 1% BSA in PBS for 10 min each under shaking at RT. Alexa Fluor 488 IgG (H+L) secondary antibody (Thermo Fisher Scientific, Waltham, MA) and Hoechst 33342 (1:100) was added for 1 h shaking in the dark. After having washed twice for 10 min with 1% BSA in PBS, and once with pure PBS under shaking in the dark, cells were covered with one drop of FluorSave™ mounding medium (Merck Millipore, Darmstadt, Germany) and sealed with a cover slip. After incubation for 30 min at RT in the dark, slides were stored until measurement at 4 °C in the dark. Laser scanning confocal microscopy images were taken with a Leica TCS SP8 microscope equipped with an HC PL APO CS2 63x/1.4 oil objective and photomultiplier (PMT) or HyD detectors, using the LAS X core software. In sequential scanning mode two frames were acquired for every channel with a scanning speed of 400 Hz and the pinhole size set to 1.0 airy units. Following excitation laser lines were applied: 405 nm and 488 nm.

3.18 *In-vitro* MMP-9 activity assay

The *in-vitro* assessment of the influence of compounds on MMP-9 enzyme activity was thankfully conducted and established by our collaboration partner Dr. Stefan Schwaiger and Dominic Mittas (University of Innsbruck). The assay is based on the fluorescence quenching by enzymatic hydrolysis of the peptide substrate Dnp-Pro-Cha-Gly-Cys(Me)-His-Ala-Lys(Nma)-NH2. In this peptide Dnp stands for dinitrophenyl which is the quencher and Nma for *N*-methylanthranillic acid, the fluorophore.[42] Therefore, in a 96-well plate (chimney well, black) a total reaction volume of 100 µl consisting of 40 µL buffer solution, 10 µl sample or blank (DMSO or 0.1 N NaOH for BR), and 25 µl human recombinant active MMP-9 enzyme dilution, and 25 µl fluorogenic substrate was pipetted and fluorescence quenching was measured using a Tecan Spark 10M multimode microplate reader (Tecan group AG). The daily fresh prepared buffer consisted of 50 mM Tris, 100 mM NaCl, 10 mM $CaCl_2$ and 0.01% of non-ionic surfactant Brij 35 and was adjusted to pH 7.4 by the addition of HCl (7%). To minimize freezing and thawing, enzyme (40 nM) and substrate (640 µM) were dissolved and aliquoted in fresh buffer and stored at – 80 °C. Prior to the experiment, thawed aliquots of enzyme and substrate were diluted with final assay medium to 4 nM and 40 µM on ice in the dark, respectively. Samples were dissolved in DMSO or 0.1 N NaOH (Br) and diluted with Tris-HCl buffer. Buffer, sample solution or control (DMSO or 0.1 N NaOH) was added to the enzyme solution (4 nM) and were preincubated at 37 °C for 10 min with ten seconds of linear shaking (1440 rpm). The reaction was initiated by adding 25 µl of fluorogenic substrate solution (40 µM) and the fluorescence intensity (ex/em: 320 nm/430nm) was measured every 30 sec for one hour at 37 °C prior to an equilibration time of 10 min with ten seconds of linear shaking (1440 rpm). Final concentration of DMSO was 1%. MMP-9 activity of mean values was calculated by subtracting the increase of fluorescence intensity of compensation wells between timepoint zero and 60 min from the increase of fluorescence of sample wells of timepoint 0 and 60 min using the formula below. For compensation of self-fluorescence, wells consisting of 90 µl Tris-HCl buffer and 10 µl sample solution without enzyme or substrate, were recorded. Controls were set to 100% MMP-9 activity and mean residual MMP-9 activity is calculated relative to the 100% active controls. At least six different concentrations were tested and subsequently IC_{50} values were calculated.

$$Residual\ MMP-9\ Activity\ [\%] = \frac{(\mathrm{T60Sample}\ -\ \mathrm{T0Sample})\ -\ (\mathrm{T60Sample\ w/o}\ -\ \mathrm{T0Sample\ w\ /\ o})}{(\mathrm{T60Blank}\ -\ \mathrm{T0Blank})\ -\ (\mathrm{T60Blank\ w/o}\ -\ \mathrm{T0Blank\ w\ /\ o})} \times 100$$

3.19 Migration of THP-1 cells by Boyden Chamber assay

For migration experiments with THP-1 cells transwells with 6.5 mm diameter and 8.0 µm pore size were used (Corning Incorporated). The chemoattractant medium consisted of 100 ng/ml MCP-1 (Peprotech) in RPMI 1640 supplemented with 10% FBS and as starving medium served RPMI 1640 supplemented with 2% FBS. THP-1 cells were harvested at a cell density of 0.8 x 10^6 cells/ml, centrifuged, resuspended in 5 ml of medium and counted with a ViCell™ XR cell counter. Cells were diluted to 1 x 10^6 cells/ml in 5 ml in a T25 flask and cells were stained by incubation at 37 °C for 30 min with Calcein-AM (Biomol GmbH) in a final concentration of 2 µM. Cells were centrifuged again, resuspended in 3 ml of starving medium, counted, and diluted to a cell concentration of 1 x 10^6 cells/ml. For a calibration curve, an aliquot of the suspension was diluted further in normal growth medium and 50 µl of each dilution was pipetted in triplets in a 96 well plate and incubated at 37 °C until the migration experiment was stopped. 700 µl of chemoattractant medium was added to the lower chamber and 200 µl of cell suspension containing compound was applied to the upper chamber. For negative control wells, starving medium was added to the lower chamber, as well as to the upper. Cells were allowed to migrate for 4 h at 37°C in an incubator. Afterwards the solution in the lower chamber was collected. The upper filter was washed with PBS and cleaned with a Q-tip. Transmigrated cells, that remained on the lower surface of the filter, were dislodged by incubation with 5 mM EDTA in PBS for 5 min. Solutions were combined in 1000 µl vials, centrifuged and cells were resuspended in normal growth medium. 50 µl aliquots were transferred in doublets to the calibration curve plate and fluorescence was measured with a Tecan plate reader at 495 nm excitation and 520 nm emission. Linearity of the measurement was present throughout the experiment and was validated by the calibration curve. After the fluorescence measurement, cell viability was checked by transferring samples to a ViCell™ XR cell counter.

3.20 Transendothelial Migration of THP-1 cells by Boyden Chamber assay

To investigate the migration of THP-1 cells through a monolayer of endothelial cells, first HUVEC cells were seeded until confluency on coated sterile filter sides of transwells with 6.5 mm diameter and 8.0 µm pore size (Corning Incorporated). Therefore, lower and upper filter sides were pre-coated with collagen G in PBS for 30 min at 37 °C (700 µl lower chamber, 100 µl upper chamber). Then, solutions were removed, and filters were air dried for a minimum of 10 min. Fibronectin solution in PBS was prepared fresh and 50 µl were

added on the top of the filter to an end-concentration of 2 µg/cm^2. After additional incubation for 45 min at 37 °C, coating solution was removed and 5 x 10^4 HUVEC cells were seeded on the dried filter slides and incubated at 37 °C. Growth medium was present in both chambers and was refreshed every two to three days. After three days, monolayer integrity was checked by applying a FITC-Dextran M_w 70 kDa (Sigma) in an end-concentration of 1 mg/ml for 20 min incubation and by measuring the fluorescence (ex: 485 nm/em: 535 m) of the solutions in the lower chamber. One day before starting the migration of THP-1 cells, adhesion proteins expression of HUVECs was induced by adding TNF-α (10 ng/ml) to the upper and lower chambers. The experimental migration part of the experiment was then conducted as explained in **3.19** with minor modifications. Briefly, compound was added to the lower and upper chambers and THP-1 cell migration was stopped after 24 hours of incubation. The collected medium of the lower chamber of each well was combined with the EDTA detachment solution in the corresponding well of the 24-well plate, and fluorescence read-out was conducted by measuring the plate without additional cell centrifugation and reseeding step.

3.21 Statistical analysis

Results display the mean of at least three independent experiments (mean ± SD), each replicated in at least three repeats, if not declared else. Statistical significance was calculated by one-way analysis of variance with post hoc analysis using Dunnett's multiple comparison test. All statistical analyses were examined with GraphPad Prism 9 or 10.

PART I

4 Part I: Phyllobilins - a bioactive natural product class contributing medicinal plants activity

4.1 Introduction

Among natural compound families, PBs are just at the beginning of being exploited as phytochemicals. Therefore, less is known about their pharmaceutical properties, including their pharmacological bioactivities, but also their potential as excipients in pharmaceutical technology. Taking the group of flavonoids as example, researchers extensively investigated the diversity of the compound structures, their impact on diverse human diseases in details, their function for the plants, the way how to handle the substances to form stable dosage forms.[43] Although the knowledge on the existence of chlorophyll breakdown has increased since 1987[44], information on the occurrence of PBs in various plants and their chemical structures remain to be fully elucidated. Here, we wanted to contribute information on both sides, further discovery of representatives and first insights on pharmaceutical technological aspects. With our work, we aimed at identifying previously unknown PBs in different plants on the one hand, but we also investigated the properties of these molecules as excipients on the stability of phytotherapeutics.

Based on strong anti-oxidative properties that were described previously[26-28, 30], we hypothesized that PBs stabilize phytotherapeutics that are susceptible to degradation. In pharmaceutical technology and food industry, antioxidants are applied to maintain and prolong the quality of their products. Following hydrolysis, oxidation is the major degradation pathway of pharmaceuticals.[45] Three different oxidation mechanisms can be defined: radical mediated (autooxidation), peroxide mediated (nucleophilic/electrophilic) and single electron to dioxygen mediated oxidations.[46] The use of antioxidants displays one prominent approach during drug product formulation to prevent instabilities.[47] Also here, depending on the way of action, different types of antioxidants can be distinguished. For example, EDTA is known to inhibit radical chain reactions and therefore is grouped into initiation inhibitors.[45] Contrarily, butylhydroxyanisole (BHA) influences the propagation, a later phase of radical chain reactions.[48] This group is named terminators of radicals. Generally, autooxidation is seen as process of three steps, initiation, propagation, and termination. By inhibiting one of the first two steps, antioxidants terminate the oxidation reaction.[49] However, also established are antioxidants in their function as reducing agents, like ascorbic acid, thiols, and polyphenols.[45, 50] Although the benefits of antioxidants as protective additives in food or pharmaceutical products is well

known, the impact of the antioxidants *in-vivo* on adverse effects is being discussed.[51] Antioxidants, their intermediates, or metabolites, can interfere with important signaling cascades, like cell survival and immune response, and are claimed to be involved in the development of allergies and asthma.[51-52] PBs are abundant ingredients in ripening plant material. The substances are part of human nutrition as they were found in lettuce and savoy cabbage, among others[28, 31], and ingredients of phytopharmaceuticals as demonstrated for tea preparations of *Urtica dioica*[27]. Potentially, they are overlooked substances in a variety of phytomedicines with unknown contribution to the pharmacological and technological properties of those. As their highly anti-oxidant potential was established before[26-28, 30], the question arose whether PBs as antioxidants influence these pharmaceutical attributes. In this regard, we isolated *Ep*-PxB-5 of senescent *Echinacea purpurea* leaves and spiked purchased medicinal extracts of the plant with this substance to analyze its impact on the anti-oxidative potential of the preparation and further the stability of major ingredients by analytical HPLC over the time.

Additionally, we examined aerial parts of medicinal plants for their PB content and characterized the derived PBs, expanding the knowledge about this family of phytopharmaceuticals. In this work, we deciphered and focused specifically on novel structures of PBs in *Humulus lupulus* L. and *Tropaeolum majus* L.

Hops (*Humulus lupulus* L.), a common member of the plant family *Cannabaceae*, is widely cultivated over the world and especially for traditional reasons in Bavaria. A third of the word wide cultivation takes place in the European Union (EU) on 26 500 ha, with 60% placed in Germany. Thereby, 50 kilotons are produced in the EU per year.[53] Brewing as well as the pharmaceutical industry glances at female inflorescences of hops for either their bitter aromatic secondary metabolites or their bioactive properties. Desirable metabolites are terpenes and sesquiterpenes, present in the essential oil of the hop cones, or prenylated phenolic compounds as acylphloroglucinols known as bitter acids from the humulone type. Briefly, associated bioactivities range from anti-carcinogenic, anti-microbial, anti-inflammatory, anti-glycemic, sedative to estrogenic effects.[54] Predominately, the known active substances in hops can be found in the inflorescences, thus much interest on bioactivities of hop leaves has not sparked yet. Apart from investigations on *in-vitro* anti-fungal activity of apolar sub-extracts of leaves, identifying xanthohumol as dominating active substance, little research has focused on the leaves.[55] 75% of leaves and stems are unused biomass waste.[56] Apparently, the chlorophyll rich

leaves degreen after harvest season in autumn, arousing the question whether PBs might be found. Indeed, novel structures of Type-II PBs appeared as elucidated by analytical HPLC und UV/Vis detection, and in the following work their anti-oxidative potential was evaluated for the first time.

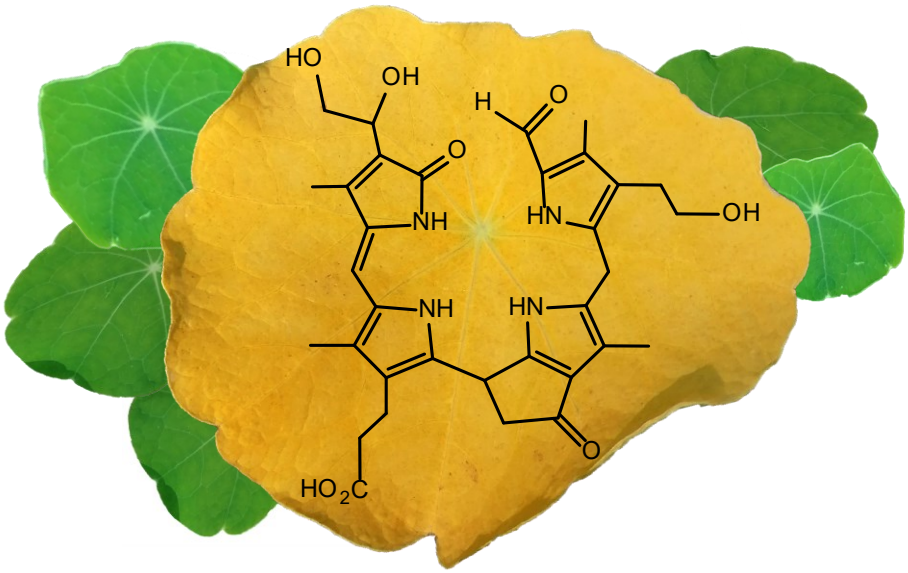

Figure 5 Graphical abstract on a naturally occurring pyPxB in yellow senescent *Tropaeolum majus* leaves

Garden nasturtium (*Tropaeolum majus* L.) is a member of the *Tropaeolaceae* family and it is, among other names, also known as indian cress or monks cress.[57] Notably, the pharmaceutically used plant still lacks full chemical characterization of its components, which is aggravated by influences of cultivation methods and environmental conditions on the chemical fingerprint.[57] The most analyzed part of the plant is its flowers. Depending on their colors, which can vary from yellow to orange or brick red, phytochemical composition was found to be different, referrable to differences in anthocyanin representatives. Bioactive compounds of the flowers are carotenoids as lutein and phenolic compounds, namely flavonoids.[57] However, a limited number of studies has investigated their leaves which describe flavonoids, such as isoquercitrin (IQ), quercetin 3-glucoside, kaempferol, fatty acids, and glucosinolates, such as glucotropaeolin and sinalbin, as ingredients.[57-58] Garden nasturtium is not only used as decorative food e.g. in salads, but also in folk medicine due to its diuretic and anti-bacterial effects.[59] In addition, *Tropaeolum majus* was listed as phytomedicine for the treatment of catarrhs of the upper respiratory tract and urinary tract infections in monographies of the commission E of Germany Nr. 162 of 1992. Gasparotto et al. further investigated nasturtium leaf extracts, revealing natriuretic and diuretic activity *in-vivo*. Thereby, semi-purified fractions with

enriched IQ were found to possess enhanced effects leading to the assumption that IQ might play a major role in leaf extracts.[60] Despite that, literature claimed also that polyphenols, mainly chlorogenic acid (CGA) and ascorbic acid are responsible for anti-oxidative and anti-inflammatory power of herb extracts of nasturtium.[61] In this part of the thesis on PBs in *Tropaeolum majus*, novel PxB structures were structurally characterized and, in comparison to the bioactive ingredients IQ and CGA, their anti-oxidative potency as well as their potential to inhibit COX-1 and -2 activity was assessed (**Figure 5**).

4.2 Results

4.2.1 Influence of phyllobilins on properties of phytopharmaceuticals

4.2.1.1 Isolation of *Ep*-PxB-5

To examine whether PBs, as antioxidants, can influence the stability of phytotherapeutics and could therefore prolong the stability of those preparations like other known substances as ascorbic acid[45, 50], *Ep*-PxB-5 (**Figure 6**) was chosen as representative PB. As published by Karg et al., six different anti-oxidative PBs of the type phylloxanthobilin (PxB) were found in senescent *Echinacea purpurea* leaves, with *Ep*-PxB-5 being the substance with highest yield.[26] Consequently, *Ep*-PxB-5 was isolated and its identity was confirmed by analytical HPLC and HR-ESI-MS analysis (**Supplementary Figure 1**). The yield arising from extracting 200 g of senescent leaves was about 5 mg as quantified by UV/Vis spectroscopy.

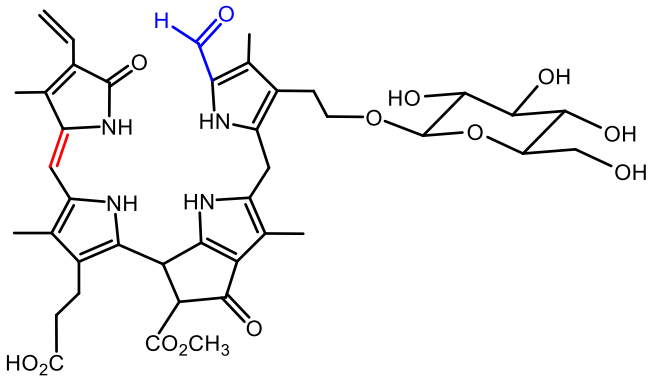

Figure 6 Chemical structure of *Ep*-PxB-5

4.2.1.2 Effects of *Ep*-PxB-5 on the stability of *Echinacea* extracts

Focusing on simple liquid dosage forms, the influence of *Ep*-PxB-5 on the stability of a purchasable Echinacea-ratiopharm® liquid extract for ingestion was tested. An appropriate HPLC method with 0.1% TFA as mobile phase was established for appropriate separation of the multicomponent mixture. To set up a simple model to investigate the influence of *Ep*-PxB-5 on the extract components, the highest peak at 28 min R_t (detection at 320 nm) was analyzed for the decline in peak area in correlation to the addition of *Ep*-PxB-5 at RT, which is the indicated storage condition of the phytomedicine (**Supplementary Figure 3-Supplementary Figure 4**). This peak at R_t =28 min showed a characteristic UV/Vis spectrum for a phenolic compound. The substance was isolated from analytical HPLC,

and the identity was tentatively assigned as caftaric acid by HR-ESI MS analysis (**Supplementary Figure 2**). Caftaric acid is known as highly abundant ingredient in *Echinacea purpurea* raw materials and liquid tincture products.[62] Over a storage time of ten days at RT the peak of caftaric acid in the *Echinacea* extract significantly diminished. However, the relative decline in the peak area was independent of *Ep*-PxB-5 addition at two different concentrations (100 µM, 200 µM) (**Figure 7**). Additionally, during this experiment, a decrease of *Ep*-PxB-5 content itself was observed by analytical HPLC peak analysis (**Supplementary Figure 5**). Owing to the fading of *Ep*-PxB-5, storage time above ten days was not conducted. To exclude an influence of potential instabilities of *Ep*-PxB-5 in the extract, controls with *Ep*-PxB-5 in the extract solvent EtOH 22% (*v/v*) were included (**Supplementary Figure 6-Supplementary Figure 7**). Indeed, as presented in **Figure 8**, we detected significant differences in peak area decline of *Ep*-PxB-5 in *Echinacea* extract vs in EtOH 22% for two different concentrations over ten days at RT. In line with that, the amount of the degradation product PrB differed between *Echinacea* extract and EtOH 22%. PrB is formed by oxidation of PxB and absorbs at longer wavelengths.[63] Significantly more PrB was formed over six days, when *Ep*-PxB-5 was added (100 µM and 200 µM) to the *Echinacea* extract than to EtOH 22%. Samples of the 100 µM batch from day 10 showed an inverse effect, potentially caused by an instability of PrB, becoming evident by the decline in peak area. Anyway, not a significant but a similar trend of peak area decrease of PrB at day 10 was observed for the 200 µM samples (**Figure 8**).

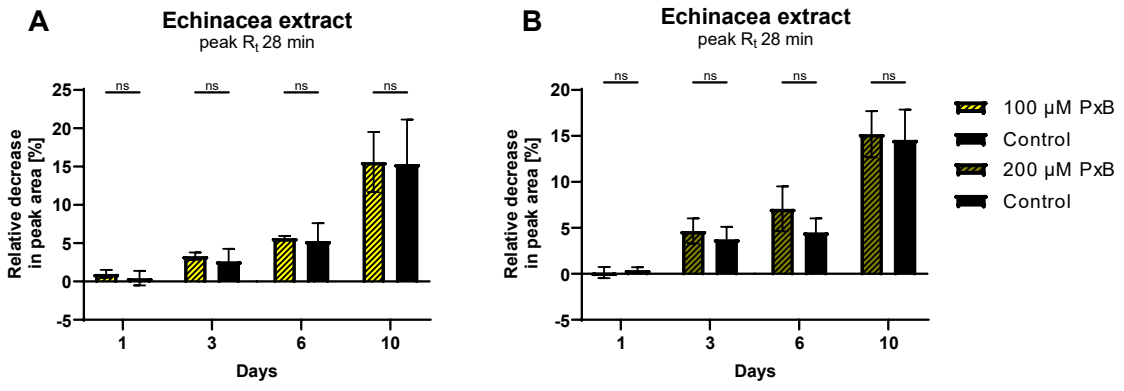

Figure 7 Influence of *Ep*-PxB-5 on the peak area of a major constituent of a purchasable *Echinacea* extract over ten days. (A) 100 µM and **(B)** 200 µM of *Ep*-PxB-5 were added to a freshly opened *Echinacea* extract**.** As vehicle control DMSO was added to the extracts, accordingly. Peak areas were analyzed by analytical HPLC. Experiments were performed as biological triplicates and statistical significance was calculated by 2way ANOVA analysis and Šídák's multiple comparisons test. (ns, not significant)

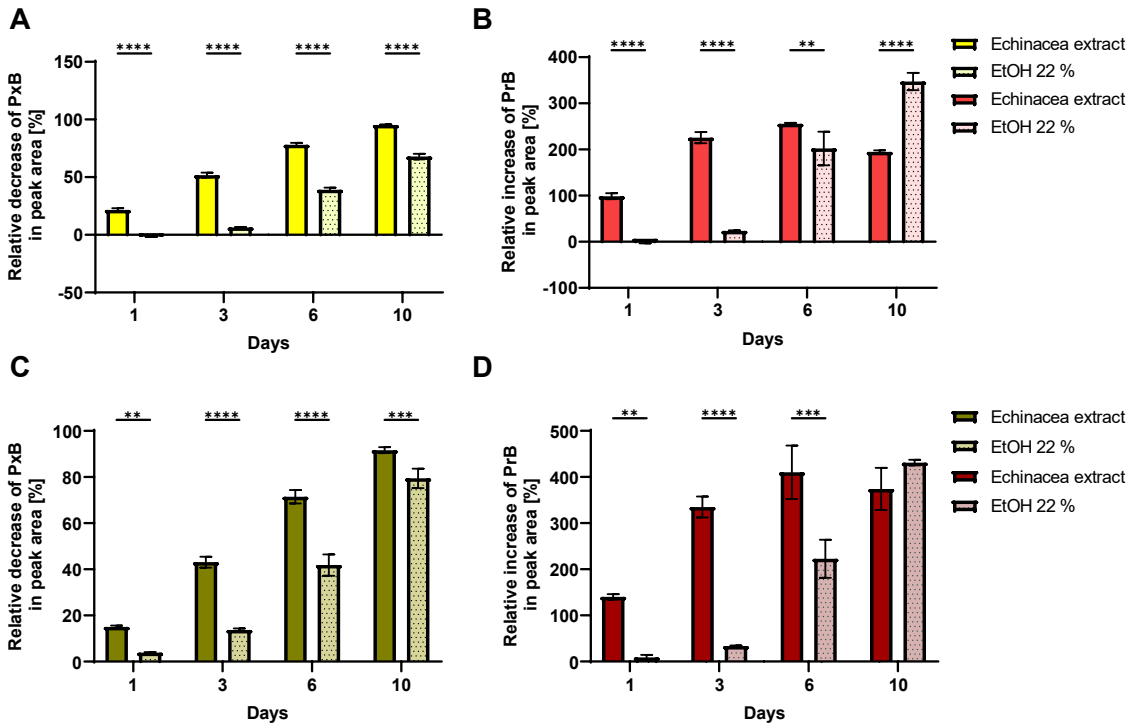

Figure 8 Stability of *Ep*-PxB-5 in *Echinacea* extract compared to EtOH 22% over ten days. (A) Relative decrease of 100 µM of *Ep*-PxB-5 in *Echinacea* extract and EtOH 22% (*v/v*) and **(B)** increase of the oxidation product PrB of the same samples was assessed by analytical HPLC analysis; **(C)** relative decrease of 200 µM samples of *Ep*-PxB-5 in the named solvents and **(D)** emergence of PrB, analogously. Quantification of PxB **(A,C)** was carried out at 420 nm HPLC trace and PrB **(B,C)** at 520 nm, respectively. Statistical significance was calculated by 2way ANOVA analysis and Šídák's multiple comparisons test. (***P* < 0.01, ****P* < 0.001, *****P* < 0.0001)

4.2.1.3 Effects of *Ep*-PxB-5 on anti-oxidative activity of *Echinacea* extract

Most bioactive ingredients of *Echinacea* are phenolic compounds, such as caffeic acid derivatives and flavonoids, or alkamides, polysaccharides, polyacetylenes, polyenes and, terpenoids.[64] To monitor the impact of *Ep*-PxB-5 on possible changes on pharmacological properties of the standardized *Echinacea* extract during storage, anti-oxidative testing was conducted. The extracts and the extract solvent EtOH 22% (*v/v*) as control, were supplemented with *Ep*-PxB-5. Samples were analyzed at the indicated timepoints, which were subsequently tested via FRAP assay, which assesses the ability of antioxidants to reduce iron ions.[36] Addition of 100 µM of *Ep*-PxB-5 showed an increase in anti-oxidative strength compared to the controls, which was significantly increased one day after addition (**Figure 9 A**). Stronger effects were visible using a higher concentration of *Ep*-PxB-5. Extracts containing 200 µM of *Ep*-PxB-5 possess significantly higher FRAP values at each timepoint over ten days than the control extracts without *Ep*-PxB-5 supplementation (**Figure 9 B**). Furthermore, the anti-oxidative stability of the model substance *Ep*-PxB-5

itself was assessed. Thereby, instead of spiking the extracts with substance, the extract medium EtOH 22% (*v/v*) was supplemented with *Ep*-PxB-5 and anti-oxidative property was tested over ten days. It was found that samples with 100 µM of *Ep*-PxB-5 were potent for six days and only showed significant reduction in anti-oxidative values for day 10. For 200 µM of *Ep*-PxB-5 in EtOH 22%, only samples taken at day 6 showed significantly reduced Trolox values, other samples did not exhibit those effects (**Figure 9 C**).

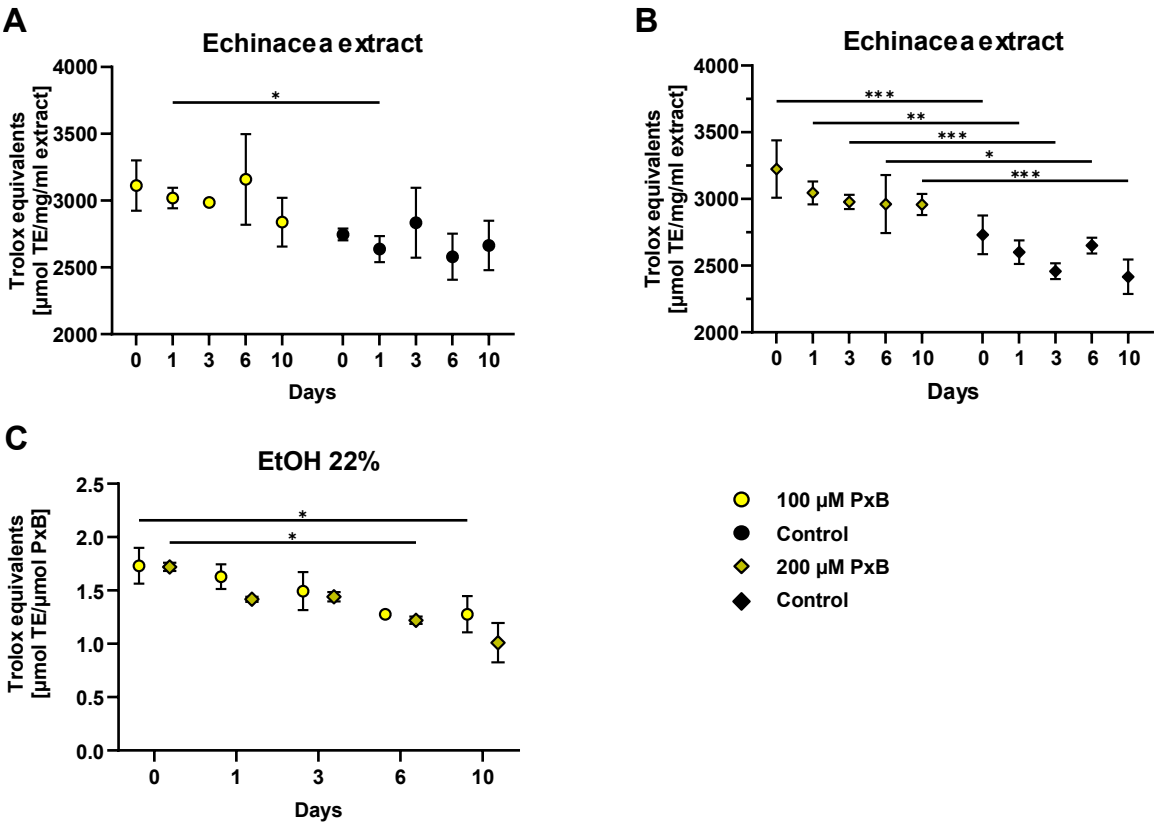

Figure 9 Time-dependent influence of *Ep*-PxB-5 on the anti-oxidative potency of a standardized *Echinacea* extract. Assessed by FRAP assay was the antioxidant ability to reduce iron ions. **(A)** *Echinacea* extract was spiked with 100 µM of *Ep*-PxB-5 and (**B)** with 200 µM. Controls were extracts supplemented with EtOH 22% (*v/v*). **(C)** FRAP values of *Ep*-PxB-5 in solvent EtOH 22% (*v/v*), 100 µM and 200 µM over ten days. Experiments were performed as **(A,B)** biological triplicates and **(C)** duplicates, statistical significance was calculated by 2way ANOVA analysis and Šídák's multiple comparisons test (**P* < 0.05, ***P* < 0.01, ****P* < 0.001)

4.2.2 Characterization of novel phyllobilins of *Humulus lupulus*

4.2.2.1 Dioxophyllobilins of hops influence leaf appearance and composition

Humulus lupulus leaves change their colors during fall in a fascinating color. Chlorophyll breakdown leads to the degreening of leaves[65] and, as it was uncovered in the past decades, a novel substance class is thereby formed, the PBs.[10a] Although hops is widely cultivated in Bavaria mostly for its cones, the raw material for brewing or pharmaceutical purposes, we here investigated the leaves in the context of this work. Thus, two dioxophyllobilins were found in senescent hops leaves with previously unknown structures. In cooperation with Christian Nadegger and Ass. Prof. Dr. Thomas Müller (University of Innsbruck) we were able to isolate the PBs. The isolation of light- and air sensitive compounds is challenging, and surprisingly, was even more so in the case of hops PBs compared to other PB isolations, already hinting at previously unknown structural features to be present. HPLC retention times and characteristic UV spectra are portrayed in **Supplementary Figure 8**. Structure elucidation was conducted by the group in Innsbruck, revealing the structures presented in **Figure 10**. In the following, PBs were labeled by the botanical source (prefix) and subclass characteristics, i.e. *Hl*-PBs for the compounds from *Humulus lupulus*.

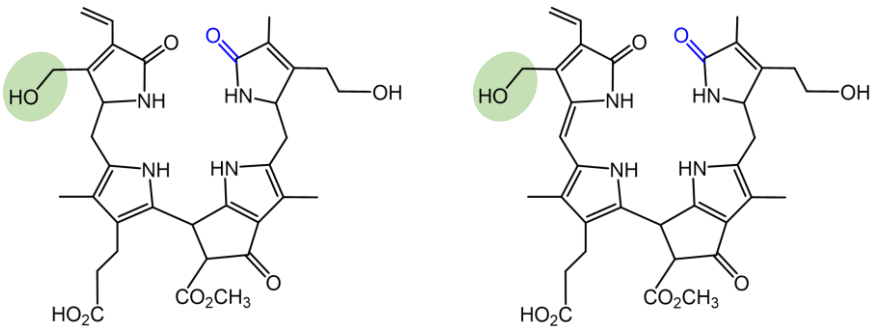

Figure 10 *Hl*-PBs of senescent hop leaves. Novel modifications are highlighted in green.

As assessed by HPLC analysis, relative abundance of *Hl*-PxB was highest in yellow hop leaves (**Figure 11**). *Hl*-DPxB shared a remarkable contribution of 40% to all peak areas at 420 nm. It was 11% for brown leaves and 4% for green leaves. PB content was rising in maturing leaves, strongly influencing the composition of hop leaves. PB formation is indicated by relative peak area attribution of PBs at 420 nm responsible for yellow coloration.

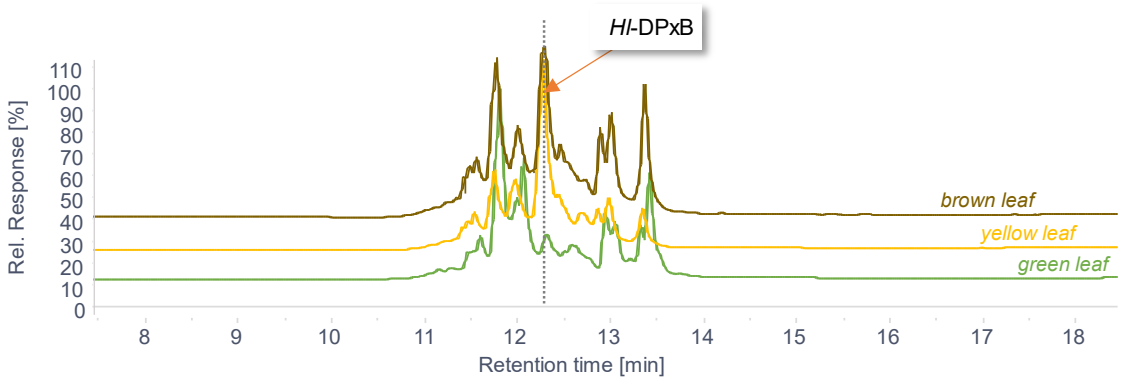

Figure 11 Analytical HPL chromatograms of *Humulus lupulus* leaves of different colors. Leaves were ground and extracted with MeOH. Peaks of DPxB were highest for yellow leaves (36,7%) followed by brownish leaves (15,1%) and green (3,31%). (420 nm, HPLC method Nr. 1)

4.2.2.2 Anti-oxidative testing of *Hl*-DPxB and *Hl*-DPleB

To extend the still limited knowledge about this branching class of Type-II PBs (**Figure 4**), the hops PBs were investigated for their antioxidant activity *in-vitro* and *in-cellulo.* Firstly, an *in-vitro* FRAP assay was performed, providing first insights on the anti-oxidative properties of the tested molecules. Whereas *Hl*-DPleB was significantly less potent in iron reducing ability as compared to the water-soluble vitamin-E derivative Trolox, a potent antioxidant and reference molecule, *Hl*-DPxB proved to have comparable effects (**Figure 12 A**). Further, we tested the PBs in a cell-based ROS scavenging assay using the cervical cancer cell line HeLa. During the experiment, intracellular ROS species are formed by stressing of the cells with H_2O_2, which can be then quantified by fluorescence detection by the radical induced conversion of H_2DCF to DCF.[38] The purity of the isolated *Hl*-DPxB sample used for cellular experiments was confirmed by HPLC (**Supplementary Figure 9**). For intracellular ROS assay, the substances were diluted in DMEM medium for subsequent cell treatment. *Hl*-DPxB and *Hl*-DPleB significantly scavenged ROS in a comparable manner as the controls Trolox and quercetin (QUE), which is a prominent antioxidant of *Humulus lupulus*[54a] (**Figure 12 B**). Notably, no influence on cell viability could be observed for Trolox, *Hl*-DPxB and *Hl*-DPleB. QUE showed a moderate reduction of cell viability (**Figure 12 C**).

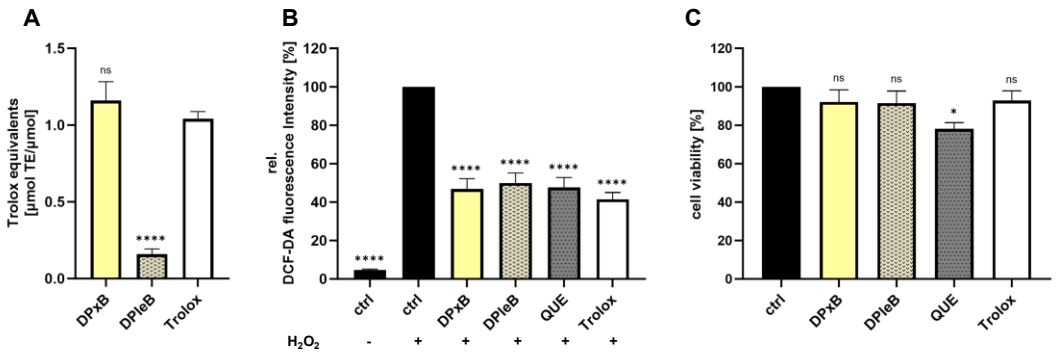

Figure 12 *Hl*-DPxB is a potent antioxidant *in-vitro* and *in-cellulo* on HeLa cells. (A) *Hl*-DPxB and *Hl*-DPleB (100 µM) were tested for *in-vitro* anti-oxidative effects via a FRAP assay. **(B)** *Hl*-DPxB and *Hl*-DPleB scavenge ROS in HeLa cells without affecting cell viability **(C)**. Cells were treated with compound (10 µM, Trolox 1 mM) for 24 h, then incubated with dye H_2DCF (30 min) and H_2O_2 (30 min). Generation of ROS was measured as conversion of H_2DCF to the fluorophore DCF, and radical scavenging activity represents the prevention of DCF formation. Trolox and Quercetin (QUE) served as positive controls. **(C)** *Hl*-DPxB, *Hl*-DPleB and Trolox do not affect cell viability at 10 µM or 1 mM for Trolox, respectively. QUE influences cell viability significantly at a concentration of 10 µM. Cell viability was assessed by a crystal violet staining after 24 h stimulation of compounds in the indicated concentrations. **(A)** Values represent mean ± SD of tree, **(B,C)** four independent experiments (ns, not significant, **P* < 0.05, *****P* < 0.0001)

4.2.2.3 Anti-proliferative effects of *Hl*-DPxB and *Hl*-DPleB

Hops cones have evoked attention due to their anti-cancer effects.[54a] To investigate if Type-II *Hl*-PBs also exhibit effects on cancer cells, a proliferation experiment was conducted using the cervix cancer cell line HeLa, with which the anti-oxidative cellular ROS experiment was performed. Clearly, *Hl*-DPleB showed no effects on the proliferation rate of the cells in the tested concentrations from 1 to 50 µM. In the highest tested concentration (50 µM), *Hl*-DPxB slightly diminished HeLa cell proliferation after 72 h (11%) (**Figure 13**). IC_{50} values for the substances could not be calculated.

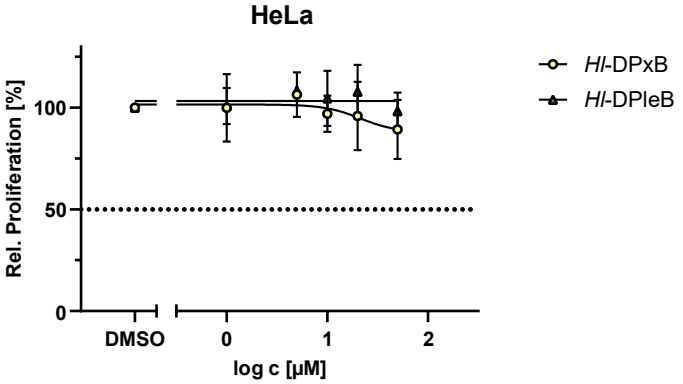

Figure 13 *Hl*-PBs do not influence cell proliferation of HeLa cells in the tested concentrations. For testing the anti-proliferative effects of PBs on HeLa cells, cells were treated for 72 h and then stained with crystal violet. IC_{50} values were calculated by nonlinear regression after normalizing to vehicle control with subtracted day zero value but were not conclusive.

This piece of work on PBs in *Humulus lupulus* is currently in manuscript writing process.

4.2.3 Structural characterization, anti-oxidative-, and anti-inflammatory activities of phylloxanthobilins in *Tropaeolum majus* L., a plant with relevance in phytomedicine

4.2.3.1 Phytochemical fingerprint of PBs in *Tropaeolum majus* and UV/Vis characteristics of *Tm*-PxB-(1-4)

During autumn months, *Tropaeolum majus* (nasturtium) leaves undergo an intense color change from green to yellow. Analytical investigations with HPLC on the fingerprint of aqueous methanolic extracts of *Tropaeolum majus* revealed four different PxBs, which were subsequently identified by their characteristic UV spectrum.[66] The PxBs were numbered according to their decreasing polarity and named *Tm*-PxB-(1-4) according to the botanical source (prefix). An analytical HPLC trace of nasturtium leaf extracts and assignment of the four PxBs is shown in **Figure 14**. Typically, a UV/Vis spectrum of a PxB shows an absorbance maximum at around 426 nm, known to originate from ring A to D possessing an extended π-electron system and carrying a vinyl residue at ring D.[23b] Indeed, this characteristic was seen for *Tm*-PxB-4 with highest retention times, thereby having maxima at 430 nm, 314 nm and 246 nm. On the contrary, *Tm*-PxB-(1-3) showed slightly different spectra with a maxima at 418 nm, besides the maxima at 314 - 316 nm and 242 - 246 nm. This shift to lower wavelengths at 418 nm indicated the presence of a dihydroxy side chain at ring D instead of a vinyl residue, as reported earlier for PxBs in *Egeria densa* and *Echinacea purpurea*. [26, 67] Retention times of the substances as well as UV/Vis data is additionally presented in the chapter **3.2.5** (spectroscopic data of isolated compounds).

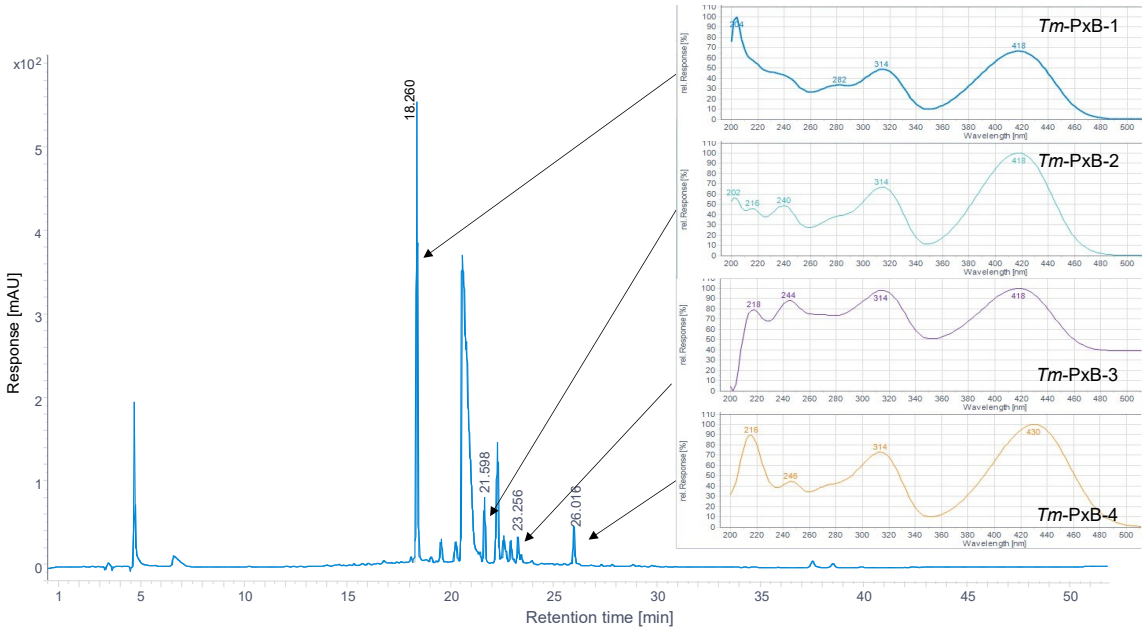

Figure 14 Analytical HPLC trace of an acidified methanolic extract of senescent *Tropaeolum majus* leaves with UV/Vis spectra. (420 nm; HPLC method Nr. 3)

High quantities of *Tm*-PxB-(1-4) were present in yellow leaves of *Tropaeolum majus*. Analyzing methanolic extracts of freshly collected yellow leaves via analytical HPLC, relative peak areas of all PxBs to the sum of all peak areas yielded a total of approximately 25% at 420 nm detection (**Supplementary Figure 10)**.

4.2.3.2 Isolation of *Tm*-PxBs

PBs of *Tropaeolum majus* were isolated as explained in the method section (**3.3.1**). Extraction of 200 g of senescent leaves yielded in 12.3 mg of *Tm*-PxB-1, 0.8 mg of *Tm*-PxB-2, 1.1 mg of *Tm*-PxB-3, and 2.3 mg of *Tm*-PxB-4 as quantified by UV/Vis spectroscopy (*Tm*-PxB-1 1.86 µmol, *Tm*-PxB-2 0.12 µmol, *Tm*-PxB-3 0.20 µM, *Tm*-PxB-4 0.36 µmol). For *Tm*-PxB-2 and *Tm*-PxB-3 less pure yields were obtained since other substances eluted at the same reaction time and thus the fractions obtained by semi-HPLC often remained contaminated.

4.2.3.3 Structure elucidation of PxBs and selected PleBs

For structure elucidation, also HR ESI-MS, MS^2 as well as NMR (*Tm*-PxB-(1,2,4)) were recorded and analyzed in addition to UV/Vis spectra. Molecular formulae were $C_{34}H_{38}N_4O_{10}$ for *Tm*-PxB-1, $C_{33}H_{38}N_4O_8$ for *Tm*-PxB-2, $C_{34}H_{39}N_4O_9$ for *Tm*-PxB-3, and $C_{34}H_{36}N_4O_8$ for *Tm*-PxB-4, as assessed by the $[M-H]^-$ as well as $[M+H]^+$ molecular ions of HR ESI-MS spectra (**Supplementary Figure 11-Supplementary Figure 14**). The

analyzed compounds have not been described previously, as evident by comparison with databases.[68] Next, we investigated the molecular side chain modification of the PBs by characteristic fragmentation reactions according to Müller et al.[69] during MS^2 fragmentations. In the positive ion-mode, characteristic fragmentations like loss of H_2O and CO_2 were seen for all four PxBs. Moreover, cleavages at the saturated meso positions between ring A and B as well as ring B and C were evident (**Supplementary Figure 15;Supplementary Figure 18**). We found that *Tm*-PxB-1 might be the corresponding oxidation product of a published PleB, namely *So*-PleB-1 (*So*-NCC-1) and *Mc*-PleB-26 (*Mc*-NCC-26), found in spinach (*Spinacia oleracea*) and ripening peels of banana (*Musa acuminata*).[10a, 70] To confirm this, methanolic spinach extracts were prepared and analyzed by analytical HPLC. Indeed, identical retention times were found for *So*-PleB-1 isolated from spinach and a PleB in the nasturtium extract. We therefore concluded that also the reduced form of *Tm*-PxB-1, identical to *So*-PleB-1 is an ingredient in nasturtium leaf extracts (**Supplementary Figure 19**). As UV/Vis and MS^2 already provided detailed insights on the molecular structures, ^{1}H-NMR spectra, as well as homo- and heteronuclear 2-D spectra (COSY, ^{1}H,^{13}C-HMQC, ^{1}H,^{13}C-HMBC) were recorded for *Tm*-PxB-1, *Tm*-PxB-2 and *Tm*-PxB-4 to further confirm the proposed structures. NMR data was evaluated in collaboration with Christian Nadegger (University of Innsbruck) and atom numbering is shown precisely in **Supplementary Figure 20** and follows the common specifications for PBs.[7] PBs have characteristic signals, e.g. four signals at 2 ppm reasoning from the methyl groups at C2, C7, C13 and C17.[23b] Another signal at 9.5 ppm typically indicates a formyl group[8a], as seen for *Tm*-PxB-1 and *Tm*-PxB-4 (**Supplementary Figure 21;Supplementary Figure 23**). Furthermore, the core structure of PxBs possesses a double bond between C15 and C16 indicated by signals at 5.96 ppm (*Tm*-PxB-1) and 6.04 ppm (*Tm*-PxB-4). Based on previous mass spectrometry and UV/Vis data, we assumed that *Tm*-PxB-1 and *Tm*-PxB-4 differ in their side chain residue at R_3 (**Figure 15**). Comparing the mid-field ^{1}H-NMR region of *Tm*-PxB-1 and *Tm*-PxB-4, differences were seen at 5.26/6.32 and 6.50 ppm (*Tm*-PxB-4), signaling from a vinyl group. Instead, *Tm*-PxB-1 showed signals shifted to high field regions, being characteristic for the dihydroxy side chain of *Tm*-PxB-1 (**Supplementary Figure 21;Supplementary Figure 23**). For *Tm*-PxB-2, only ^{1}H-NMR was evaluated due to the low quality of the homo- and heteronuclear 2-D spectra (**Supplementary Figure 22**). Nevertheless, the typical signal pattern of the PxBs could be clearly detected. Namely, the four methyl groups were seen in singlets at 2.16, 1.98, 2.06 and 2.15 ppm, as well as the dihydroxy side chain of C18 (R_3) at 4.47 ppm and 3.46/3.68 ppm, respectively. Additionally, the pyrrole nitrogen bound protons at

around 10 ppm were clearly pronounced. A signal at 5.98 ppm supported further the presence of a PxB as this signal can be attributed to the proton at C15, resulting from the double bond there. By proving the core structure of a PxB, knowing the residue at R_3 and the elemental composition by HR-ESI MS (**Supplementary Figure 12**) in combination with MS^2 fragmentations (**Supplementary Figure 16**) and UV/Vis spectra (**Figure 14**), we concluded that *Tm*-PxB-2 lacks a carbon residue at R_2. PBs possessing this feature are named pyroPhylloxanthobilins (pyPxB) and were as far as to our knowledge only semi-synthesized before and are to date not found to occur naturally, apart from iPBs with rearrange carbon skeleton found in fern.[24, 71] NMR data of *Tm*-PxB-1/-4 is additionally presented in the chapter **3.2.5** (spectroscopic data of isolated compounds) and all ^1H NMR spectra are attached to the Supplementary (**Supplementary Figure 21-Supplementary Figure 23**).

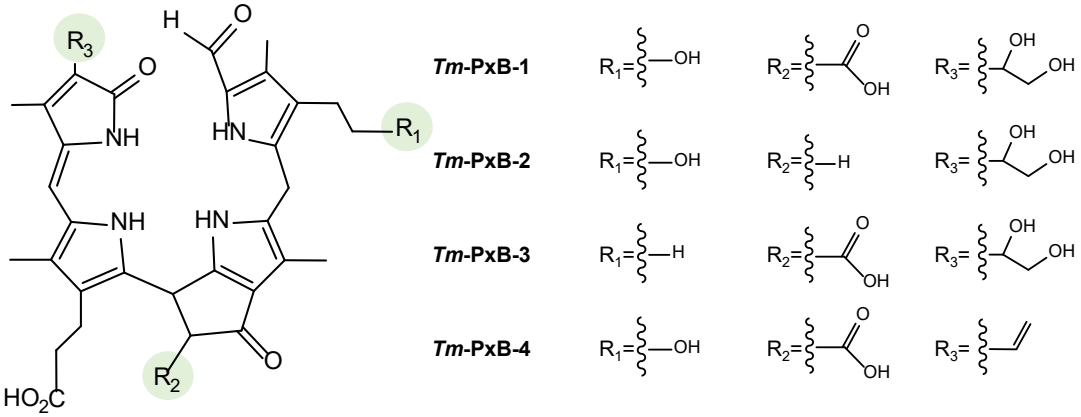

Figure 15 Chemical structure of *Tm*-PxB core and side chain modifications of the identified *Tm*-PxBs

4.2.3.4 *Tm*-PxB-2 is a genuine phytochemical in nasturtium

Having identified the first natural occurring pyPxB, we needed to verify that *Tm*-PxB-2 is indeed a native ingredient of nasturtium leaves and not an artefact of the extraction process derived by decarboxylation of *Tm*-PxB-1. Particularly, *Tm*-PxB-2 could theoretically be formed through decarboxylation of *Tm*-PxB-1, as evident by known MS fragmentation reactions.[69] Consequently, we tested the stability of *Tm*-PxB-1 in solvents that were used during extraction by analytical HPLC, including acidic PBS, and we additionally performed leaf spray MS of freshly harvested yellow nasturtium leaves. *Tm*-PxB-1 showed no reduction in peak area for one hour of incubation at RT in PBS at pH 7 and pH 5.2. Samples that were acidified with AcOH (pH 3.5) were less stable. When incubating them at RT overnight, the peak area of *Tm*-PxB-1 declined in AcOH pH 3.5 by

22%, accompanied by forming 4% of *Tm*-PxB-2, 0.3% of *Tm*-PxB-3, and 1.6% of *Tm*-PxB-4. Following further acidification of *Tm*-PxB-1 in PBS (pH 2.5), samples were analyzed by analytical HPLC and by LC-MS, to potentially characterize degradation products. After overnight incubation, *Tm*-PxB-1 showed a diminished peak area of 18% and 4% formation of signals for *Tm*-PxB-2, 1.3% of *Tm*-PxB-3 and 0.7% of *Tm*-PxB-4. Summarizing, under acidic conditions (pH 2.5; pH 3.5), *Tm*-PxB-1 is slightly degraded to form the other three PxBs, likely by decarboxylation (*Tm*-PxB-2) and dehydrogenation (*Tm*-PxB-(3-4)). Thus, leaf spray MS was performed by our cooperation partner (Christian Nadegger, University of Innsbruck) using freshly harvested, yellow nasturtium leaves to answer the question whether *Tm*-PxB-2 is truly a native ingredient. Leaf spray MS offers the opportunity to analyze leaf compositions without extraction. Therefore, cut outs of leaf samples are held directly in front of the ion source.[72] By applying this method, indeed, all four PxBs were detectable (**Figure 16**). In accordance with analytical HPLC results, *Tm*-PxB-1 showed highest abundance. Relatively to the signal intensity of $[M+Na]^+$ *Tm*-PxB-1, amounts of the identified sodium adducts were 92% for *Tm*-PxB-2, 9% for *Tm*-PxB-3, and 67% for *Tm*-PxB-4. Moreover, additional adducts were observed for *Tm*-PxB-2, which were $[M+Na]^+$, $[M+K]^+$ and $[M+2K]^+$ ions. Taken together, by utilizing leaf spray ionization experiments, we were able to find distinct proof that *Tm*-PxB-2 is a genuine ingredient of senescent plant leaves.

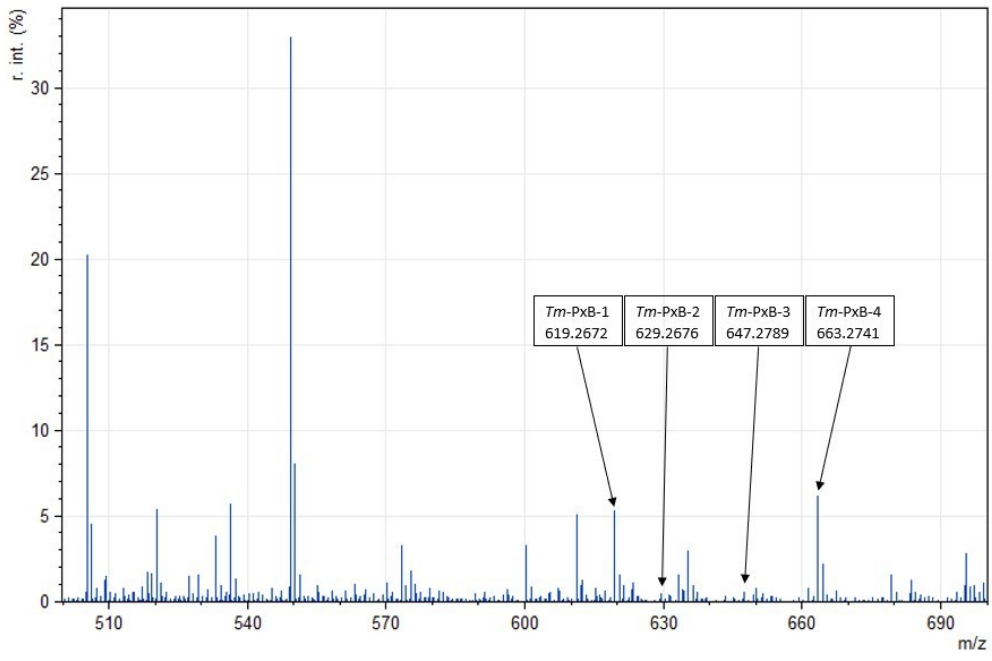

Figure 16 Leaf spray mass spectrum of a freshly harvested senescent leaf of *Tropaeolum majus*. Leaf spray MS was recorded by Christian Nadegger (University of Innsbruck).

4.2.3.5 Anti-oxidative properties of isolated *Tm*-PxBs

Following up the work on structural characterization, potential bioactivities were assessed as a next step. Here, we focused on anti-oxidative and anti-inflammatory properties, based on the fact, that *Tropaeolum majus* is commonly used as “over the counter” drug against symptoms of the common cold and urinary tract infections.[59] *In-vitro*, *Tm*-PxB-1 and *Tm*-PxB-3 significantly exhibited stronger anti-oxidative strength relative to Trolox in a FRAP assay (**Figure 17 A**). Effects of *Tm*-PxB-1 were thereby twice as high as Trolox and *Tm*-PxB-3 even showed tree times stronger anti-oxidative potency than the standard Trolox. No significant difference to Trolox was seen for *Tm*-PxB-2 and *Tm*-PxB-4. As Trolox itself is already a strong antioxidant, even comparable effects, are characterizing the compounds as potential antioxidants. The flavonoid isoquercitrin (IQ) and the phenolic acid chlorogenic acid (CGA) were tested as well as they are both bioactive components of the plant’s leaves.[57-58, 61] Similar effects were observed for IQ and CGA as for the tested PxBs, whereby IQ and CGA significantly exhibited higher values than Trolox. Trolox equivalents for IQ and CGA were in accordance with published literature (**Figure 17 A**).[73] Going further, to assess the anti-oxidative potential on a cellular basis, we therefore conducted intracellular ROS experiments on HeLa cells (**Figure 17 B**). Antioxidants reduce intracellular ROS production by functioning as radical scavengers.[49] The formation of ROS can be monitored by the intracellular conversion of a dye to a fluorophore after stressing the cells with H_2O_2 by fluorometric detection. *Tm*-PxB-1 and *Tm*-PxB-4 exhibited a significant reduction of ROS production to 36% and 39% relative to H_2O_2 treated cells, respectively. Comparable effects were seen for CGA with a significant reduction in ROS formation by 37% (**Figure 17 B**). Cell viability after the treatment was subsequently assessed by crystal violet staining to exclude influences of a diminished cell viability on ROS production. No significant impact was detected (**Figure 17 C**).

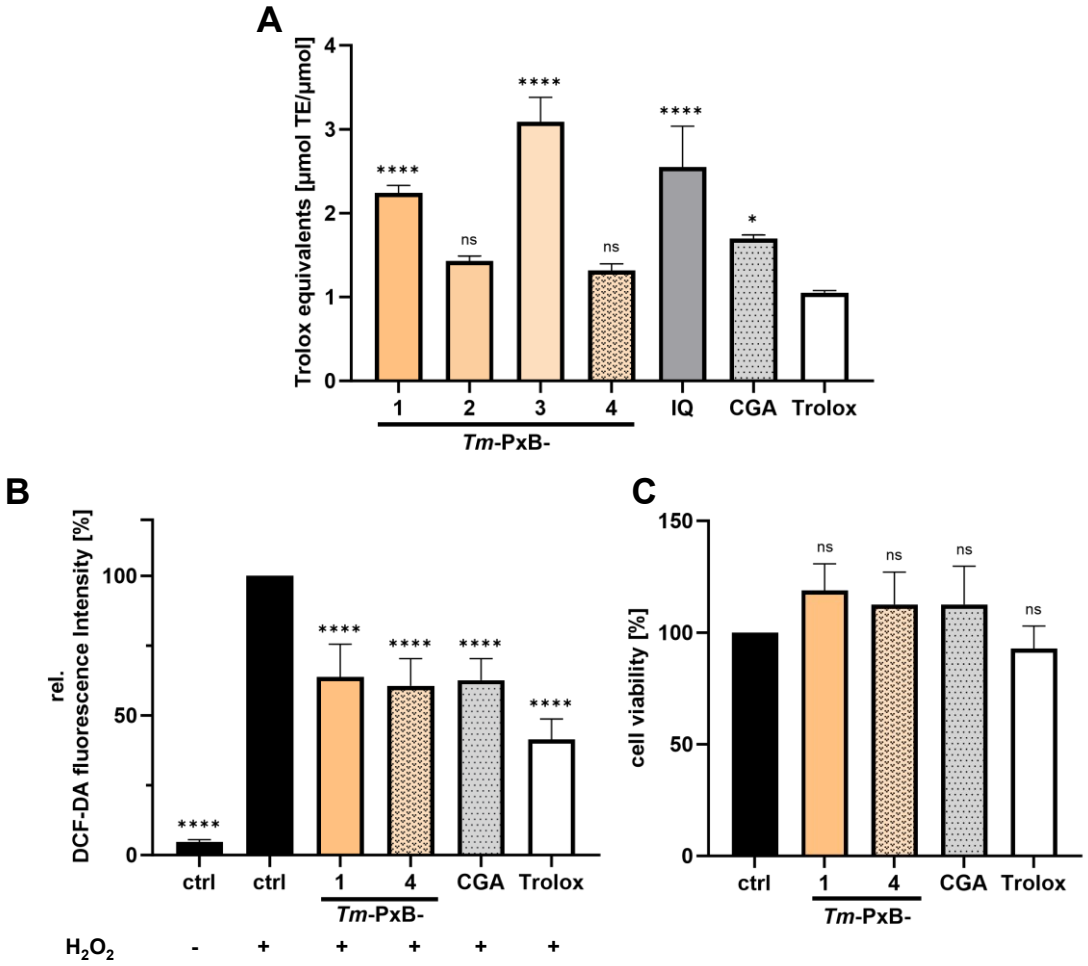

Figure 17 *Tm*-PxBs possess strong anti-oxidative potential *in-vitro* and *in-cellulo*, as determined in a (A) FRAP and (B) in an intracellular ROS assay. (A) *In-vitro* anti-oxidative potency was expressed as Trolox equivalents (µmol TE/µmol), *Tm*-PxB-1 and *Tm*-PxB-3 showed 2 and 3-fold higher anti-oxidative power, respectively, and *Tm*-PxB-2 and *Tm*-PxB-4 were comparable to Trolox. CGA and IQ, known ingredients of *Tropaeolum*, exhibited significantly stronger activity than Trolox. **(B)** PxBs of *Tropaeolum majus* scavenge ROS in Hela cells **(C)** without influencing cell viability. **(B)** Cells were stimulated with compound (10 µM, Trolox 1 mM) for 24 h, then treated with dye (30 min) and H_2O_2 (30 min). Radical scavenging activity was measured as the ability to prevent the conversion of the dye H_2DCF to the fluorophore DCF. **(C)** *Tm*-PxB-1, *Tm*-PxB-2, Trolox, and CGA did not affect cell viability at 10 µM (1 mM for Trolox). Cell viability was tested after 24 h by a crystal violet staining after stimulation of compounds under the same conditions. **(A)** Values represent mean ± SD of three, **(B,C)** of four independent experiments (ctrl, control, ns, not significant, **P* < 0.05, *****P* < 0.0001)

4.2.3.6 Anti-inflammatory potential of *Tm*-PxB-1 and *Tm*-PxB-4 on COX-1 and -2

Indications of *Tropaeolum majus* preparations are urinary tract infections, among others. Investigations revealed that mainly anti-bacterial properties of isothiocyanates are responsible for the therapeutic effects. Enriched extract combinations of nasturtium herb and horseradish roots favor those ingredients, commonly used for the treatment of mild diseases.[74] Further, it has been reported that *Tropaeolum majus L*. herb inhibits COX-1 enzyme activity.[61] Detailed investigations on the herb extract constitution and its relation

to COX-1 inhibition are still missing. But first evidence accumulated that IQ, a major and active component of nasturtium leaves[58a, 75], inhibits COX-2 enzyme activity, especially.[76] The downregulation of COX-1 activity by IQ was only reported for high concentrations so far by reaching IC_{50} values above 100 µM.[77] The enzymes COX-1 and especially COX-2 are of major importance during inflammatory cascades, making them suitable targets in cystitis, notably.[78] Investigating influence of nasturtium substances on those enzymes can help to understand the effects of nasturtium constituents in this established indication. *Tm*-PxB-1 and *Tm*-PxB-4 were tested as most and less polar candidate found in the leaves, respectively. Indeed, experiments on influences of *Tm*-PxB-1 and *Tm*-PxB-4 on COX-1 and COX-2 revealed inhibitory effects in low micromolar concentrations in a similar manner to IQ (**Figure 18**). Both, *Tm*-PxB-1 and *Tm*-PxB-4, showed similar potential to inhibit COX-2 with an IC_{50} of around 1 µM. IC_{50} of IQ (IC_{50} 0.95 µM) and *Tm*-PxBs on COX-2 activity inhibition were comparable, whereas CGA was less potent (IC_{50} 30.0 µM) (**Figure 18 B**). Differences were observed on COX-1 inhibition. *Tm*-PxB-4 showed stronger effects with an IC_{50} of 8 µM, whereas *Tm*-PxB-1 was much less potent with an IC_{50} of 57 µM. IC_{50} values of CGA and IQ for COX-1 inhibition could not be calculated for the tested concentration range (**Figure 18 A**). Summarizing the data on COX-1 inhibition, only one candidate, *Tm*-PxB-4 exhibited pronounced effects.

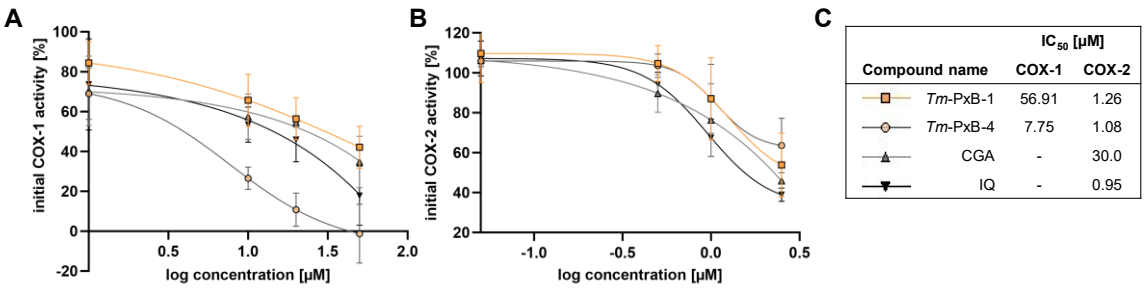

Figure 18 *In-vitro* dose-dependent inhibition of (A) COX-1 and (B) COX-2 activity by *Tm*-PxB-1, *Tm*-PxB-4, CGA, and IQ. For IC_{50} determination, data of three independent experiments are calculated by nonlinear regression of percentages of initial activities after normalizing to the positive control with 100% activity.

This piece of work on PBs in senescent *Tropaeolum majus* leaves is currently in revision (Planta Medica).

4.3 Discussion

The beautiful yellowish to reddish coloration of leaves during autumn is a fascinating phenomenon. For a long time, PBs have been regarded as bare side products of a detoxification process, accumulating upon the programmed degradation of chlorophyll. Hence, researchers have proven different in the last years. Especially yellow chlorophyll catabolites of the type PxB, have demonstrated interesting bioactive properties, establishing their relevance as ingredients of medicinal plants.[26-27]

PBs are potent antioxidants.[26-28, 30] By now, we are aware of this attribute as we routinely test novel candidates of the PB family for their anti-oxidative potential in our laboratory. Most of them at least as potent as the standard Vitamin-E derivative Trolox, especially PxBs and DPxBs (**Figure 4**).[26, 28, 30] Trolox is used as gold standard and reference for testing food, herbs, phytochemicals and plant extracts for their anti-oxidative potential.[36, 79] It is not known whether PBs are present in phytomedicines apart from *Urtica dioica* tea preparations, in which they were found as ingredients, lately.[27] A strategic testing of phyto-preparations for potential PB content has not yet been realized so far. We hypothesized that PBs, as antioxidants, potentially impact properties of phytomedicines and could serve as excipients. In a small setting, we investigated the influence of *Ep*-PxB-5 on the stability of caftaric acid, a major component of a commercially available *Echinacea* extract, by spiking the extract with the substance. Adding different concentrations (100 µM, 200 µM) of *Ep*-PxB-5, however, did not increase or preserve the metabolic stability of caftaric acid at RT. Instead, we observed a decrease of *Ep*-PxB-5 concentration, which was accompanied by the rise of its oxidation product, a PrB. Interestingly, for both concentrations, the decrease in *Ep*-PxB-5 was significantly greater in the *Echinacae* extract than in the control (EtOH 22%). EtOH 22% was the extractant of the commercially available industrial *Echinacea* extract. Summarizing, we could not prove, that *Ep*-PxB-5 enhanced the stability of the *Echinacea* extract. Besides, the experiments showed some disadvantages and limitations: Oxidation processes are usually accompanied by a reduction. The degradation of *Ep*-PxB-5 and the increase of the oxidation product provokes the question of what was reduced in the extract and if *Ep*-PxB-5 potentially influenced the extract by maintaining the content of other ingredients. This question cannot be answered by our experiments, as one disadvantage in the experimental setup was that the selected extract was dominated by one main substance in high quantity. Consequently, the extract had to be diluted for analytical HPLC which

reduced the peak area of minor ingredients and made peak area analysis of other minor substances unevaluable. For future approaches, an extract should be chosen with several constituents of similar quantity for investigating the decline of multiple peaks over the time. Another limitation of the experimental setup is the significance of an experiment at room temperature. Generally, accelerated stress tests are conducted in pharmaceutical technology to investigate the stability of pharmaceuticals. However, preliminary experiments revealed a fast degradation of *Ep*-PxB-5 and were as a matter of that not continued. Although we could not verify *Ep*-PxB-5 to impair the degradation of the extract, we could determine strong effects of *Ep*-PxB-5 on its anti-oxidative potency. Interestingly, when adding *Ep*-PxB-5 to the *echinacea* extract, its anti-oxidative properties are significantly increased when compared to the unmodified extracts over the tested period of 10 days. Thereby, *Ep*-PxB-5 was stable in potency in the controls until timepoint day 6 (200 µM) and day 10 (100 µM), respectively.

In addition, we described novel PB candidates in the two medicinal plants *Humulus lupulus* (hops) and *Tropaeolum majus* (Nasturtium) and conducted first evidence on the bioactivities, anti-oxidative and beyond, of the new structures, as well.

Investigating *Humulus lupulus*, we identified two Type-II PB with a replacement of the characteristic aldehyde function of Type-I PB by an oxo group. Given their high abundance in senescent hops leaves (36.7%), the visible yellowing of the leaves in autumn is likely to be influenced by the increase of PB content. Having been overlooked so far, *Hl*-DPxB, a yellow pigment, occurs in high amounts in yellow hops leaves. In the past yellowing of plants during autumn was attributed to carotenoids and flavonoids content mainly[80], but findings on yellow chlorophyll catabolites proved different.[23b] Our work further emphasizes that PBs are main components of yellowish plants. Likewise, hops leaves also receive little attention as they do not contain the established bioactive content as hop cones. Pharmaceutically, hop cones are known for their anti-oxidative, anti-carcinogenic, anti-microbial, anti-inflammatory, anti-glycemic, sedative, and estrogenic effects. Researchers put the focus on the chalcone xanthohumol as dominating bioactive substance, while being unspecific, and interacting with multiple biological targets.[54] Among the known bioactivities, we focused mainly on the anti-oxidant properties associated with hops. Notably, we could show that *Hl*-DPxB possesses similar effects as the strong antioxidant Trolox in a FRAP assay. *Hl*-DPleB, which only structurally differs in a reduced C^2 bond, showed remarkably lower potency than its counterplayer *Hl*-DPxB.

The FRAP assay followed an established protocol of Benzie and Strain and is commonly used by researchers to measure anti-oxidative activity based on iron reduction.[36] The differences between *Hl*-DPleB and *Hl*-DPxB might be attributed to the differences in their delocalized electron system. Electrons of *Hl*-DPxB can distribute over a bigger part of the molecule via the double bound at C^{15}, which may result in a higher iron reducing ability. Additionally, the significant loss of antioxidant potential by *Hl*-DPleB could be explained by the poor solubility of *Hl*-DPleB in the solvent 75% EtOH during the experiment. Nevertheless, *in-cellulo* experiments using HeLa cells revealed no differences in potency between the two substances. Interestingly, *Hl*-DPleB and *Hl*-DPxB scavenged ROS on cells in a similar manner indicating that possible differences in cellular uptake or intracellular metabolism are of relevance. As the read-out of this experiment is conducted by an intra-cellular conversion of the dye to a fluorochrome, the substances are taken up by the cells. In addition to focusing on the anti-oxidative potential, we also examined the anti-proliferative effect of the substances on HeLa cells. PxBs possess strong anti-cancer effects by inducing apoptosis and decreasing proliferation of cancer cells.[25] Hence, the described effects in literature focused on Type-I PBs by showing promising potential for PxBs. With this work, we investigated Type-II PBs for their effects on cancer cell proliferation. In comparison to the strong anti-proliferative effects of *Cj*-PxB described in literature[25], *Hl*-DPxB, as Type-II PB, did not show strong anti-proliferative effects on HeLa cells in the tested concentrations. We therefore conclude, that the aldehyde function of Type-I PBs correlates with the anti-cancer effects of PBs, whereas the replacement by an oxogroup leads to a loss of potency. Undoubtedly, further investigations must be conducted in the future to understand the strong anti-oxidative differences of the *in-vitro* and *in-cellulo* results between these two interesting compounds *Hl*-DPleB and *Hl*-DPxB. Additionally, we could identify the aldehyde function as molecular moiety determining the anti-proliferative activity of cancer cells by testing hops PBs on cellular proliferation, thereby opening the field for more structure-effect investigations on this exciting class of natural products. Furthermore, considering the immense unused biomass waste, which accounts to 75% of leaves and stems[56] that could be recycled, establishing the leaves as source for other bioactive substances is promising. Generally, harvesting for hop inflorescences is conducted in August, thereby reaching their maximum in second metabolite content.[81] Methods for recycling of the leaves and stems, e.g. as composting mixtures usable in horticultural crops[82] or investigations on drying procedures on the phytochemical profile of hops leaves[83] came up only recently. Besides, hops stems are found to be a promising source for cellulose nanofibers, as they obtain 44% of cellulose.[84]

By discovering these novel structures as powerful antioxidants, we are also opening another opportunity for the utilization of hop leaves after harvest season, while tackling hops biomass wastage.

By investigating another medicinal plant, *Tropaeolum majus*, we identified four PxBs with novel structures in yellowing leaves which contribute up to 25% to the yellow coloration of seasonal leaves during autumn. Among them, by the loss of the carboxyl function, *Tm*-PxB-2 showed a special structural feature at C8^2, which is why we named the substance by the additional prefix pyro, pyro-PxB (pyPxB). To our knowledge, no pyPxB has yet been found to occur naturally. Interestingly, Erhard et al. found PBs with rearranged carbon skeletons at ring A which also lack a carboxyl unit at C8^2. The substances that were found in bracken fern have not been named pyro-derivates. Instead, these exceptional structures were considered iso-phyllobilins (iPB), as they were isolated of a seedless vascular plant of evolutionary old heritage underlying a differing chlorophyll breakdown than angiosperms.[24] Though, pyPxB was partially synthesized by Li et al., firstly. Thereby, a pyPleB and after further oxidation a pyPxB was formed by exposing *Cj*-PleB to harsh conditions in several steps.[71] During the biosynthesis of PBs, the decarboxylation at C8^2 by 13^2-carboxy-pyro-pheophorbidase a[85] and corresponding molecules (RCC) to pyPheo a and pyRCC,[86] respectively, relatively quickly, driven by the stabilization of the decarboxylated products. Contrarily, the spontaneous loss of CO_2 by 8^2-carboxy-PleBs is described in literature to proceed notably slowly.[70a, 71, 87] Other pyro-representatives that share a Chl-derived linear tetrapyrrole structure are the bioluminescent emitter in Krill (*Euphausia pacifica*)[88] and luciferin of dinoflagellates.[89] However, by utilizing leaf spray MS, we could proof that all four identified PxBs occur genuinely in the plant, which supports the assumption that *Tm*-PxB-2 is the first described naturally occurring pyPxB. Inevitably, more research must be undertaken to understand the mechanisms in the plant to produce those rare candidates. By investigating the anti-oxidative bioactive potential of those compounds *in-vitro*, it becomes evident that pyPxB is comparable to Trolox. By now, the anti-oxidative testing of PBs established as tool to initially classify potency of novel PBs. Hereby, no extraordinary outstanding in potency of *Tm*-PxBs is seen compared to data of Karg et al. on PxBs from *Echinacea purpurea*[26], *Urtica dioica*[27] or *Brassica oleracea* var. *sabauda* (Savoy cabbage)[28]. Nevertheless, *Tm*-PxBs are strong antioxidants, similar to the standard Trolox. *Tropaeolum majus* is used in traditional medicine as phytomedicine to treat mild symptoms of the common cold and urinary tract infections.[59] The strong anti-oxidative power of *Tm*-PxBs may contribute to the plant's

activity here.[61] Furthermore, we could unravel further inhibitors of COX-1 and COX-2 in low micromolar range. Thereby, COX-2 inhibition was likely more pronounced than COX-1 inhibition. Moreover, strong COX-2 inhibition was seen for IQ, which is an active flavonoid and known for a pronounced COX-2 inhibition, mainly.[76] Contrary, IQ does only possess inhibitory effects on COX-1 in high concentrations with IC_{50} values above 100 µM[77], which is in alignment with our findings. During inflammation COX-2 expression is highly induced and is therefore a common target to treat excessive inflammation and pain, as well.[90] *Ud*-PxB demonstrated similar potential in inhibiting COX-1 and COX-2.[27] Again, no distinct superiority of the isolated PxB of *Tropaeolum majus* was detected. Taken together, these results indicate that small structural changes in the molecular structure do not strongly influence the biological potency among PxBs. Nevertheless, compared to commercially available and established COX-2 inhibitors, such as celecoxib (IC_{50} 0.96 µM)[91], the strong potential of PxBs (IC_{50} *Tm*-PxB-(1/-4) 1.26/1.08) becomes evident. Importantly, inhibition of COX-2 is believed to prevent chronic and recurrent cystitis.[92] Of note, C-phycocyanin, a biliprotein isolated from *Spirulina platensis*, inhibited bladder inflammation through inhibition of COX-2 and prostaglandin E receptor 4 expression and thereby relieved symptoms of cystitis in mice.[93] to sum it up, our results emphasize that *Tm*-PxBs contribute to the anti-inflammatory properties of this medicinal plant by expanding the so far investigated pharmacologically active phytochemical constitution.

PART II

5. Part II: Comparison of the anti-atherosclerotic potential of phyllobilins and bilirubin on early stages of atherosclerosis

5.1 Introduction

The heme degradation substance Bilirubin (BR) is known to influence diseases related to oxidative stress. The endogenous and continuously produced BR is slightly elevated in serum of patients with Morbus Meulengracht, also known as Gilbert syndrome. The mild hyperbilirubinemia of those patients correlated in several observational studies to a decrease of developing oxidative-stress mediated diseases as hypertension, type-2-diabetes mellitus, metabolic syndrome, obesity, cardiovascular disease, and cancer development.[94] Further studies indicated a relationship between high serum BR levels and the prevention of atherosclerotic plaque formation.[95] In contrast, low levels are connected to an increased risk of serious deep white matter lesions (DWMLs) which raise the risk of impaired cognitive function and stroke.[96] By acting as an agonist on PPARα, BR inhibits lipid accumulation, assigning it a key role in adiposity related diseases and diabetes.[97] Taken together, there is strong evidence for the anti-oxidative effect of BR on mainly age-related diseases. Several factors, however, including BR's low solubility and bioavailability, and its toxicity, limit its therapeutic use.[98] By being water soluble and with a potentially better bioavailability, which needs to be determined, PBs, BR's plant counterparts, might overcome these limitations (**Figure 19**).

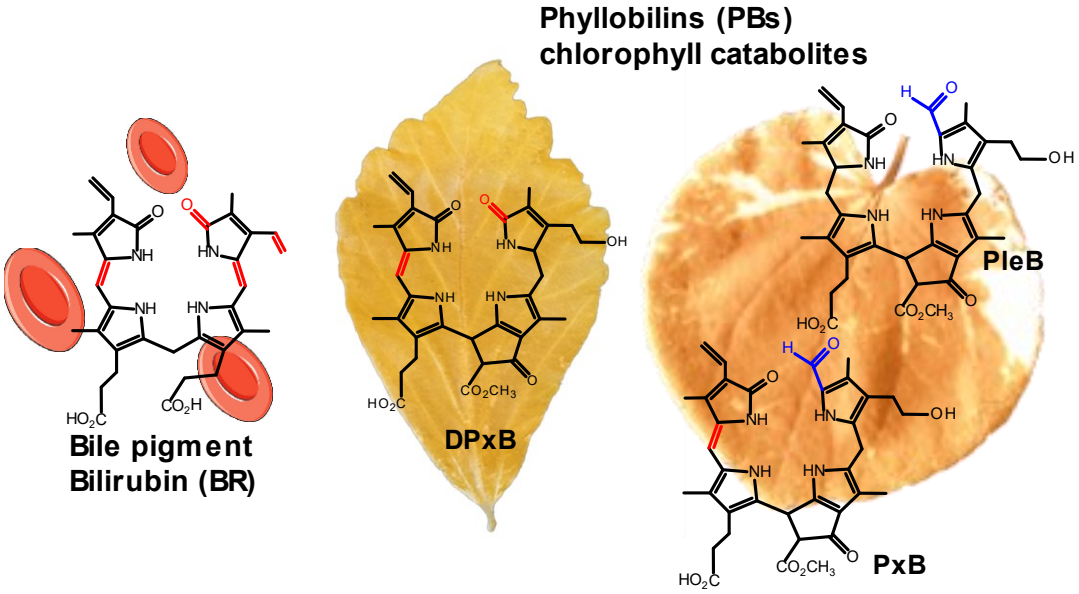

Figure 19 Molecular structures of Bilirubin (Br) and phyllobilin (PB) candidates DPxB, PleB and PxB.

Atherosclerosis is a wide-spread disease that is associated with risk factors such as high blood pressure, obesity, and smoking, among others. Progressive lesion formation in the arteries and consequent narrowing of the lumen condition coronary artery disease (CAD) and cerebrovascular diseases.[99] To date, CAD encounters for one third of deaths with 17.8 million deaths worldwide per year.[100] Eventually, acute coronary syndrome (ACS), myocardial infarction or stroke appear as result of plaque rupture or thrombosis.[99] Systematically, atherosclerosis progression can be divided into characteristic steps and six stages of lesion formation. The so-called early lesions, stage I and II, encompass the development of small to bigger lipid deposits in the intimal layer and the formation of macrophage derived foam cells in the arterial wall, which is favored by oxidated LDL (oxLDL). Late or advanced lesions of stage III, manifest in the massive recruitment of lipids, foam cells and immune cells. Moreover, intima, media and adventitia thicken, and the artery wall shows signs of deformation, which is finally extensively aggravated in the lesion dependent subtype stages IV- VI.[101] Overall, chronic inflammation and endothelial dysfunction are driver of atherosclerosis progression.[102]

Endothelial dysfunction resembles an imbalance of redox status and manifests in enhanced lipoprotein oxidation and permeability, increased leucocyte accumulation as well as adhesion, changes in extracellular matrix metabolism, thereby contributing to a dysregulated hemostatic-thrombotic state. Further nitric oxide metabolism and vascular reactivity are affected.[103] Redox imbalance is manifested by an overproduction of reactive oxygen species (ROS) or reactive nitrogen species (RNS) or an impaired degradation or malfunctional antioxidant defense mechanisms of the cell, thereby causing an excess presence of ROS.[104] ROS candidates are the molecules H_2O_2, superoxide anion ($O_2^{-\bullet}$), and hydroxy free radical (•OH) which participate in numerous redox signaling pathways interacting as signaling molecules and affect other signaling molecules.[105] Under normal conditions, low amounts of ROS are continuously produced either as by-products of mitochondrial cell metabolisms or as product of reactions of enzymes as the heme oxygenase 1, xanthine oxidase, and enzymes of the NADPH oxidase (NOX) family.[106] Moreover, also exogenous factors like radiation are sources of ROS.[107]

The NOX family consists of seven isoforms including NOX1, NOX2, NOX3, NOX4, NOX5 and, the dual oxidases Duox1 and Duox2. In phagocytic leukocytes, NOX2 was the first discovered oxidase. By activation and production of ROS, NOX2 supports the anti-microbial activity of phagocytes and the destruction of phagocytosed organisms. Hence,

NOX2 got titled phagocyte NOX or gp91*phox* by contributing to host defense mechanisms, as it was also found for the Duox oxidases.[108] After the discovery of the other non-phagocytic NOX isoforms also in other cells, knowledge about the contribution of the enzymes to signaling pathways and cardiovascular[109], neurodegenerative[110], cancer[111] and metabolic diseases[112] and other pathophysiological functions accumulated.[107, 109a] As members of the NOX family differ in the assembly of subunits, activation and tissue localization, the NOX family was characterized in subgroups.[113] The structure of the various NOX proteins is complex. Predominantly of cardiovascular relevance are NOX2 and NOX4 with high abundancy of NOX4 in endothelial cells, in particular.[114] All NOX share the membrane bound gp91-*phox* subunit, which was due to the discovery of the first NOX2, also long-time known as NOX2 subunit and β subunit. gp91-*phox* together with membrane bound p22-*phox* (α subunit) forms the flavocytochrome b558. Further subunits are p40-*phox*, p47-*phox* and p67-*phox*. Under basal conditions they are located as complex in the cytosol.[113] Activation of NOX2 appears upon phosphorylation of p47-*phox* and subsequent translocation of the subunit complex to the membrane, thereby binding to the flavocytochrome b558. Known p47-*phox* dependent activators are TNF-α and protein kinase C (PKC)-activating phorbol esters.[115] Moreover, Angiotensin II can activate NADPH oxidases.[116] After initial activation, a signaling cascade with EGF receptor transactivation, PI3-K and subsequent Rac activation, lead to a prolonged activation and ROS generation.[115, 117] Whereas NOX2 activity is strongly influenced by the subunit complex, NOX4 activity depends only on p22-*phox*, not on the cytosolic subunits or Rac, and therefore is considered as constitutively active.[118] Uniformly, for all NOX members, essential for the superoxide production is the central catalytic (gp91-*phox*) core consisting of six transmembrane domains, four heme-binding histidine, responsible for trans-membrane electron transport, and two NADPH and FAD binding cytoplasmic C-terminal sides. Eventually, by the transmembrane transport of single electrons by the NOX enzymes, oxygen is reduced to superoxide via NADPH, FAD and heme.[119] NOX4 was discussed to produce rather H_2O_2 than superoxide anions.[118] However, NOX4 is located intracellular so that release of superoxide anions into the lumen would rapidly convert into H_2O_2, which can reach the extracellular space by diffusing membranes.[119]

Characteristically, adhesive proteins are involved in early stages of atherosclerosis. Generally, four families of adhesive proteins exist: cadherins, integrins, selectins and immunoglobulin-like adhesion molecules. During the infiltration of immune cells during atherosclerosis, the vascular-cell adhesion molecule 1 (VCAM-1) and intercellular

adhesion molecule-1 (ICAM-1) are important players. Both proteins are up-regulated in endothelial cells at early sites of lesion formation.[120] Factors as blood flow, cholesterol and oxidized LDL, inflammatory cytokines as TNF-α or IL-1β activate endothelial cells.[121] Generally, the production of inflammatory cytokines, not only by immune cells but also by endothelial cells and later by foam cells[122] and vascular smooth muscle cells (VSMC)[123], drives the progression of lesion formation.[102] Activated endothelium stimulates the expression of adhesion molecules and induces multiple steps of recruitment of circulating monocytes by rolling, adhesion and subsequent endothelial transmigration into the intima. By interaction of selectins with glycoprotein ligands, weak binding of immune cells with endothelial cells is favored and adhesion processes are initiated.[124] Together with P- and E-selectin, VCAM-1 mediates the first stage of tethering and rolling of monocytes and lymphocytes as well as the second stage arrest and firm adhesion. ICAM-1 is involved in arrest and firm adhesion of monocytes, lymphocytes, and neutrophils (**Figure 20**).[125] After transmigration into the intima, monocytes differentiate to macrophages. By ingesting oxidized LDL (oxLDL), they derive to foam cells and contribute to VSMC migration and proliferation and eventually fibrous lesions formation (**Figure 20**).[121]

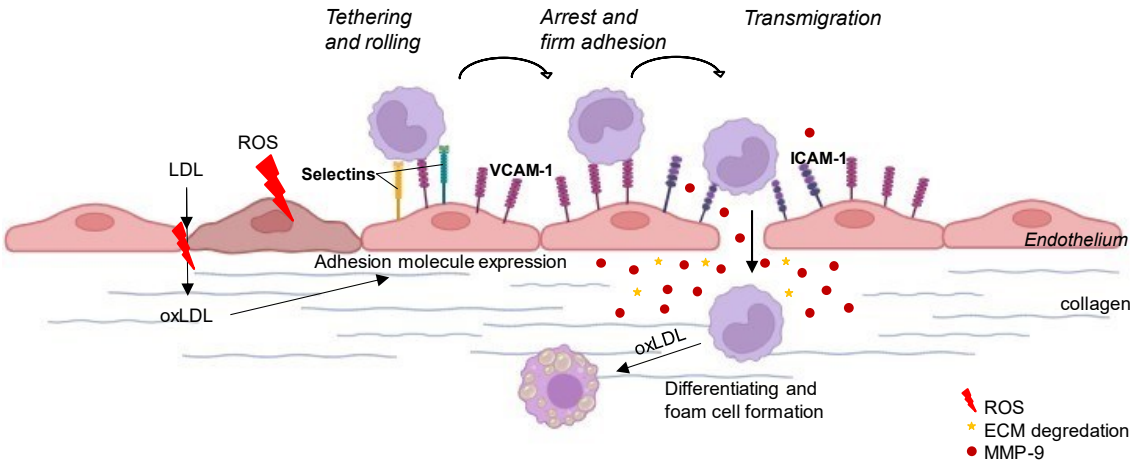

Figure 20 Process of monocyte transmigration across endothelium involves adhesion protein expression and MMP-9 activation. The figure was adapted from George et al.[126].

Matrix metalloproteinases (MMPs) are zinc-dependent endopeptidases with tissue remodeling functions. The proteolytic enzymes can be classified in five groups, depending on the substance that they degrade: collagenases, gelatinases, stromelysins, matrilysins and membrane types. Collagen cleaving MMPs are MMP-1, -2, -8, -9, -14.[127] Of cardiovascular relevance is MMP-9, also named type IV collagenase or gelatinase B, by degrading extracellular matrix (ECM), collagen IV and V, gelatin, fibronectin and elastin,

and non-ECM proteins. MMP-9 is upregulated in pathophysiological inflammatory diseases as atherosclerosis, among others.[128] Moreover, MMP-9 activates proangiogenic factors as vascular endothelial growth factor (VEGF) and fibroblast growth factor-2 (FGF). Cells secreting MMP-9 involve immune cells as neutrophils, macrophages, but also fibroblasts and VSMC.[127b] MMPs are secreted as pro-MMPs and get activated extracellularly by modification of the pro-form with cleavage of the connection of the zinc molecule in the catalytic core and a cysteine switch in the pro-domain. Further, apart from proteolytic enzymes and tissue and plasma proteases, MMPs are activated by pro-MMPs or homogenic by other MMPs.[127a] Hence, evidence accumulated recently indicating that also an intracellular activation might be possible.[129] MMP-9 activity is endogenously inhibited by tissue inhibitors of metalloproteinases (TIMPs), thereby binding to both pro-MMP-9 and MMP-9. IL-1, TNF-α, and platelet-derived growth factor induce MMP-9 activity. ECM remodeling is understood as balance between MMPs and TIMPs.[127b, 130] MMP-9 was found to play a key role in the progression of atherosclerosis, as it is highly upregulated during the growth until the rupture of plaques and is involved in the diapedesis of macrophages.[127b, 131] Apart from MMP-9, also MMP-2 is connected to facilitate monocyte and lymphocyte transmigration (**Figure 20**).[126]

In the following part of the work, we investigated PBs and BR as potential mediators to interfere with atherosclerosis, an oxidative stress triggered disease, in early stages of the progression with focus on their anti-oxidative potential.

5.2 Results

5.2.1 Isolation and characterization of *Pp*-DPxB (*Vv*-DPxB), *Cj*-PxB and *Cj*-PleB

Leaves of *Parrotia persica* tree show a remarkable change in color during autumn. Investigating the yellow leaves by analytical HPLC analysis revealed a PB with the characteristic UV spectrum of a DPxB (**Figure 21; Supplementary Figure 24**).[68]

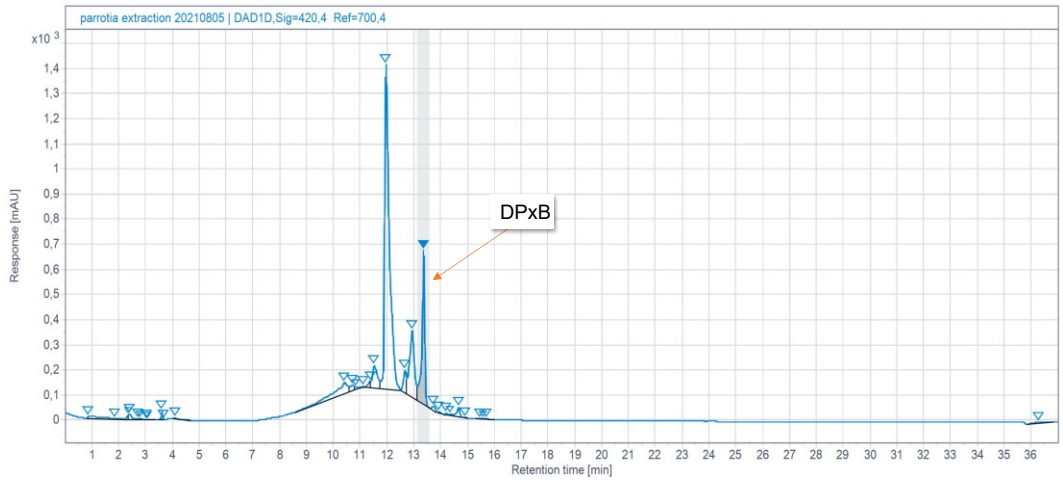

Figure 21 Fingerprint HPL chromatogram of a methanolic extract of a yellow *Parrotia persica* leaf and peak of a DPxB. (420 nm, HPLC method Nr. 2)

Subsequently, the substance was named *Pp*-DPxB according to the botanical source in the prefix. As quantified by UV/Vis spectroscopy, the pure compound *Pp*-DPxB was obtained with a yield of 3.6 mg (5.69 µmol) by extracting a total of 200 g of the leaves. For further characterization, HR ESI-MS spectra (**Supplementary Figure 25**) as well as NMR were recorded (**Supplementary Figure 28**). By the $[M-H]^-$ as well as $[M+H]^+$ molecular ions of HR ESI-MS spectra the chemical formula of $C_{34}H_{38}N_4O_8$ was deduced which is connected to an already published structure found in *Vitis vinifera* namely *Vv*-DPxB.[20, 132] Indeed, NMR proved that *Pp*-DPxB and *Vv*-DPxB are the same substances, thus we established *Parrotia persica* as novel source for this substance. NMR data of *Pp*-DPxB *(Vv*-DPxB*)* is presented in the chapter **3.2.5** (spectroscopic data of isolated compounds) and ^1H NMR spectrum is attached to the Supplementary (**Supplementary Figure 28**).

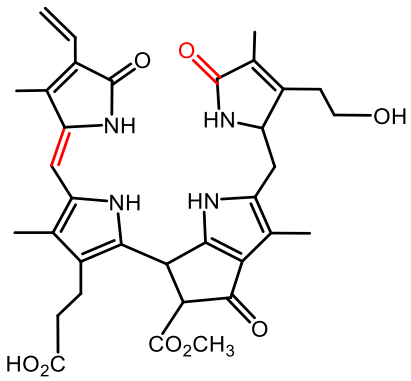

Figure 22 *Pp*-DPxB of senescent *Parrotia persica* leaves is identical to *Vv*-DPxB of fading *Vitis vinifera* leaves.

As the extraction of *Cj*-PleB and partial-synthesis of *Cj*-PxB was previously established by Karg et al[25] in our lab, identity of the substances is portrayed by HR ESI MS spectra in the appendix (**Supplementary Figure 26;Supplementary Figure 27**). Accordingly, *Cj*-PleB was isolated from senescent *Cercidiphyllum japonicum*. After subsequent oxidation on silica gel, *Cj*-PxB was formed. *Cj*-PleB, *Cj*-PxB and *Vv*-DPxB were tested in the following part II of this thesis and structures are presented in **Figure 19**. The naming of the substances was abbreviated by omitting the prefix for clarity.

5.2.2 Effects of PBs on endothelial cell proliferation

Firstly, the PBs were tested for their influence on proliferation of HUVEC cells to subsequently perform cellular experiments in a concentration range in which proliferation is not affected by the compounds. Thereby differences in potency among the candidates were detected. PxB inhibited proliferation in low micromolar concentrations with an IC_{50} value of 8.0 µM. Interestingly, this effect was not seen for its structural counterplayers DPxB and PleB in the tested concentrations (**Figure 23**). As cytotoxic effects are already known for PxB[25], proliferation experiments were crucial to ensure cellular testing under nontoxic concentrations. In the literature, BR is described to exhibit cytotoxic effects in high concentrations with IC_{50} values above 75 µM as accessed with several cell lines.[133] BR concentrations within the normal physiological range are between 3-20 µM for woman and between 5-29 µM for men, respectively.[134] Furthermore, solubility of BR in the cell culture medium of HUVEC cells above 50 µM is challenging. We therefore considered a maximum of 20 µM of BR as nontoxic working concentration within physiological relevance for the previous experiments.

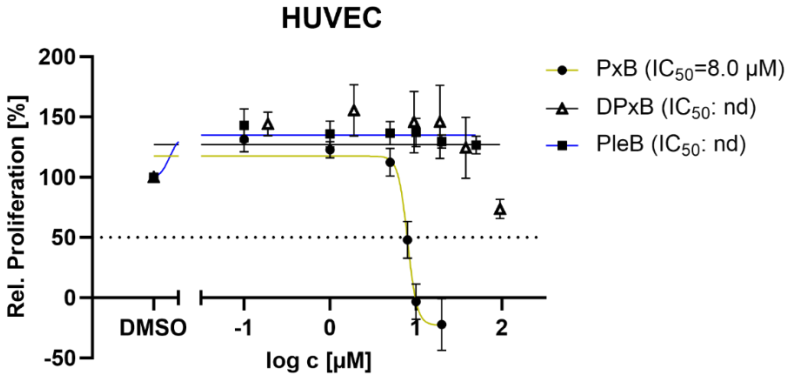

Figure 23 PBs differently influence proliferation of endothelial cells. For testing anti-proliferative effects of PBs on HUVEC, cells were treated for 72 h and then stained with crystal violet. IC_{50} values were calculated by nonlinear regression after normalizing to vehicle control with subtracted day zero value.

5.2.3 Anti-oxidative potential of phyllobilins in the context of atherosclerosis

Next, we investigated the antioxidant properties of PBs and BR *in-vitro* (**Figure 24 A, B**) and *in-cellulo* (**Figure 24 C**) on endothelial cells in nontoxic concentrations. Atherosclerosis is a progressive disease mediated by oxidative stress, influencing not only early steps as driver for endothelial dysfunction, but also lipid oxidation and foam cell formation of macrophages.[135] Measuring the ferric iron reducing power (FRAP), strongest anti-oxidative power, twice as potent as Trolox, was observed for BR (**Figure 24 A**). Similar results were obtained in an experiment based on the ability to scavenge radicals of DPPH, a stable free radical. Although this time no significant difference was detectable compared to Trolox, scavenging activities of BR were at least as high as for the tested PBs (**Figure 24 B**). For both experiments, PleB was the weakest one, indicating that the C15 double bond is crucial for potency. Next, anti-oxidative properties were investigated in the cellular setting. Of note, by utilizing an intracellular ROS assay, PleB significantly scavenged ROS in nanomolar concentrations to 32%. Only BR had stronger potency (44%). Despite that, PxB (22%) and DPxB (16%) showed anti-oxidative effects on endothelial cells, too (**Figure 24 C**). A crystal violet staining ensured that compounds were not cytotoxic under the chosen conditions (**Figure 24 D**).

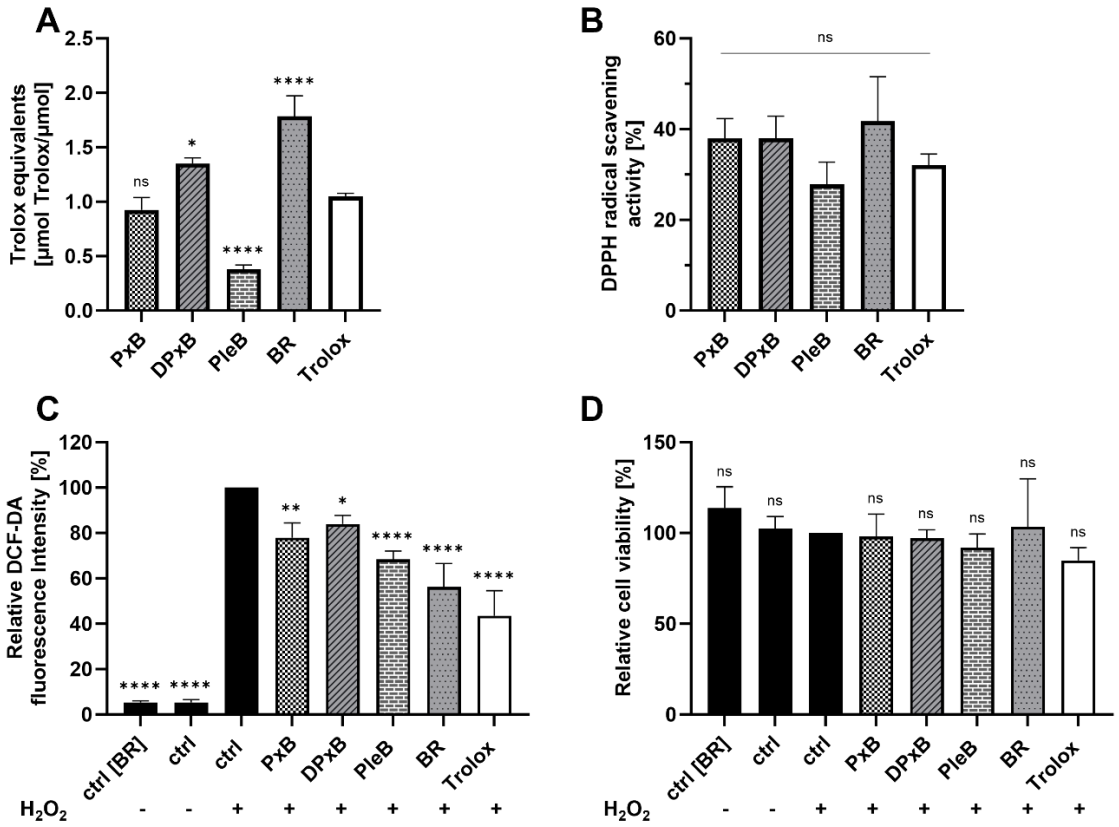

Figure 24 PBs are potent antioxidants *in-vitro* and *in-cellulo* on HUVEC cells. (A) Ferric reducing ability of compounds (100 µM) was tested via FRAP assay. **(B)** *In-vitro* radical scavenging activity was assessed by a DPPH assay, indicating comparable properties to the control Trolox. Thereby 50 µM of compounds were added to the radical DPPH for 30 min of incubation and absorption was measured afterwards. **(C)** PBs scavenge ROS in HUVEC cells as assessed by intracellular ROS assay without affecting cell viability **(D)**. **(C)** Cells were stimulated with compounds (100 nM) and Trolox (100 µM) for 24 h. BR strongly acted as radical scavenger in HUVEC cells. **(B,C)** For solubility reasons, BR was dissolved in NaOH, BR ctrl was NaOH in medium; all other compounds were dissolved in DMSO. **(D)** Cell viability was assessed by crystal violet staining after the ROS assay. Values represent mean ± SD of three independent experiments. (ns, not significant, *$P < 0.05$, **$P < 0.01$, ****$P < 0.0001$)

5.2.4 PBs impact NADPH oxidase activity and protein levels

Recently, Zheng et al. published influences of BR, BV and phycocyanobilin on NADPH oxidase activity of normal human mesangial cells (NHMC).[136] In literature, the oxidases are presented over all as the major dominating source of ROS species in cells and are, under normal conditions, essential for cellular redox balance.[106] In a state of redox imbalance, e.g. caused by disturbed ROS production, excess amount of ROS can result in severe pathophysiologic conditions, notably endothelial dysfunction and related diseases as atherosclerosis, hypertension, diabetes and acute, respiratory distress syndrome (ARDS).[137] We investigated whether or not PBs and BR can potentially inhibit NADPH oxidases in endothelial cells. Firstly, we established a chemiluminescence assay to determine the NADPH oxidase activity. Being the most potent substance, DPxB

significantly decreased the enzyme activity by 60%, followed by PxB (45%) and BR (44%). Although no significancy was calculated for PleB, a reduction of NAPDH oxidase activity was observed (20%) (**Figure 25**).

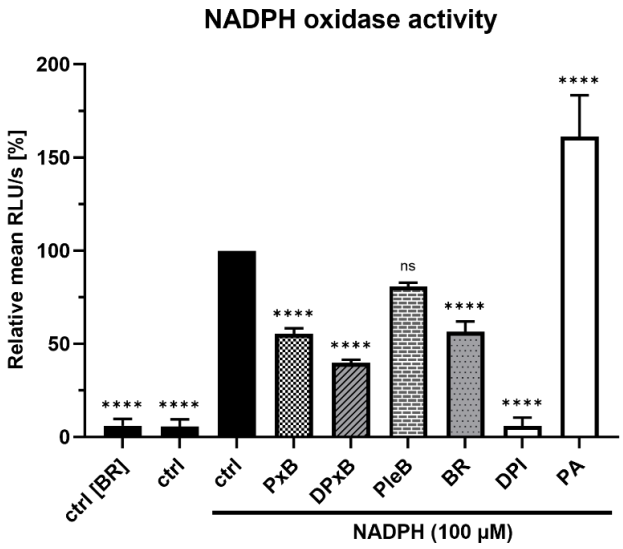

Figure 25 PBs and BR decrease NADPH oxidases activity as assessed in a chemiluminescence assay. PxB, DPxB and BR significantly inhibit NADPH oxidases activity. Prior to the addition of compounds and cell lysate supernatant, lucigenin was dark-adapted for 10 min in a white 96 well plate. After initial chemiluminescence reading for 10 min, reaction was started by adding NADPH. Luminescence was measured for 30 min. Final concentrations for compounds and lucigenin were 20 µM, for NADPH 100 µM were applied. NADPH oxidase activity was normalized to the NADPH added control after subtraction of background reading. DPI and PA were controls for inhibitor and inducer. BR was dissolved in NaOH, BR ctrl was NaOH in Krebs-HEPES buffer; all other compounds were dissolved in DMSO. Values represent mean ± SD of three independent experiments. (ns, not significant, ****$P < 0.0001$)

Secondly, we elucidated the influence of PBs and BR on NOX4 protein and mRNA levels, as NOX4 was found to be the major dominating NOX subtype in HUVECs.[114] Apart from influencing NADPH activity, further evidence from the literature reveals downregulation of NOX4 protein and mRNA level by BR and BV treatment on angiotensin II stimulated cultured human mesangial cells.[138] Immunoblotting of HUVECs, that were stimulated with PB for 24 h also showed a visible downregulation of NOX4 protein levels in HUVECs, which was significantly reduced only for BR (**Figure 26 A, B**). Levels of NOX4 mRNA and p22phox were not significantly altered by PB or BR treatment (**Figure 26 C, D**). Additionally, qPCR experiments were conducted with 30 min of pre-stimulation with PBs and BR and TNF-α incubation for 24 h to induce NOX4. Contrary to the literature[139], however, no significant induction of NOX4 mRNA was detected under these conditions (**Supplementary Figure 29**).

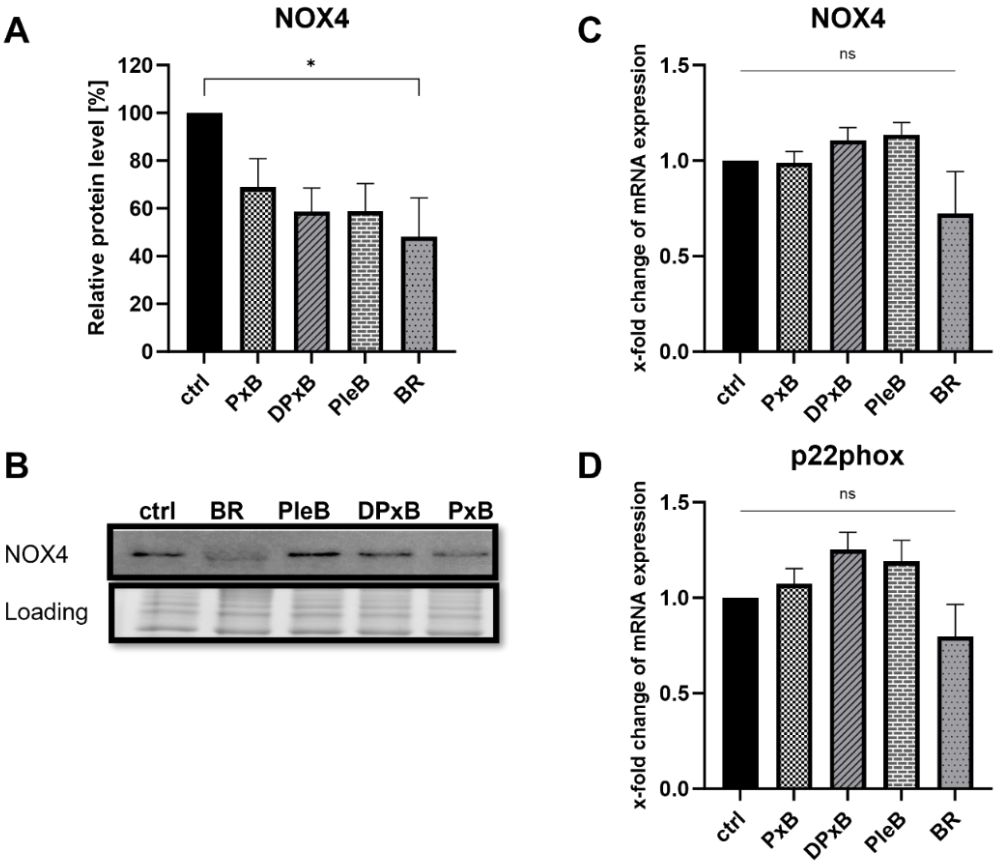

Figure 26 Influence on NOX4 protein and mRNA levels and p22phox subunit mRNA expression. (A,B) HUVEC cells were treated for 24 h and NOX4 protein levels were analyzed by immunoblotting. **(A)** Relative quantification of protein levels of **(B)**. **(C,D)** mRNA levels were quantified by qPCR after 24 h of treatment. **(A-D)** Cells were stimulated with 20 µM of DPxB, PleB, BR and 5 µM of PxB. **(A,B)** Values represent mean ± SEM of four independent experiments or **(C,D)** of three independent experiments. (ns, not significant, **P* < 0.05)

5.2.5 PBs and BR effect monocyte migration and endothelial transmigration

The invasion of monocytes and their following transmigration into the intima is an early hallmark in the pathogenesis of atherosclerosis displays. In a transwell setup, Keshavan et al. and Vogel et al. showed inhibitory effects of BR on endothelial THP-1 transmigration.[95, 140] So far, little is known about the mechanisms of BR affecting monocyte transmigration. To start this chapter as a driving part during atherosclerosis progression, we tested the anti-migratory influence of PBs and BR on THP-1 cells in a transwell setup, keeping the experimental setup similar to the published experiments performed with BR.[95, 140] After 4 h of migration, PxB, DPxB as well as BR showed significant effects on the migration of THP-1 monocytes (**Figure 27**).

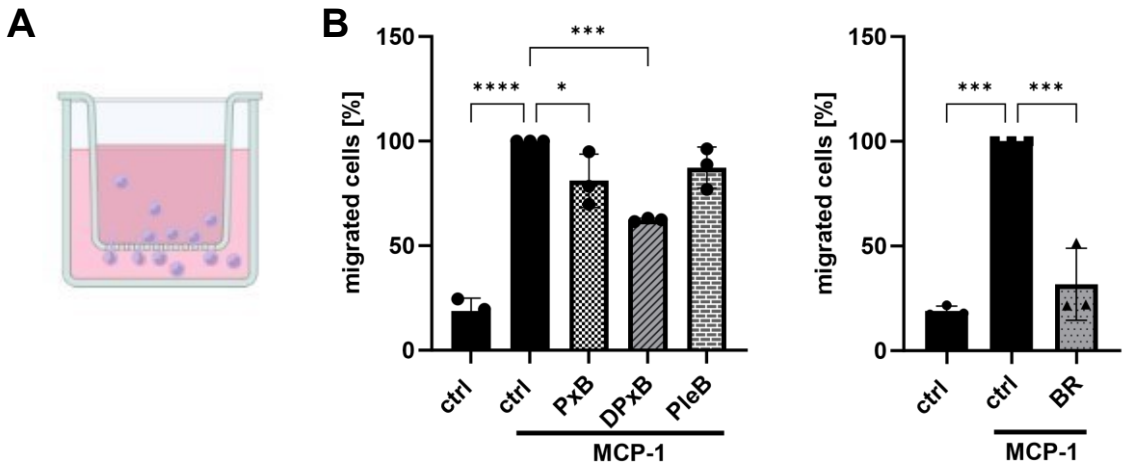

Figure 27 PBs and BR inhibit THP-1 monocyte migration. (A) Schematic presentation of a Boyden chamber transwell. 100 ng/ml MCP-1 in RPMI medium supplemented with 10% FBS served as attracting medium in the lower chamber. Upper chamber consisted of starving medium with 2% FBS. **(B)** Calcein-AM stained THP-1 cells were treated with compounds PxB (8 µM), DPxB, PleB, BR (20 µM) and were led to migrate for 4 h in a transwell. Fluorescence of migrated cells was measured at 495/520 nm (ex/em) and normalized to the DMSO or NaOH control. BR was dissolved in NaOH, analogue BR ctrl was NaOH in medium; all other compounds were dissolved in DMSO. Values represent mean ± SD of three independent experiments. (*P < 0.05, ***P < 0.001, ****P < 0.0001)

Further, we investigated the transmigratory properties of THP-1 cells through a monolayer of endothelial cells in a two-cellular model. PxB significantly reduced transendothelial migration of THP-1 cells (**Figure 28 B**). For the two other compounds, DPxB and PleB, no significant influence on transendothelial migration of monocytes was observed. In contrast to the experiment in **Figure 27**, in this two-cellular model the migration of the monocytes was diminished by the endothelial monolayer, and so the difference between unstimulated and migration-induced controls was low (**Figure 28 B**). To compensate the low migration rate of the cells, the relative induced migration was additionally evaluated (**Figure 28 C**). PxB, DPxB and PleB, show significant effects on the calculated induced migration of THP-1 cells.

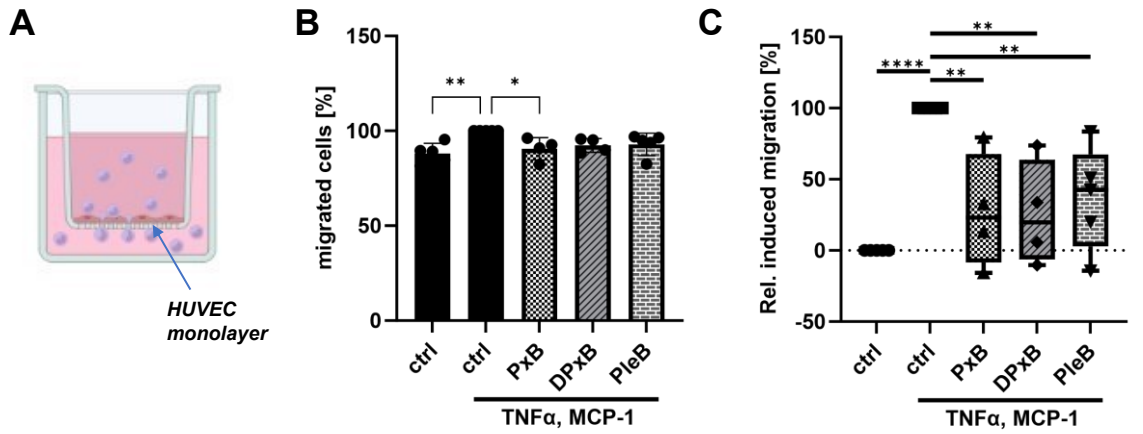

Figure 28 PBs influence THP-1 monocyte migration through a monolayer of HUVEC. (A) HUVEC cells were seeded on collagen G and fibronectin coated filters of Boyden chamber transwells. **(B,C)** Upon reaching confluency, HUVECs were treated with TNF-α (10 ng/ml) for 24 h. PxB (8 µM), DPxB, PleB (20 µM) were added to upper and lower chamber. Calcein-AM labelled THP-1 were seeded in the upper chamber and migration was stopped after 24 h. Fluorescence of migrated cells was measured at 495/520 nm (ex/em) and **(B)** normalized to the DMSO control. **(C)** Quantification of data of **(B)** as relative induced migration by normalizing to the mean difference of positive and negative control. Values represent mean ± SD of five independent experiments. (*P < 0.05, **P < 0.01, ****P < 0.0001)

5.2.6 PBs and BR do not modulate protein and mRNA expression of adhesion proteins

Adhesion of monocytes to endothelial cells is mediated by adhesion proteins as VCAM-1, ICAM-1 as well as selectins that are expressed on the surface of the endothelium.[125] Common investigations on anti-atherosclerotic drugs are often related to the inhibition or downregulation of those surface proteins.[141] Therefore, we tested PBs and BR for their influence to impact TNF-α induced protein and mRNA levels HUVECs. However, on protein as well as on mRNA level, no significant impact of the chemical treatment was observed (**Figure 29-Figure 30**). Of note, BR concentration had to be limited to 5 µM due a strong autofluorescence of BR to ensure no interference on the VCAM-1 PE labeled antibody detection (**Supplementary Figure 30**).

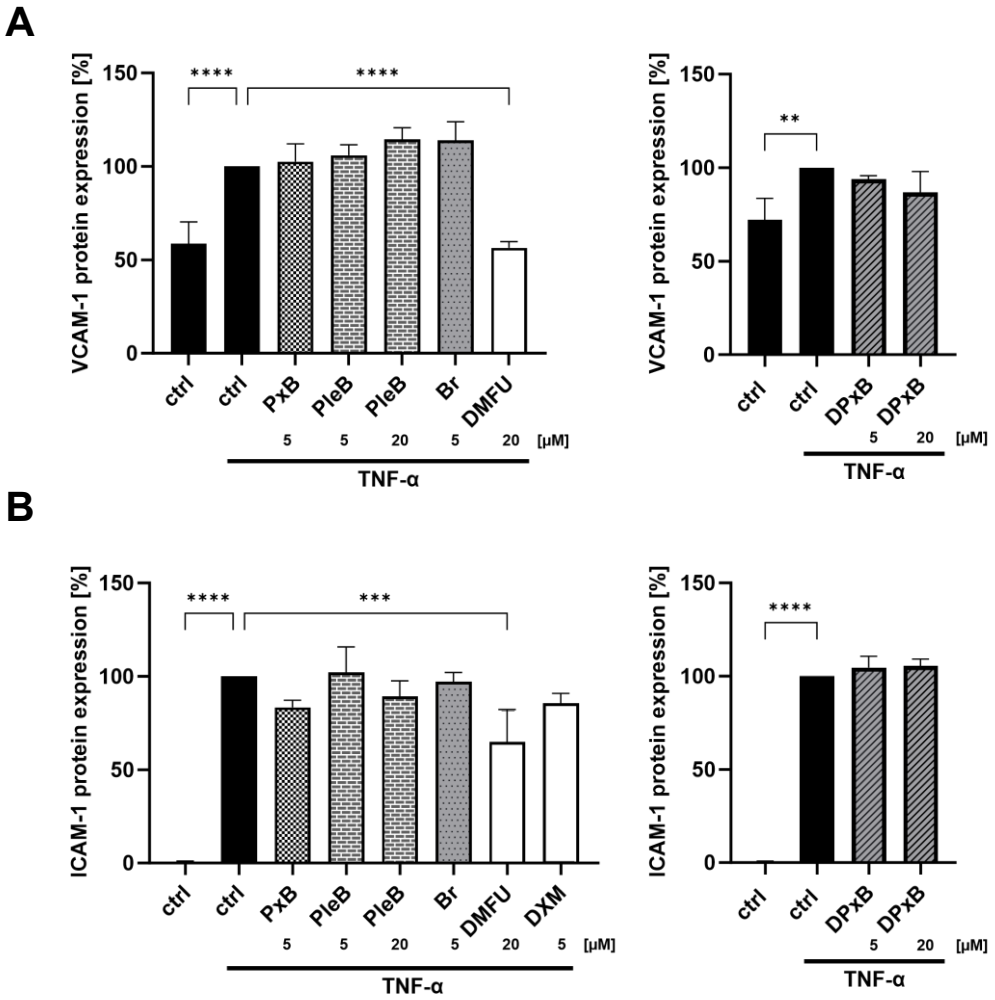

Figure 29 PBs and BR do not influence VCAM-1 and ICAM-1 protein expression levels. (A) VCAM-1 and **(B)** ICAM-1 protein expression levels were analyzed by Flow cytometry after incubation of cells with 10 ng/ml TNF-α for 16 h with a pre-stimulation time of 30 min with compounds or controls as indicated. DMFU and DXM served as positive controls for VCAM-1 and/or ICAM-1 expression inhibitors. Values represent mean ± SD of three independent experiments. (***P* < 0.01, ****P* < 0.001, *****P* < 0.0001)

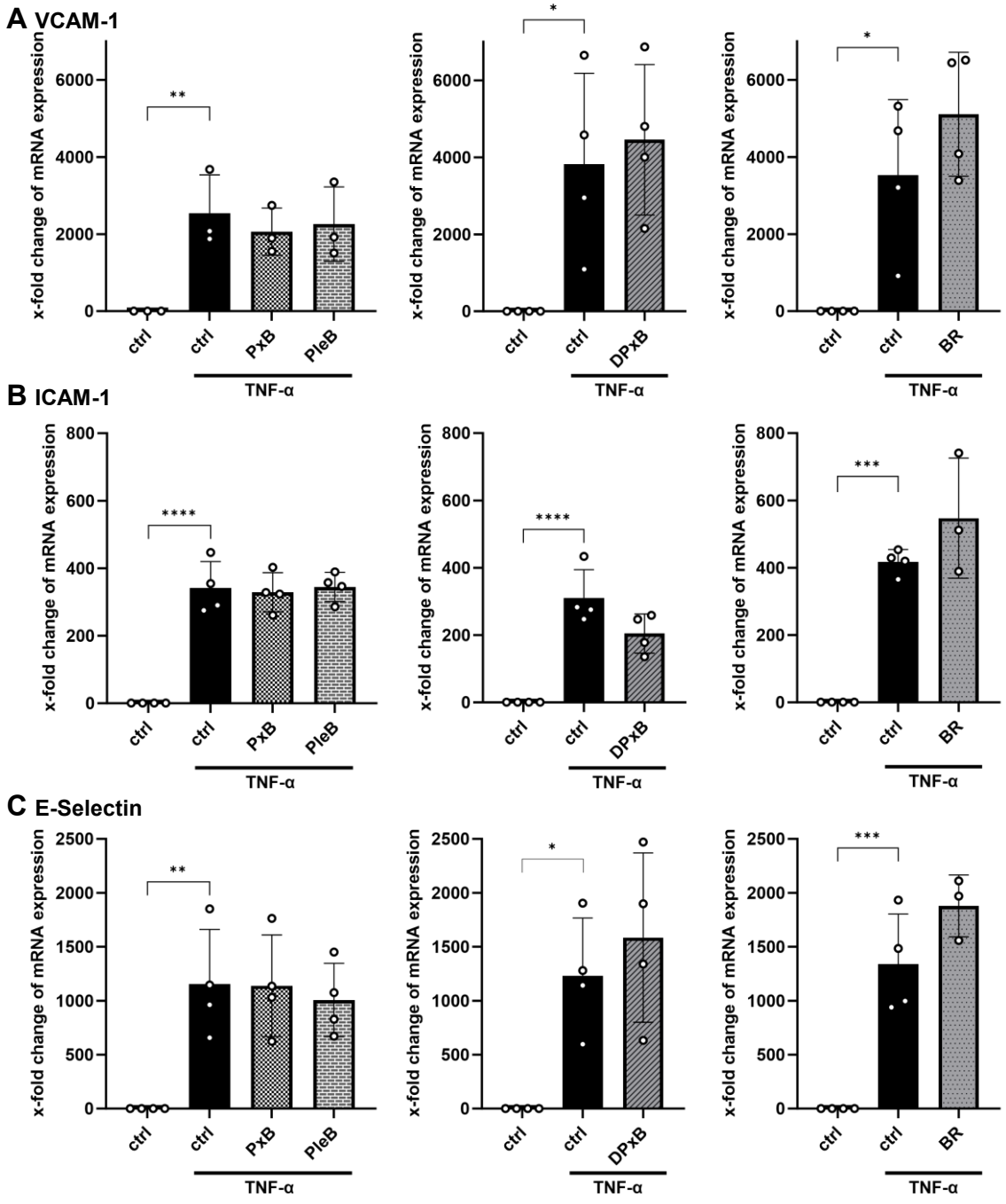

Figure 30 PBs and BR do not affect mRNA expression levels of VCAM-1, ICAM-1 and E-selectin after 4 h. HUVEC cells were pre-stimulated for 30 min with 20 μM of DPxB, PleB, BR and 8 μM of PxB prior to addition of TNF-α (10 ng/ml) for 4 h. Values represent mean ± SD of three or four independent experiments, as graphically presented. (*P < 0.05, **P < 0.01, ***P < 0.001, ****P < 0.0001)

5.2.7 Modulation of MMP activity by PBs and BR

MMPs play a critical role in endothelial remodeling processes and are upregulated pathologically in atherosclerosis. They are produced by macrophages and endothelial cells and subsequently secreted into the surrounding environment. Collagenases are members of the MMP family which degrade ECM.[128] Furthermore, inhibiting MMP activity is related to negatively affect monocyte transmigration through the endothelium and maintaining endothelial function. [127b, 131] Consequently, targeting MMP activity is therefore a promising approach to impact this key step of atherosclerosis progression. To investigate potential inhibitory effects of PBs on MMP-9 activity, firstly a confocal experiment was conducted based on the ability of MMPs of the endothelium to degrade collagen IV, visible by the formation of perforations in the stained collagen. NNGH served as positive control that is known to inhibit multiple MMPs.[142] Remarkably, BR and PxB altered on the intactness of the collagen IV lawn as evident by increased fluorescence intensity of collagen IV. Not significant, were effects on the endothelium of the other tested PBs, DPxB and PleB (**Figure 31 A**). The results obtained from confocal microscopy indicate that PBs mainly inhibit MMP-9 activity. MMP-9 is a highly expressed important collagenase in vascular endothelium which contributes to endothelial dysfunction in atherosclerosis.[143] Thus, the compounds were tested to directly influence MMP-9 activity in an *in-vitro* approach performed by the group of Dr. Stefan Schwaiger (University of Innsbruck, Austria) (**Figure 31 B**). Indeed, strong inhibitory effects in low micromolar concentrations (IC_{50} 11.53 µM) was detected for PxB. Additionally, PleB, DPxB, and BR inhibited the enzyme at higher concentrations. IC_{50} values were 23.07 µM for PleB, 33.10 µM for DPxB, and 52.24 µM for BR, respectively. Next, we analyzed protein levels of HUVEC and THP-1 cell lysates for MMP-2 and MMP-9, to investigate whether the compounds alter the expression of MMPs (**Figure 31 C**). MMP-2 is involved in the process of lymphocyte diapedesis.[126] However, no influences on the protein expression of MMP-2 in HUVEC and MMP-2 and MMP-9 in THP-1 cell lysates was found. Of note, as MMPs are secreted into the surrounding environment, high amounts of MMPs are detectable in cell suspensions.

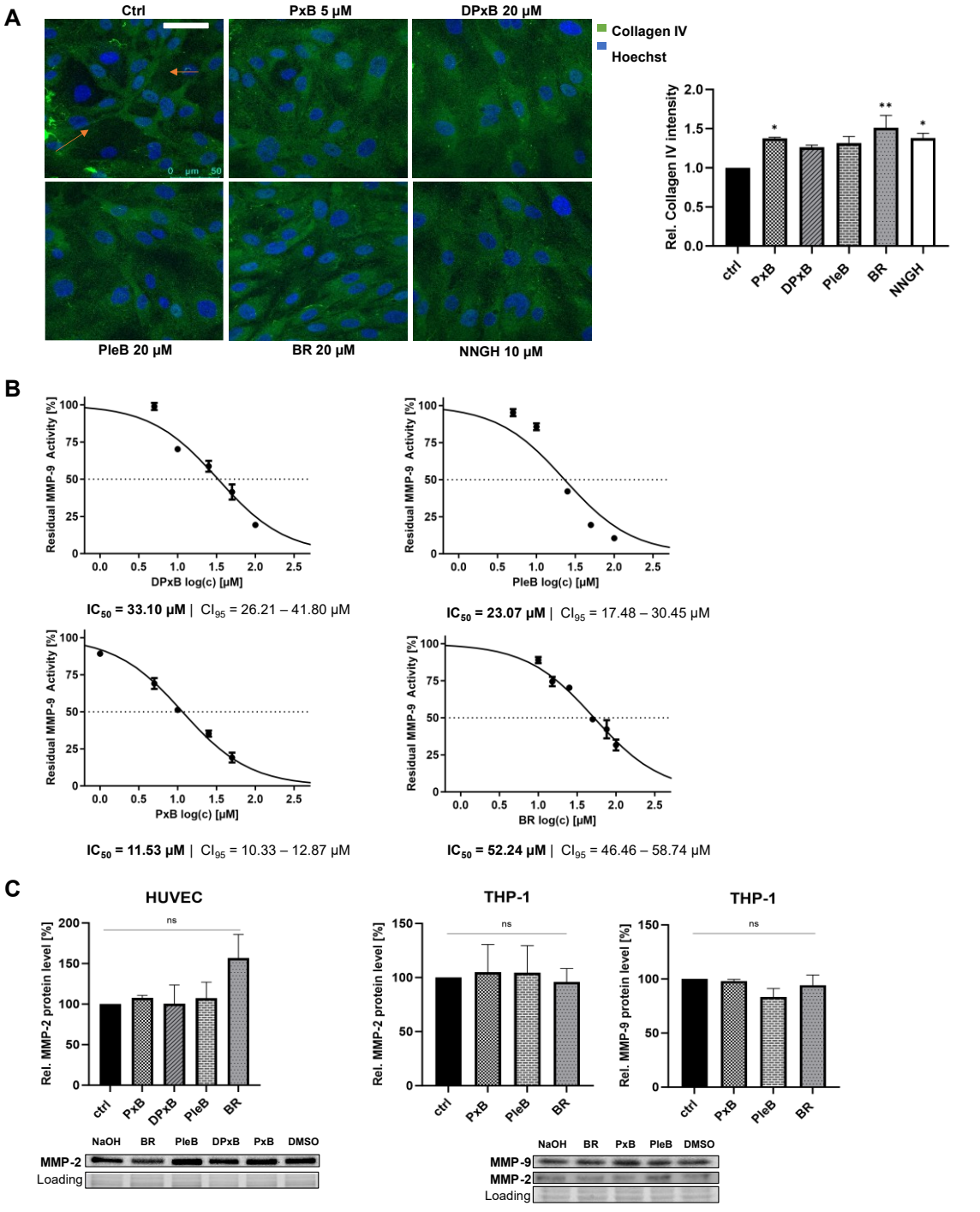

Figure 31 PBs and BR influence MMP-9 activity without affecting cellular protein expression levels *in-vitro* and *in-cellulo*. (A) HUVEC cells were seeded on collagen IV coated slides and treated for 24 h with substances as indicated, before staining with anti-collagen IV antibody (green) and Hoechst (nuclei, blue), and analysis by confocal microscopy using ImageJ. Scale bar 50 µm. One representative image out of three independent experiments is shown. **(B)** *In-vitro* MMP-9 activity assay was performed by the group of Dr. S. Schwaiger (University of Innsbruck, Austria). Residual MMP-9 activity was normalized to vehicle control after compensation of the self-fluorescence of the substances and IC_{50} values were calculated by nonlinear regression analysis. **(C)** Protein levels of MMP-2 in HUVEC lysates and MMP-2 and MMP-9 in THP-1 cell lysates after treatment with 20 µM of DPxB, PleB, BR and 5 µM of PxB for 24 h as analyzed by Western blotting and subsequent quantification. One representative Western blot out of three is shown. **(A,B,C)** Values represent mean ± SEM of three independent experiments. (ns, not significant, **P* < 0.05, ***P* < 0.01)

5.3 Discussion

Inevitably, the investigations on novel sources and molecules from plants are drivers for therapeutic drug research. Monocyte migration and transmigration are hallmarks in atherosclerotic plaque formation, which is a major complication in CAD leading to 17.8 million deaths word wide annually.[100] Predominately, atherosclerosis is a lifestyle influenced disease triggered by oxidative stress.[135] Even though the disease is well understood, apart from treating hypercholesterolemia, preventative therapies are not commonly pursued as the disease manifests years after its progression and the optimal timepoint of starting preventative interventions remains to be determined.[144] PBs potentially open a promising approach to interfere with early stages of atherosclerotic plaque formation as they are part of human daily nutrition. Oxidative stress is the major disruptor of the proper functionality of the endothelium. Damages in its cell monolayer contribute to activate the endothelium which then favors inflammation processes by secretion of cytokines.[102, 145] The balance between oxidative stress markers, such as superoxide anions, and stress cleaving mechanisms is disturbed.[104] Based on the structural similarities to BR and its known anti-atherosclerotic properties, we could find parallel activities of PBs with regards to impacting monocyte transmigration and oxidative stress influenced mechanisms in the early stages of atherosclerosis. We investigated three different PBs, two of which were isolated from *Cercidiphyllum japonicum* (PleB, PxB). DPxB was identified in senescent *Parrotia persica* leaves and matches the modifications of *Vv*-DPxB, thus providing a new source for this molecule, that was previously only known as a component of senescent grapevine leaves.[132]

5.3.1 *In-cellulo* anti-oxidative radical scavenger ability of PBs and BR is potentially mediated by the inhibition of NADPH oxidase activity and impacts endothelia function maintenance

Radical oxygen species (ROS) act as signaling molecules at a physiological level, thus being important for cellular biological feedback mechanism and the regulation of pathways such as PI3K, MAPK, Nrf2 and Ref1-mediated redox cellular signaling or iron homeostasis, among others.[105] To maintain a balanced level in ROS amount and to limit the pathophysiological side effects of cell death and apoptosis, ROS are cleaved and degraded by cells. However, the balance can be disturbed by extensive ROS production, which subsequently cannot be compensated by the cells.[104] As during atherosclerosis, this equilibrium is disturbed by an extensive amount of ROS and manifests in endothelial

dysfunction.[145-146] Our data underline the potential to interfere with oxidative-triggered endothelial disruption by acting as potent radical scavenger on endothelial cells in nanomolar range. Additionally, our results clearly demonstrate that PBs are taken up by the cells and exert pharmacological effects. The major producer of ROS species in the vascular endothelium is the membrane bound oxidase NOX4, consisting of the central core unit gp91-*phox* and the subunit p22-*phox*. NOX enzymes reduce oxygen to superoxide (ROS) via NADPH, FAD and heme.[119] NOX4 is activated by several factors attributed to atherosclerosis like oxLDL, hypertension or shear stress.[117-118] Moreover, by induction of oxidative stress in cells, NOX4 contributes to endothelial cell damage by blocking cell replication.[147] We found that PBs and BR significantly decrease NOX4 activity in HUVEC lysates after a short incubation time of 30 min. This leads to the conclusion that PBs directly interfere the production of ROS in endothelial cells. By revealing that bilins scavenge ROS in endothelial cells and inhibit NOX activity, it can be summarized that the tested bilins are not only scavenger but also destroyer of the production of oxidative stress. Of note, the ability to inhibit NOX4 activity is not new for bilins. Investigations on diabetic nephropathy previously showed that BR and Biliverdin (BV) inhibited NOX activity on living human renal mesangial cells after incubation for 48 h. Furthermore, downregulation of NOX4 mRNA and protein levels was observed for angiotensin II stimulated cultured human mesangium cells by BR and BV treatment.[138] These results are substantiated by studies of other bilins, phycocyanin and phycocyanobilin from *Spirulina platensis*, on diabetic nephropathy. Again, dose-dependent inhibitory effects of bilins, including BR, BV, and phycocyanobilin were detected on superoxide production in cultured human mesangial cells. Preventative effects on NOX4 expression were found after oral administration of phycocyanin and phycocyanobilin in diabetic mice.[136] Similar to atherosclerosis, diabetic nephropathy is strongly connected to cellular dysfunction induced by oxidative stress. Therefore, inhibiting vascular NOX as main source of ROS also in the kidney is regarded as therapeutic approach to conquer diabetic vascular nephropathy.[148] Additionally, evidence on the inhibitory potential of BR on the NOX activity of macrophages was found, which might rely on an inhibition of NOX2 activity, mainly.[149] NOX2 is the major NOX subtype in phagocytic cells. However, contrary to the findings in cultured human mesangium cells[138], BR did not exhibit influences on the subunit expression levels of gp91-*phox*, p22-*phox*, and p47-*phox* proteins in the LPS stimulated macrophages RAW 264.7.[149] Summarizing the current evidence from literature, contradictory findings of BR on protein or mRNA expression of

NOX enzymes are reported. However, there is consensus on the ability of BR to inhibit the activity of NOX enzymes to produce ROS.[136, 138, 149]

Theories on the underlying mechanisms of BR, BV but also others, such as protoporphyrin IX and hemin, are focusing on the process of enzyme activation. It is assumed that, due to the hydrophobic properties, interactions with hydrophobic cytosolic components of the enzyme lead to a dysfunctional translocation of the cytosolic components to the membrane bound subunits, which is necessary for the activation of the enzyme. Therefore, bilins do not inhibit the active enzyme but the subunit assembly of the oxidase.[150] Our findings are in line with this hypothesis as the activity of the NOX enzymes is significantly inhibited by PBs and BR over a short timeline of only 30 min.

Apart from the NOX activity inhibition by BR and PBs, we found that BR significantly decreases NOX4 protein level in HUVEC cell lysates, whereas effects were not significant for the PBs PxB, DPxB, and PleB. Further, investigations on mRNA levels did not reveal significant influences of all the substances on NOX4 and the expression of its active subunit p22-*phox* for TNF-α activated cells as well as for non-activated control cells. Thus, TNF-α stimulation of the cells did not show an expected induction in mRNA expression, which is contrary to reports in literature.[139] To summarize, although effects of PBs on mRNA and protein expression of NOX4 were non-elusive, PBs and BR clearly reduced NOX activity.

Comparing the potency of PB candidates in the different experiments, no correlations can be found. BR was the most anti-oxidative candidate in *in-vitro* and *in-cellulo* approaches. However, this does not account for the ability to inhibit NOX activity. PleB was the weakest to incorporate electrons or radicals *in-vitro*, potentially due to its smaller delocalized electron system, as assessed by FRAP and DPPH assay. This finding is in line of the fact that PleB inhibits superoxide production in the NOX activity assay in cell lysates. Other than that, stronger effects were seen on *in-cellulo* ROS scavenging ability. Potentially other influences like improved cellular uptake amplifies the effects of PleB in living cells, which remains to be elucidated. DPxB inhibited NOX activity as most potent candidate but possessed a similar ROS-scavenging capability to PxB in HUVEC cells. Therefore, conducting several experiments are necessary to evaluate the full picture of the anti-oxidative potential of bilins, including *in-vitro* and *in-cellulo* approaches.

Taken together, strong evidence hints towards a direct inhibition of NOX enzymes activation by bilins, including PBs, leading to suppression of ROS production in endothelial cells. We are the first research group that shows that PBs diminish endothelial NOX activity. By acting as radical scavenging molecules together with the preventative ability to shutdown ROS production via NOX4 inhibition in endothelial cells, PBs can potentially interfere with the manifestation of endothelial dysfunction during early stages of atherosclerosis.

5.3.2 Effects of PB and BR on diapedesis of monocytes is not mediated by the expression of adhesive proteins

Indisputably, a hallmark in atherosclerosis development is the infiltration of immune cell across the endothelium into the intima. We could prove that PBs and BR slow down the migration of monocytes across a membrane attracted by a chemotactic agent. Moreover, monocyte diapedesis across activated endothelial cell monolayers is influenced by PBs, most pronounced for one candidate PxB. As a result, we could demonstrate that PBs potentially interfere atherosclerosis progression during the early stages of plaque formation.

BR is known to inhibit transendothelial lymphocyte migration, but not adhesion of the lymphocytes to endothelial cells. Accordingly, regulation of adhesive protein expression was not found to be altered under treatment with BR.[95, 140] Mechanisms that mediate lymphocyte diapedesis are most likely to involve adhesive proteins.[120] Consistent with previous reports on BR[95, 140], our results show that PBs do not influence TNF-α induced VCAM-1, ICAM-1, and E-selectin mRNA and protein expression levels of HUVECs as other natural products, Flavopiridol[151], for instance. Consequently, the decreased monocyte migration must be attributed to some other pathway. Literature vaguely hypothesizes that BR interferes the signaling cascades of ROS in endothelial cells by its strong anti-oxidative properties. ROS is produced in downstream pathways as a response to the activation of VCAM-1 and ICAM-1 by leukocyte binding via integrins.[152] Subsequently, BR is speculated to prevent the effects of intracellular ROS, which modifies endothelial junctions, thereby promoting transmigration of leukocytes.[95] Theoretically, this could also be feasible for PBs as well, as our results outline that PBs are antioxidants that scavenge ROS in endothelial cells.

As we detected inhibitory potency of BR and PBs on the migration of monocytes itself this effect needs to be considered while interpreting the inhibitory potential of the substances on transendothelial migration of monocytes. To our knowledge, monocyte migration studies were not conducted for BR so far. Recently, BR and PBs were found to inhibit actin dynamics and cell migration of adherent cells.[29a] Without affecting cell viability, disruption of the actin cytoskeleton and silencing of dynamic podosomes leads to an inhibition of monocyte and macrophage migration as found by research on the drug angiostatin.[153] Considering the anti-migratory effects of PBs and BR on monocytes, it can be hypothesized that PBs and BR exhibit influences on the deceleration of monocyte migration by interacting with actin on the monocyte cell surface. Thereby, our findings could open a new vista for a different mode of action of bilins in affecting transendothelial migration of monocytes, which is potentially not only limited to the disease atherosclerosis.

5.3.3 Reduced monocyte migration by PBs and BR is potentially related to NOX4 and MMP-9 enzyme activity inhibition

Our work is the first report on a direct inhibition of MMP-9 enzyme activity by PBs *in-vitro* and *in-cellulo* in a low micromolar range. Similarly, BR inhibited MMP-9 activity, which is in accordance with existing literature. BR is reported to block anti-VCAM-1 activation of MMP-2 and MMP-9 produced by endothelial cells, as well as the VCAM-1 dependent trans-endothelial migration of lymphocytes. Involvement of the ROS scavenging ability of BR was underlined as its non-antioxidant conjugate ditaurobilirubin does not inhibit migration.[140] Besides, to our knowledge, IC_{50} of BR on *in-vitro* MMP-9 has not been determined yet by other groups. Investigations on other natural products on MMP-9 inhibition as caffeate and silbenoids exhibit IC_{50} values of 1-15 µM, and flavonoids obtain IC_{50} values from 2-32 µM. Natural products are reported to act selectively on MMPs, being superior to synthetic, highly potent MMP-inhibitors that reach low nanomolar IC_{50} < 10 nM, but suffer in selectivity.[154] To summarize, PBs show *in-vitro* inhibition in low micromolar ranges on MMP-9 activity similar to other potent natural compounds, while PBs (IC_{50} 12-33 µM) are notably superior the activity of BR (IC_{50} 52 µM). Whether the effects of PBs on MMP-9 are selective among the other MMPs must be elucidated by testing different MMPs on activity inhibition in the future.

In addition, our findings on MMP-9 inhibition strongly indicate that PBs and BR potentially reduce monocyte migration across activated endothelium by influencing the downstream signaling of VCAM-1 with an involvement of the endothelial-associated MMP and NOX

enzymes. In atherosclerosis, highly elevated MMP-9 levels are related to the formation, destabilization, and rupture of plaques. It was shown that loss of MMP-9 activity diminished macrophage diapedesis and reduced atherosclerotic plaque growth in mice.[127b, 131] In this regard, an involvement of MMPs on monocyte and T lymphocyte transmigration through ECM was found to be related to VCAM-1 inducing MMPs secreted by the endothelium not by lymphocytes[155], thereby facilitating the infiltration of immune cells by extracellular matrix (ECM) degradation.[126]

Moreover, while mediating lymphocyte migration, VCAM-1 signaling was found to impact not only MMP activity but also endothelial NOX. More precisely, the activation of VCAM-1 induces NOX enzymes of the endothelium which consequently produce H_2O_2, in other words ROS, which subsequently leads to an induction of endothelial-cell associated MMP activity. Consequently, NOX and MMPs are required for the diapedesis of the immune cells and inhibition of the enzymes NOX, MMPs as well as scavenging endothelial ROS is a promising approach to break down leukocyte transendothelial migration.[156] Inhibitors of NOX activity as diphenyleneiodonium chloride (DPI) and apocynin are capable to block migration without affecting adhesion of lymphocytes. Same was found for molecules that scavenge ROS in cells, since binding to VCAM-1 was found to induce ROS production in endothelial cells by stimulating NOX enzyme activity.[157] By proving the strongly pronounced potential of PBs to scavenge endothelial ROS, inhibit NOX and MMP-9 activity, we open a chapter for PBs as phytochemical substances to counter atherosclerosis.

As a result of the downstream VCAM-1 signaling effects, the activity of the substances on *in-vivo* MMP inhibition and their ability to inhibit NOX activity in endothelial cell lysates may be connected. As discussed above, numerous hints are pointing out that ROS, which are produced by the NOX family enzymes, are involved in the regulation of MMP expression and/or activation.[119] This fact could potentially explain our results, in which differences in the potency of the bilins on *in-vitro* and *in-cellulo* MMP-9 inhibition was visible. For BR, for instance, strongest *in-cellulo* inhibition on endothelial MMP-9 activity, as assessed by reduced collagen IV degradation, was detected. Contrary, BR obtained highest IC_{50} on MMP-9 inhibition *in-vitro*, among the tested bilins. It can be hypothesized that *in-cellulo* the potency of BR is favored by stronger inhibition of NOX enzyme activity which compensates the high IC_{50} on in-vitro MMP-9 activity.

5.3.4 Inhibition of MMP-9 by PBs and BR can impact endothelial dysfunction and VSMC migration

On the one hand, apart to the impact of bilins on MMPs involved in leukocyte transmigration, our findings on MMP-9 activity inhibition by PBs and BR, support also our hypothesis that bilins could maintain endothelial functionality. MMP-9 is involved in the activation of endothelial cells and acts in a pro-inflammatory and pro-apoptotic manner on the endothelium.[143b] Consequently, inhibition of MMP-9 supports our findings on NOX activity inhibition by our compounds, providing evidence that bilins diminish pathological dysfunctional endothelium.

On the other hand, our findings also build the foundation for other research opportunities regarding the impact of bilin treatment in later stages of atherosclerosis progression. In lesions, MMP-9 is secreted from distinct cell types including macrophage foam cells and SMCs as response to inflammatory stimuli.[127a] MMP-9 is involved in all stages of atherosclerosis and for example enhances infiltration of smooth muscle cells (SMC) to migrate into lesions by degrading the surrounding ECM. Eventually, MMP-9 enables proliferation of SMCs. By secreting collagen and ECM proteins, SMCs induce a so-called fibrous cap formation. Finally, MMP-9 was also reported to be responsible for plaque rupture and destabilization by excessive proteolysis.[127a, 158] Summing up, the potential of PBs and BR to interfere MMP-9 induced mechanisms in later stages of atherosclerosis as plaque formation is a promising approach for future investigations.

5.3.5 Potential impact of PBs in next stages of atherosclerosis progression

Existing data suggest that BR interferes cholesterol biosynthesis[159], cholesterol metabolism[160] and lipid peroxidation[161]. Hypercholesterolemia and elevated LDL levels are risk factors of atherosclerosis. In particular, oxidized LDL has an impact on the release of phospholipids, which can activate the endothelium and induce atherosclerosis.[162] Further, oxLDL can trigger the production of ROS via NOX activation, which as discussed leads to the activation of endothelial cells and macrophages.[135] To conclude, investigating if PBs, as antioxidants, potentially also interfere with cholesterol and LDL associated mechanisms during atherosclerosis progression may be a promising direction for future research.

CONTRIBUTION

6. Contribution: Redox-Mediated Amination of Pyrogallol-Based Polyphenols

6.1 Introduction

For the testing of anti-oxidative capacity of substances, various methods and assays are available, assessing different mechanisms of anti-oxidative reactions. Generally, two major reaction types can be named, Hydrogen Atom Transfer (HAT) and Single Electron Transfer (SET) mechanisms. HAT mechanisms are defined by hydrogen donation of antioxidants to fend off radicals. In contrast, in SET-based reactions, the reducing ability of antioxidants is based on electron transfer to other substances. Often, both mechanisms go hand in hand and occur in parallel with one mechanism being more pronounced than the other.[79] As HAT reactions are strongly influenced by the bond dissociation enthalpy (BDE) of phenolic antioxidants, low BDE provokes a faster reaction with radicals. For polyphenols, it has been postulated that mainly HAT reactions are responsible for the anti-oxidative scavenging ability.[163] To examine the anti-oxidative activity of polyphenols structurally related to baicalein (BA) (provided by Salavat Ashirbaev, AK. Zipse, LMU Munich), a FRAP assay, which targets SET-mechanisms, and an ORAC assay to examine underlying HAT reactions, were performed.[79] The obtained dataset was correlated, with computed thermodynamic properties (BDE, proton affinity) to better understand the underlying oxidative mechanisms of the coupling reactions between polyphenol compounds and amines of amyloid polypeptides as amylin (Natércia Brás, AK. Zipse, LMU Munich/Universidade do Porto). Notably, in the following part, only the results that contributed to the publication are shown and described, and, consequently, our *in-vitro* data were not integrated into the results focusing on compound chemistry.

This piece of work is currently in manuscript writing process.

6.2 Library of pyrogallol-derived polyphenols

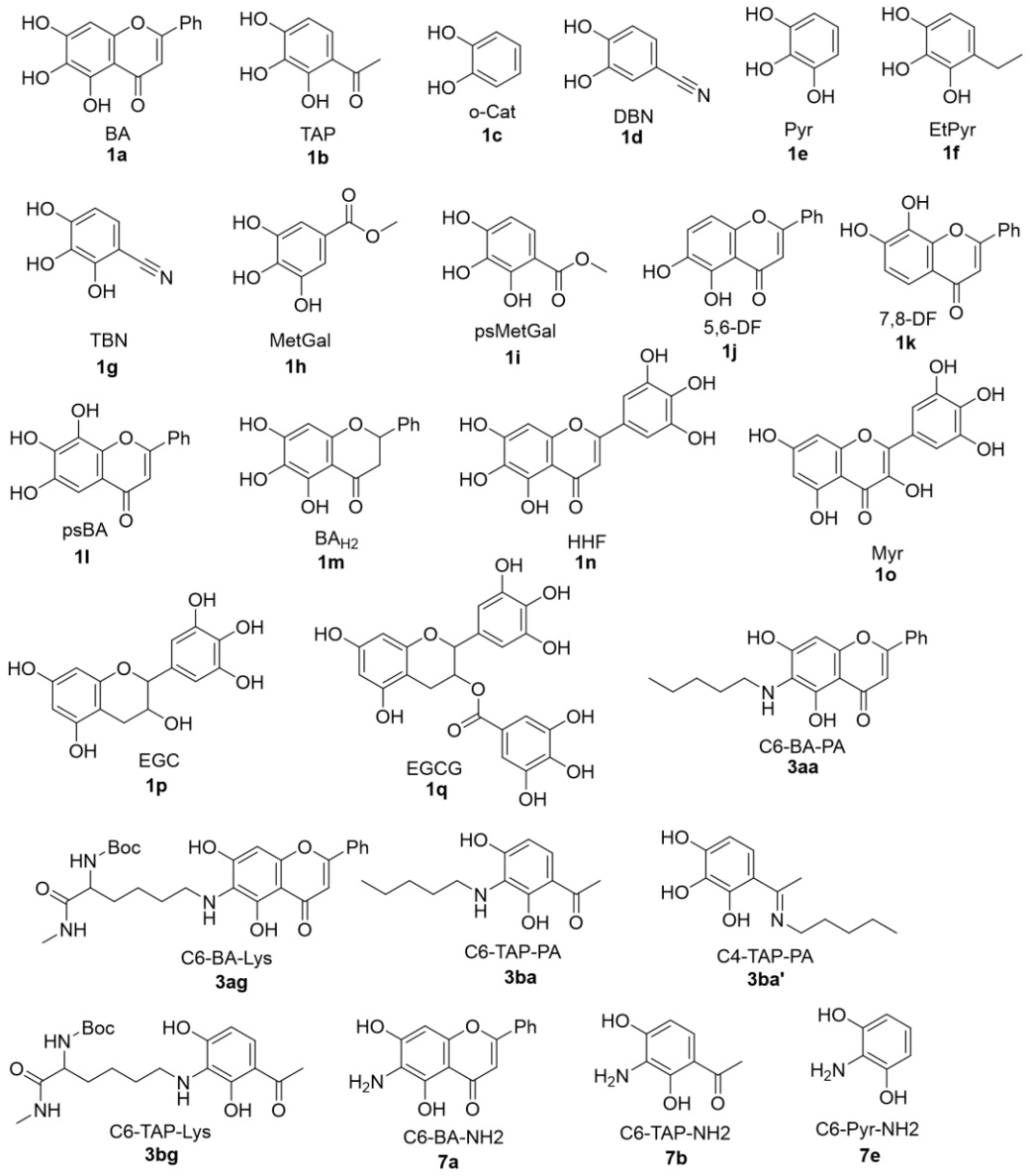

Figure 32 Structures of the pyrogallol-derived polyphenol library. Compounds were provided and C4 and C6 adducts were synthesized by Salavat Ashirbaev (Prof. Zipse, LMU Munich). Molecule drawings in this figure are originated from Salavat Ashirbaev.

6.3 Screening of a library of pyrogallol-derived polyphenols for anti-oxidative properties

Observed FRAP values were highest for psBA (3.40), HHF (3.06) and EGCG (3.05), and lowest for C4-TAP-PA (1.26) and C6-BA-NH_2 (1.24) (**Figure 33 A**). C4-TAP-PA showed significantly reduced FRAP potency compared to TAP, while other C6-TAB derivatives

possessed comparable anti-oxidative potency. psBA, which differs from BA only in the location of a hydroxyl functionality, exhibited a threefold higher FRAP value compared to BA. BAH2 and BA showed comparable anti-oxidative potency in the FRAP setup. Comparing C6-Pyr-NH_2 to Pyr, a distinct loss in anti-oxidative capacity was observed. The ORAC assay is based on hydrogen atom transfer (HAT) mechanisms of antioxidants and unlike other methods, also reaction kinetics of substances are expressed by the ORAC value.[164] Among the tested polyphenols, DBN (4.87), Myr (4.40), and o-Cat (3.96) exhibited highest ORAC values, C6-TAP-Lys (1.77), psBA (1.66), and EtPyr (1.23) showed lowest anti-oxidative potential (**Figure 33 B**). Comparing TAP (2.14) with its derivatives, no significant change in ORAC value was detectable, apart from C6-TAP-Lys (1.77), which showed a significant loss in anti-oxidative power. For BA derived polyphenols, no significant change in ORAC values compared to BA (2.43) was observed, except for a significantly reduced ORAC value for psBA (1.66). ORAC values of C6-Pyr-NH_2 were comparable to Pyr, whereas values of EtPyr were significantly decreased. EGC and EGCG, which were included as reference substances, yielded ORAC values that are in accordance to published literature.[165]

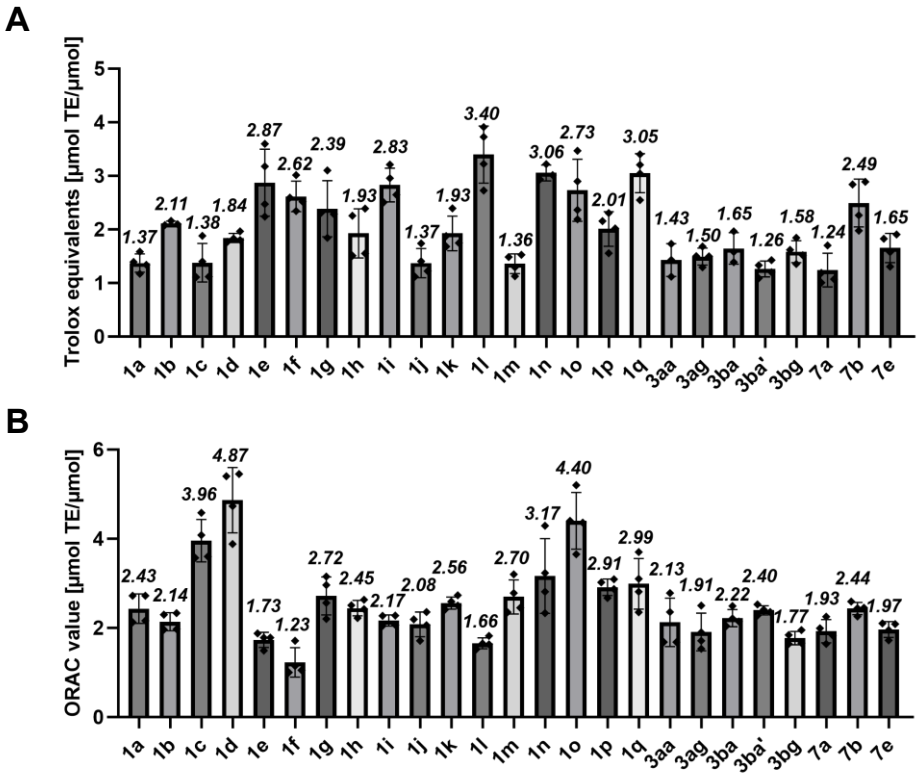

Figure 33 Anti-oxidative potency of polyphenols *in-vitro* as assessed by (A) FRAP-assay and **(B)** ORAC assay. **(A)** Values represent mean ± SD of three or four independent experiments. Two outliers were omitted based on Grubbs' Test (α=0.05). **(B)** Values represent mean ± SD of four independent experiments.

REFERENCES

7. References

[1] D. A. Dias, S. Urban, U. Roessner, *Metabolites* **2012**, *2*, 303-336.
[2] G. M. Cragg, D. J. Newman, *Pure and Applied Chemistry* **2005**, *77*, 7-24.
[3] B. Waltenberger, A. Mocan, K. Šmejkal, E. H. Heiss, A. G. Atanasov, *Molecules* **2016**, *21*.
[4] A. Endo, *Proc Jpn Acad Ser B Phys Biol Sci* **2010**, *86*, 484-493.
[5] C. Bailey, C. Day, *Practical Diabetes International* **2004**, *21*, 115-117.
[6] P. Wang, C. A. Karg, N. Frey, J. Frädrich, A. M. Vollmar, S. Moser, *Archiv der Pharmazie* **2021**, *354*, 2100061.
[7] B. Kräutler, *Chemical Society Reviews* **2014**, *43*, 6227-6238.
[8] aS. Moser, T. Erhart, S. Neuhauser, B. Kräutler, *Journal of Agricultural and Food Chemistry* **2020**, *68*, 7132-7142; bC. Mittelberger, H. Yalcinkaya, C. Pichler, J. Gasser, G. Scherzer, T. Erhart, S. Schumacher, B. Holzner, K. Janik, P. Robatscher, T. Müller, B. Kräutler, M. Oberhuber, *Journal of Agricultural and Food Chemistry* **2017**, *65*, 2651-2660.
[9] S. Hörtensteiner, B. Kräutler, *Biochimica et Biophysica Acta (BBA) - Bioenergetics* **2011**, *1807*, 977-988.
[10] aB. Kuai, J. Chen, S. Hörtensteiner, *Journal of Experimental Botany* **2017**, *69*, 751-767; bY. Shimoda, H. Ito, A. Tanaka, *The Plant Cell* **2016**, *28*, 2147-2160.
[11] aY. Shimoda, H. Ito, A. Tanaka, *Plant J* **2012**, *72*, 501-511; bS. HÖRTENSTEINER, F. VICENTINI, P. MATILE, *New Phytologist* **1995**, *129*, 237-246.
[12] S. Schelbert, S. Aubry, B. Burla, B. Agne, F. Kessler, K. Krupinska, S. Hörtensteiner, *The Plant Cell* **2009**, *21*, 767-785.
[13] S. Hörtensteiner, M. Hauenstein, B. Kräutler, in *Advances in Botanical Research, Vol. 90* (Ed.: B. Grimm), Academic Press, **2019**, pp. 213-271.
[14] aA. Pruzinská, G. Tanner, I. Anders, M. Roca, S. Hörtensteiner, *Proc Natl Acad Sci U S A* **2003**, *100*, 15259-15264; bB. Kräutler, W. Mühlecker, M. Anderl, B. Gerlach, *Helvetica Chimica Acta* **1997**, *80*, 1355-1362.
[15] A. Pružinská, I. Anders, S. Aubry, N. Schenk, E. Tapernoux-Lüthi, T. Müller, B. Kräutler, S. Hörtensteiner, *The Plant Cell* **2007**, *19*, 369-387.
[16] K. L. Wüthrich, L. Bovet, P. E. Hunziker, I. S. Donnison, S. Hörtensteiner, *Plant J* **2000**, *21*, 189-198.
[17] M. Hauenstein, B. Christ, A. Das, S. Aubry, S. Hörtensteiner, *The Plant Cell* **2016**, *28*, 2510-2527.
[18] B. Christ, I. Süssenbacher, S. Moser, N. Bichsel, A. Egert, T. Müller, B. Kräutler, S. Hörtensteiner, *The Plant Cell* **2013**, *25*, 1868-1880.
[19] B. Christ, S. Schelbert, S. Aubry, I. Süssenbacher, T. Müller, B. Kräutler, S. Hörtensteiner, *Plant Physiology* **2011**, *158*, 628-641.
[20] C. Li, T. Erhart, X. Liu, B. Kräutler, *Chemistry* **2019**, *25*, 4052-4057.
[21] aM. Oberhuber, J. Berghold, K. Breuker, S. Hortensteiner, B. Krautler, *Proc Natl Acad Sci U S A* **2003**, *100*, 6910-6915; bB. Kräutler, *Angewandte Chemie International Edition* **2016**, *55*, 4882-4907.
[22] I. Süssenbacher, S. Hörtensteiner, B. Kräutler, *Angewandte Chemie International Edition* **2015**, *54*, 13777-13781.

[23] aM. Ulrich, S. Moser, T. Müller, B. Kräutler, *Chemistry – A European Journal* **2011**, *17*, 2330-2334; bS. Moser, M. Ulrich, T. Müller, B. Kräutler, *Photochemical & Photobiological Sciences* **2008**, *7*, 1577-1581.
[24] T. Erhart, S. Vergeiner, C. Kreutz, B. Kräutler, T. Müller, *Angewandte Chemie* **2018**, *130*.
[25] C. A. Karg, P. Wang, F. Kluibenschedl, T. Müller, L. Allmendinger, A. M. Vollmar, S. Moser, *European Journal of Organic Chemistry* **2020**, *2020*, 4499-4509.
[26] C. A. Karg, P. Wang, A. M. Vollmar, S. Moser, *Phytomedicine* **2019**, *60*, 152969.
[27] C. A. Karg, C. Doppler, C. Schilling, F. Jakobs, M. C. S. Dal Colle, N. Frey, D. Bernhard, A. M. Vollmar, S. Moser, *Food Chemistry* **2021**, *359*, 129906.
[28] C. A. Karg, C. M. Schilling, L. Allmendinger, S. Moser, *Journal of Porphyrins and Phthalocyanines* **2019**, *23*, 881-888.
[29] aC. A. Karg, S. Wang, N. Al Danaf, R. P. Pemberton, D. Bernard, M. Kretschmer, S. Schneider, T. Zisis, A. M. Vollmar, D. C. Lamb, S. Zahler, S. Moser, *Angew Chem Int Ed Engl* **2021**, *60*, 22578-22584; bT. D. Pollard, J. A. Cooper, *Science* **2009**, *326*, 1208-1212.
[30] C. A. Karg, L. Parráková, D. Fuchs, H. Schennach, B. Kräutler, S. Moser, J. M. Gostner, *Antioxidants* **2022**, *11*, 2056.
[31] C. A. Karg, C. M. Neubig, J. Roosen, S. Moser, *npj Science of Food* **2021**, *5*, 19.
[32] G. Pizzino, N. Irrera, M. Cucinotta, G. Pallio, F. Mannino, V. Arcoraci, F. Squadrito, D. Altavilla, A. Bitto, *Oxid Med Cell Longev* **2017**, *2017*, 8416763.
[33] M. Strohalm, D. Kavan, P. Novák, M. Volný, V. Havlícek, *Anal Chem* **2010**, *82*, 4648-4651.
[34] T. Müller, M. Rafelsberger, C. Vergeiner, B. Kräutler, *Angewandte Chemie International Edition* **2011**, *50*, 10724-10727.
[35] C. Vergeiner, M. Ulrich, C. Li, X. Liu, T. Müller, B. Kräutler, *Chemistry – A European Journal* **2015**, *21*, 136-149.
[36] I. F. F. Benzie, J. J. Strain, *Analytical Biochemistry* **1996**, *239*, 70-76.
[37] J. M. Gostner, S. Schroecksnadel, M. Jenny, A. Klein, F. Ueberall, H. Schennach, D. Fuchs, *Journal of the American College of Nutrition* **2015**, *34*, 212-223.
[38] A. YOKOMIZO, M. MORIWAKI, *Bioscience, Biotechnology, and Biochemistry* **2006**, *70*, 1317-1324.
[39] T. J. Guzik, K. M. Channon, in *Hypertension: Methods and Protocols* (Eds.: J. P. Fennell, A. H. Baker), Humana Press, Totowa, NJ, **2005**, pp. 73-89.
[40] S. Fleige, V. Walf, S. Huch, C. Prgomet, J. Sehm, M. W. Pfaffl, *Biotechnol Lett* **2006**, *28*, 1601-1613.
[41] M. M. Bradford, *Anal Biochem* **1976**, *72*, 248-254.
[42] D. Mittas, T. Kaserer, L. Siewert, S. Schwaiger, H. Stuppner, *Planta Med* **2022**, *88*, P-120.
[43] aM. C. Dias, D. Pinto, A. M. S. Silva, *Molecules* **2021**, *26*; bY. F. Zverev, A. Y. Rykunova, *Applied Biochemistry and Microbiology* **2022**, *58*, 1002-1020; cW. Wang, C. Sun, L. Mao, P. Ma, F. Liu, J. Yang, Y. Gao, *Trends in Food Science & Technology* **2016**, *56*, 21-38; dU. Mathesius, *Plants* **2018**, *7*, 30.

[44] G. A. F. Hendry, J. D. Houghton, S. B. Brown, *New Phytol* **1987**, *107*, 255-302.
[45] A. Gabrič, Ž. Hodnik, S. Pajk, *Pharmaceutics* **2022**, *14*, 325.
[46] K. C. Waterman, R. C. Adami, K. M. Alsante, J. Hong, M. S. Landis, F. Lombardo, C. J. Roberts, *Pharm Dev Technol* **2002**, *7*, 1-32.
[47] EMA, *Commitee for proprietary medicinal products (CPMP) & Committee for veterinary medicinal products (CVMP)* **1997**, https://www.ema.europa.eu/en/documents/scientific-guideline/note-guidance-inclusion-antioxidants-antimicrobial-preservatives-medicinal-products_en.pdf; accessed 28th August 2023.
[48] N. V. L. Yanishlieva, E. M. Marinova, *Lipid / Fett* **1992**, *94*, 374-379.
[49] F. Shahidi, P. K. Janitha, P. D. Wanasundara, *Critical Reviews in Food Science and Nutrition* **1992**, *32*, 67-103.
[50] D. Njus, P. M. Kelley, Y.-J. Tu, H. B. Schlegel, *Free Radical Biology and Medicine* **2020**, *159*, 37-43.
[51] J. M. Gostner, K. Becker, F. Ueberall, D. Fuchs, *Food and Chemical Toxicology* **2015**, *80*, 72-79.
[52] D. Zaknun, S. Schroecksnadel, K. Kurz, D. Fuchs, *Int Arch Allergy Immunol* **2012**, *157*, 113-124.
[53] E. Commission, **2023**, https://agriculture.ec.europa.eu/farming/crop-productions-and-plant-based-products/hops_de; accessed 27th August 2023.
[54] aL. Bocquet, S. Sahpaz, J. L. Hilbert, C. Rambaud, C. Rivière, *Phytochemistry Reviews* **2018**, *17*, 1047-1090; bJ. L. Bolton, T. L. Dunlap, A. Hajirahimkhan, O. Mbachu, S.-N. Chen, L. Chadwick, D. Nikolic, R. B. van Breemen, G. F. Pauli, B. M. Dietz, *Chemical Research in Toxicology* **2019**, *32*, 222-233.
[55] S. Moureu, J. Jacquin, J. Samaillie, C. Deweer, C. Rivière, J. Muchembled, *Microorganisms* **2023**, *11*.
[56] J. Gardea-Torresdey, M. Hejazi, K. Tiemann, J. G. Parsons, M. Duarte-Gardea, J. Henning, *J Hazard Mater* **2002**, *91*, 95-112.
[57] K. Jakubczyk, K. Janda, K. Watychowicz, J. Aukasiak, J. Wolska, *Roczniki Panstwowego Zakladu Higieny* **2018**, *69 2*, 119-126.
[58] aA. Gasparotto Junior, T. B. Prando, S. Leme Tdos, F. M. Gasparotto, E. L. Lourenço, Y. D. Rattmann, J. E. Da Silva-Santos, C. A. Kassuya, M. C. Marques, *J Ethnopharmacol* **2012**, *141*, 501-509; bA. Gasparotto Junior, F. M. Gasparotto, E. L. Lourenço, S. Crestani, M. E. Stefanello, M. J. Salvador, J. E. da Silva-Santos, M. C. Marques, C. A. Kassuya, *J Ethnopharmacol* **2011**, *134*, 363-372; cM. Kleinwächter, E. Schnug, D. Selmar, *J Agric Food Chem* **2008**, *56*, 11165-11170.
[59] aJ. Brondani, C. Cuelho, L. Marangoni, R. Lima, C. Guex, I. Bonilha, M. Manfron, *Boletin Latinoamericano y del Caribe de Plantas Medicinales y Aromaticas* **2016**, *15*; bP. N. Ravindran, G. S. Pillai, M. Divakaran, in *Handbook of Herbs and Spices (Second Edition)* (Ed.: K. V. Peter), Woodhead Publishing, **2012**, pp. 557-582.
[60] A. Gasparotto, Jr., M. A. Boffo, E. L. Lourenço, M. E. Stefanello, C. A. Kassuya, M. C. Marques, *J Ethnopharmacol* **2009**, *122*, 517-522.

[61] A. Bazylko, S. Granica, A. Filipek, J. Piwowarski, J. Stefańska, E. Osińska, A. K. Kiss, *Industrial Crops and Products* **2013**, *50*, 88-94.
[62] P. N. Brown, M. Chan, L. Paley, J. M. Betz, *J AOAC Int* **2011**, *94*, 1400-1410.
[63] C. Li, M. Ulrich, X. Liu, K. Wurst, T. Müller, B. Kräutler, *Chemical Science* **2014**, *5*, 3388-3395.
[64] R. Fu, P. Zhang, Z. Deng, G. Jin, Y. Guo, Y. Zhang, *Industrial Crops and Products* **2021**, *170*, 113699.
[65] B. Kräutler, P. Matile, *Accounts of Chemical Research* **1999**, *32*, 35-43.
[66] C. A. Karg, M. Taniguchi, J. S. Lindsey, S. Moser, *Planta Med* **2022**.
[67] D. Wakana, H. Kato, T. Momose, N. Sasaki, Y. Ozeki, Y. Goda, *Tetrahedron Letters* **2014**, *55*, 2982-2985.
[68] C. A. Karg, M. Taniguchi, J. S. Lindsey, S. Moser, *Planta Med* **2023**, *89*, 637-662.
[69] S. Vergeiner, B. Kräutler, *International Journal of Mass Spectrometry* **2014**, *365*.
[70] aJ. Berghold, K. Breuker, M. Oberhuber, S. Hörtensteiner, B. Kräutler, *Photosynth Res* **2002**, *74*, 109-119; bS. Moser, T. Müller, A. Holzinger, C. Lütz, B. Kräutler, *Chemistry* **2012**, *18*, 10873-10885; cS. Moser, T. Müller, M. Oberhuber, B. Kräutler, *European Journal of Organic Chemistry* **2009**, *2009*, 21-31.
[71] C. Li, K. Wurst, J. Berghold, M. Podewitz, K. R. Liedl, B. Kräutler, *Chemistry – A European Journal* **2018**, *24*, 2987-2998.
[72] aJ. Liu, H. Wang, R. G. Cooks, Z. Ouyang, *Analytical Chemistry* **2011**, *83*, 7608-7613; bJ. Liu, H. Wang, N. E. Manicke, J. M. Lin, R. G. Cooks, Z. Ouyang, *Anal Chem* **2010**, *82*, 2463-2471.
[73] aR. Apak, K. Güçlü, B. Demirata, M. Özyürek, S. E. Çelik, B. Bektaşoğlu, K. I. Berker, D. Özyurt, *Molecules* **2007**, *12*, 1496-1547; bX. Li, Q. Jiang, T. Wang, J. Liu, D. Chen, *Molecules* **2016**, *21*, 1246.
[74] U. Albrecht, K. H. Goos, B. Schneider, *Curr Med Res Opin* **2007**, *23*, 2415-2422.
[75] A. Gasparotto Junior, F. M. Gasparotto, M. A. Boffo, E. L. B. Lourenço, M. É. A. Stefanello, M. J. Salvador, J. E. da Silva-Santos, M. C. A. Marques, C. A. L. Kassuya, *Journal of Ethnopharmacology* **2011**, *134*, 210-215.
[76] E.-H. Lee, H.-J. Park, H.-Y. Jung, I.-K. Kang, B.-O. Kim, Y.-J. Cho, *3 Biotech* **2022**, *12*, 100.
[77] C. Gerhäuser, in *Beer in Health and Disease Prevention* (Ed.: V. R. Preedy), Academic Press, San Diego, **2009**, pp. 669-684.
[78] T. Hannan, P. Roberts, T. Riehl, S. van der Post, J. Binkley, D. Schwartz, H. Miyoshi, M. Mack, R. Schwendener, T. Hooton, T. Stappenbeck, G. Hansson, W. Stenson, M. Colonna, A. Stapleton, S. Hultgren, *EBioMedicine* **2014**, *28*.
[79] R. L. Prior, X. Wu, K. Schaich, *Journal of Agricultural and Food Chemistry* **2005**, *53*, 4290-4302.
[80] Q. Xiao, Y. Zhu, G. Cui, X. Zhang, R. Hu, Z. Deng, L. Lei, L. Wu, L. Mei, *Frontiers in Plant Science* **2022**, *13*.

[81] J. D. Keukeleire, I. Janssens, A. Heyerick, G. Ghekiere, J. Cambie, I. Roldan-Ruiz, E. V. Bockstaele, D. D. Keukeleire, *J Agric Food Chem* **2007**, *55*, 61-66.
[82] S. Afonso, M. Arrobas, E. L. Pereira, M. Â. Rodrigues, *Journal of Environmental Management* **2021**, *284*, 112105.
[83] V. Macchioni, V. Picchi, K. Carbone, *Plants (Basel)* **2021**, *11*.
[84] N. Kanai, K. Nishimura, S. Umetani, Y. Saito, H. Saito, T. Oyama, I. Kawamura, *ACS Agricultural Science & Technology* **2021**, *1*, 347-354.
[85] F. C. Pennington, H. H. Strain, W. A. Svec, J. J. Katz, *Journal of the American Chemical Society* **1964**, *86*, 1418-1426.
[86] N. Engel, C. Curty, A. Gossauer, *Plant Physiology and Biochemistry* **1996**, *34*, 77-83.
[87] W. Mühlecker, B. Kräutler, S. Ginsburg, P. Matile, *Helvetica Chimica Acta* **1993**, *76*, 2976-2980.
[88] H. Nakamura, B. Musicki, Y. Kishi, O. Shimomura, *Journal of the American Chemical Society* **1988**, *110*, 2683-2685.
[89] H. Nakamura, Y. Kishi, O. Shimomura, D. Morse, J. W. Hastings, *Journal of the American Chemical Society* **1989**, *111*, 7607-7611.
[90] A. A. Khan, M. Iadarola, H. Y. Yang, R. A. Dionne, *J Pain* **2007**, *8*, 349-354.
[91] S. Chan, S. Boyce, C. Brideau, S. Charleson, W. Cromlish, D. Ethier, J. Evans, A. Ford-Hutchinson, M. Forrest, J. Gauthier, R. Gordon, M. Gresser, J. Guay, S. Kargman, B. Kennedy, Y. Leblanc, S. Leger, J. Mancini, Neill, Riendeau, *Iranian Journal of Pharmacology and Therapeutics* **1999**, *290*.
[92] T. J. Hannan, P. L. Roberts, T. E. Riehl, S. van der Post, J. M. Binkley, D. J. Schwartz, H. Miyoshi, M. Mack, R. A. Schwendener, T. M. Hooton, T. S. Stappenbeck, G. C. Hansson, W. F. Stenson, M. Colonna, A. E. Stapleton, S. J. Hultgren, *EBioMedicine* **2014**, *1*, 46-57.
[93] X.-q. Bao, Y.-c. Huang, F. Chen, *Evidence-Based Complementary and Alternative Medicine* **2019**, *2019*, 8424872.
[94] aL. Vitek, C. Bellarosa, C. Tiribelli, *Clin Pharmacol Ther* **2019**, *106*, 568-575; bL. Vítek, M. Jirsa, M. Brodanová, M. Kalab, Z. Marecek, V. Danzig, L. Novotný, P. Kotal, *Atherosclerosis* **2002**, *160*, 449-456.
[95] M. E. Vogel, G. Idelman, E. S. Konaniah, S. D. Zucker, *J Am Heart Assoc* **2017**, *6*, e004820.
[96] S. Higuchi, Y. Kabeya, J. Uchida, K. Kato, N. Tsukada, *Scientific reports* **2018**, *8*, 6473-6473.
[97] aD. E. Stec, K. John, C. J. Trabbic, A. Luniwal, M. W. Hankins, J. Baum, T. D. Hinds, Jr., *PLoS One* **2016**, *11*, e0153427-e0153427; bD. M. Gordon, S. H. Hong, Z. A. Kipp, T. D. Hinds, Jr., *Molecules (Basel, Switzerland)* **2021**, *26*, 2975.
[98] C. P. Soto Conti, *Arch Argent Pediatr* **2021**, *119*, e18-e25.
[99] C. Weber, H. Noels, *Nat Med* **2011**, *17*, 1410-1422.
[100] J. C. Brown, T. E. Gerhardt, E. Kwon, in *StatPearls*, StatPearls Publishing
Copyright © 2023, StatPearls Publishing LLC., Treasure Island (FL) ineligible companies. Disclosure: Thomas Gerhardt declares no relevant financial relationships with ineligible companies. Disclosure: Edward Kwon declares no relevant financial relationships with ineligible companies., **2023**.

[101] M. Kloc, A. Uosef, J. Z. Kubiak, R. M. Ghobrial, *International Journal of Molecular Sciences* **2021**, *22*, 216.
[102] G. K. Hansson, *N Engl J Med* **2005**, *352*, 1685-1695.
[103] M. A. Gimbrone, Jr., G. García-Cardeña, *Cardiovasc Pathol* **2013**, *22*, 9-15.
[104] D. Berg, M. B. Youdim, P. Riederer, *Cell Tissue Res* **2004**, *318*, 201-213.
[105] P. D. Ray, B. W. Huang, Y. Tsuji, *Cell Signal* **2012**, *24*, 981-990.
[106] A. Shaito, K. Aramouni, R. Assaf, A. Parenti, A. Orekhov, A. E. Yazbi, G. Pintus, A. H. Eid, *Front Biosci (Landmark Ed)* **2022**, *27*, 105.
[107] K. Brieger, S. Schiavone, F. J. Miller Jr, K.-H. Krause, *Swiss Medical Weekly* **2012**, *142*, w13659.
[108] aW. M. Nauseef, *Current Opinion in Immunology* **2019**, *60*, 130-140; bR. Rastogi, X. Geng, F. Li, Y. Ding, *Frontiers in Cellular Neuroscience* **2017**, *10*.
[109] aA. L. Sylvester, D. X. Zhang, S. Ran, N. S. Zinkevich, *Biomolecules* **2022**, *12*, 823; bS. Rajagopalan, S. Kurz, T. Münzel, M. Tarpey, B. A. Freeman, K. K. Griendling, D. G. Harrison, *J Clin Invest* **1996**, *97*, 1916-1923.
[110] aR. Russo, F. Cattaneo, P. Lippiello, C. Cristiano, F. Zurlo, M. Castaldo, C. Irace, T. Borsello, R. Santamaria, R. Ammendola, A. Calignano, M. C. Miniaci, *Neurobiology of Aging* **2018**, *68*, 123-133; bU. Ganguly, U. Kaur, S. S. Chakrabarti, P. Sharma, B. K. Agrawal, L. Saso, S. Chakrabarti, *Oxidative Medicine and Cellular Longevity* **2021**, *2021*, 7086512.
[111] aM. Romo-González, C. Ijurko, Á. Hernández-Hernández, *Frontiers in Immunology* **2022**, *13*; bI. Szanto, *Int J Mol Sci* **2022**, *23*.
[112] aS. Elumalai, U. Karunakaran, J.-S. Moon, K.-C. Won, *Cells* **2021**, *10*, 1573; bA. Nascè, K. Gariani, F. R. Jornayvaz, I. Szanto, *Antioxidants* **2022**, *11*, 1131.
[113] A. Panday, M. K. Sahoo, D. Osorio, S. Batra, *Cellular & Molecular Immunology* **2015**, *12*, 5-23.
[114] *Antioxidants & Redox Signaling* **2005**, *7*, 308-317.
[115] N. Xia, S. Tenzer, O. Lunov, M. Karl, T. Simmet, A. Daiber, T. Münzel, G. Reifenberg, U. Förstermann, H. Li, *Frontiers in Physiology* **2021**, *12*.
[116] K. K. Griendling, C. A. Minieri, J. D. Ollerenshaw, R. W. Alexander, *Circulation Research* **1994**, *74*, 1141-1148.
[117] R. P. Brandes, J. Kreuzer, *Cardiovasc Res* **2005**, *65*, 16-27.
[118] K. D. Martyn, L. M. Frederick, K. von Loehneysen, M. C. Dinauer, U. G. Knaus, *Cell Signal* **2006**, *18*, 69-82.
[119] K. Bedard, K. H. Krause, *Physiol Rev* **2007**, *87*, 245-313.
[120] Y. Nakashima, E. W. Raines, A. S. Plump, J. L. Breslow, R. Ross, *Arteriosclerosis, Thrombosis, and Vascular Biology* **1998**, *18*, 842-851.
[121] A. J. Lusis, *Nature* **2000**, *407*, 233-241.
[122] K. J. Moore, F. J. Sheedy, E. A. Fisher, *Nat Rev Immunol* **2013**, *13*, 709-721.
[123] A. C. Doran, N. Meller, C. A. McNamara, *Arteriosclerosis, Thrombosis, and Vascular Biology* **2008**, *28*, 812-819.
[124] B. A. Imhof, M. Aurrand-Lions, *Nature Reviews Immunology* **2004**, *4*, 432-444.
[125] aK. Konstantopoulos, S. Kukreti, C. W. Smith, L. V. McIntire, *J Leukoc Biol* **1997**, *61*, 179-187; bW. A. Muller, *Annu Rev Pathol* **2011**, *6*, 323-344.

[126] S. J. George, *Curr Opin Lipidol* **1998**, *9*, 413-423.
[127] aA. Yabluchanskiy, Y. Ma, R. P. Iyer, M. E. Hall, M. L. Lindsey, *Physiology (Bethesda)* **2013**, *28*, 391-403; bY. Konstantino, T. T. Nguyen, R. Wolk, R. J. Aiello, S. G. Terra, D. A. Fryburg, *Biomarkers* **2009**, *14*, 118-129.
[128] aG. V. Halade, Y. F. Jin, M. L. Lindsey, *Pharmacol Ther* **2013**, *139*, 32-40; bR. Fridman, M. Toth, I. Chvyrkova, S. O. Meroueh, S. Mobashery, *Cancer and Metastasis Reviews* **2003**, *22*, 153-166.
[129] A. M. Pereira, M. Strasberg-Rieber, M. Rieber, *Clin Exp Metastasis* **2005**, *22*, 285-295.
[130] H. Nagase, R. Visse, G. Murphy, *Cardiovascular Research* **2006**, *69*, 562-573.
[131] A. Luttun, E. Lutgens, A. Manderveld, K. Maris, D. Collen, P. Carmeliet, L. Moons, *Circulation* **2004**, *109*, 1408-1414.
[132] T. Erhart, C. Mittelberger, X. Liu, M. Podewitz, C. Li, G. Scherzer, G. Stoll, J. Valls, P. Robatscher, K. R. Liedl, M. Oberhuber, B. Kräutler, *Chemistry – A European Journal* **2018**, *24*, 17268-17279.
[133] J. Saffari-Chaleshtori, A. Shojaeian, E. Heidarian, S. M. Shafiee, *Cancer Invest* **2021**, *39*, 721-733.
[134] S. D. Zucker, P. S. Horn, K. E. Sherman, *Hepatology* **2004**, *40*, 827-835.
[135] U. Förstermann, N. Xia, H. Li, *Circ Res* **2017**, *120*, 713-735.
[136] J. Zheng, T. Inoguchi, S. Sasaki, Y. Maeda, M. F. McCarty, M. Fujii, N. Ikeda, K. Kobayashi, N. Sonoda, R. Takayanagi, *American Journal of Physiology-Regulatory, Integrative and Comparative Physiology* **2013**, *304*, R110-R120.
[137] R. S. Frey, M. Ushio-Fukai, A. B. Malik, *Antioxid Redox Signal* **2009**, *11*, 791-810.
[138] M. Fujii, T. Inoguchi, S. Sasaki, Y. Maeda, J. Zheng, K. Kobayashi, R. Takayanagi, *Kidney Int* **2010**, *78*, 905-919.
[139] F. Xia, C. Wang, Y. Jin, Q. Liu, Q. Meng, K. Liu, H. Sun, *J Atheroscler Thromb* **2014**, *21*, 768-783.
[140] P. Keshavan, T. Deem, S. Schwemberger, G. Babcock, J. Cook-Mills, S. Zucker, *Journal of immunology (Baltimore, Md. : 1950)* **2005**, *174*, 3709-3718.
[141] M. Yin, C. Li, J. jiang, J. Le, B. Luo, F. Yang, Y. Fang, M. Yang, Z. Deng, W. Ni, J. Shao, *Biochemical Pharmacology* **2021**, *186*, 114471.
[142] H. Laronha, I. Carpinteiro, J. Portugal, A. Azul, M. Polido, K. T. Petrova, M. Salema-Oom, I. Barahona, J. Caldeira, *Biomedicines* **2021**, *9*.
[143] aA. Mauro, M. Buscemi, A. Gerbino, *Journal of Molecular Histology* **2010**, *41*, 367-377; bJ. M. Florence, A. Krupa, L. M. Booshehri, T. C. Allen, A. K. Kurdowska, *PLoS One* **2017**, *12*, e0171427.
[144] C. Napoli, L. O. Lerman, F. d. Nigris, M. Gossl, M. L. Balestrieri, A. Lerman, *Circulation* **2006**, *114*, 2517-2527.
[145] M. A. Gimbrone, Jr., G. García-Cardeña, *Circ Res* **2016**, *118*, 620-636.
[146] S. Sitia, L. Tomasoni, F. Atzeni, G. Ambrosio, C. Cordiano, A. Catapano, S. Tramontana, F. Perticone, P. Naccarato, P. Camici, E. Picano, L. Cortigiani, M. Bevilacqua, L. Milazzo, D. Cusi, C. Barlassina, P. Sarzi-Puttini, M. Turiel, *Autoimmunity Reviews* **2010**, *9*, 830-834.

[147] B. Lener, R. Kozieł, H. Pircher, E. Hütter, R. Greussing, D. Herndler-Brandstetter, M. Hermann, H. Unterluggauer, P. Jansen-Dürr, *Biochem J* **2009**, *423*, 363-374.
[148] T. Inoguchi, H. Nawata, *Curr Drug Targets* **2005**, *6*, 495-501.
[149] S. Lanone, S. Bloc, R. Foresti, A. Almolki, C. Taillé, J. Callebert, M. Conti, D. Goven, M. Aubier, B. Dureuil, J. El-Benna, R. Motterlini, J. Boczkowski, *Faseb j* **2005**, *19*, 1890-1892.
[150] J. Y. Kwak, K. Takeshige, B. S. Cheung, S. Minakami, *Biochim Biophys Acta* **1991**, *1076*, 369-373.
[151] U. K. Schmerwitz, G. Sass, A. G. Khandoga, J. Joore, B. A. Mayer, N. Berberich, F. Totzke, F. Krombach, G. Tiegs, S. Zahler, A. M. Vollmar, R. Fürst, *Arteriosclerosis, Thrombosis, and Vascular Biology* **2011**, *31*, 280-288.
[152] Q. Wang, C. M. Doerschuk, *J Immunol* **2000**, *164*, 6487-6494.
[153] S. R. Perri, B. Annabi, J. Galipeau, *The FASEB Journal* **2007**, *21*, 3928-3936.
[154] L. Wang, X. Li, S. Zhang, W. Lu, S. Liao, X. Liu, L. Shan, X. Shen, H. Jiang, W. Zhang, J. Huang, H. Li, *Bioorganic & Medicinal Chemistry* **2012**, *20*, 4164-4171.
[155] T. L. Deem, J. M. Cook-Mills, *Blood* **2004**, *104*, 2385-2393.
[156] J. Cook-Mills, *Cellular and molecular biology (Noisy-le-Grand, France)* **2006**, *52*, 8-16.
[157] H. E. Matheny, T. L. Deem, J. M. Cook-Mills, *The Journal of Immunology* **2000**, *164*, 6550-6559.
[158] P. E. Szmitko, C.-H. Wang, R. D. Weisel, G. A. Jeffries, T. J. Anderson, S. Verma, *Circulation* **2003**, *108*, 2041-2048.
[159] G. Wen, L. Yao, Y. Hao, J. Wang, J. Liu, *Journal of Translational Medicine* **2022**, *20*, 1.
[160] J. Liu, H. Dong, Y. Zhang, M. Cao, L. Song, Q. Pan, A. Bulmer, D. B. Adams, X. Dong, H. Wang, *Scientific Reports* **2015**, *5*, 9886.
[161] J. Neuzil, R. Stocker, *J Biol Chem* **1994**, *269*, 16712-16719.
[162] aI. A. Sobenin, J. T. Salonen, A. V. Zhelankin, A. A. Melnichenko, J. Kaikkonen, Y. V. Bobryshev, A. N. Orekhov, *BioMed Research International* **2014**, *2014*, 205697; bH. Esterbauer, J. Gebicki, H. Puhl, G. Jürgens, *Free Radical Biology and Medicine* **1992**, *13*, 341-390.
[163] J. S. Wright, E. R. Johnson, G. A. DiLabio, *Journal of the American Chemical Society* **2001**, *123*, 1173-1183.
[164] S. Dudonné, X. Vitrac, P. Coutière, M. Woillez, J. M. Mérillon, *J Agric Food Chem* **2009**, *57*, 1768-1774.
[165] D. Huang, B. Ou, M. Hampsch-Woodill, J. A. Flanagan, R. L. Prior, *Journal of Agricultural and Food Chemistry* **2002**, *50*, 4437-4444.

APPENDIX

8. Appendix

8.1 Supplementary Information

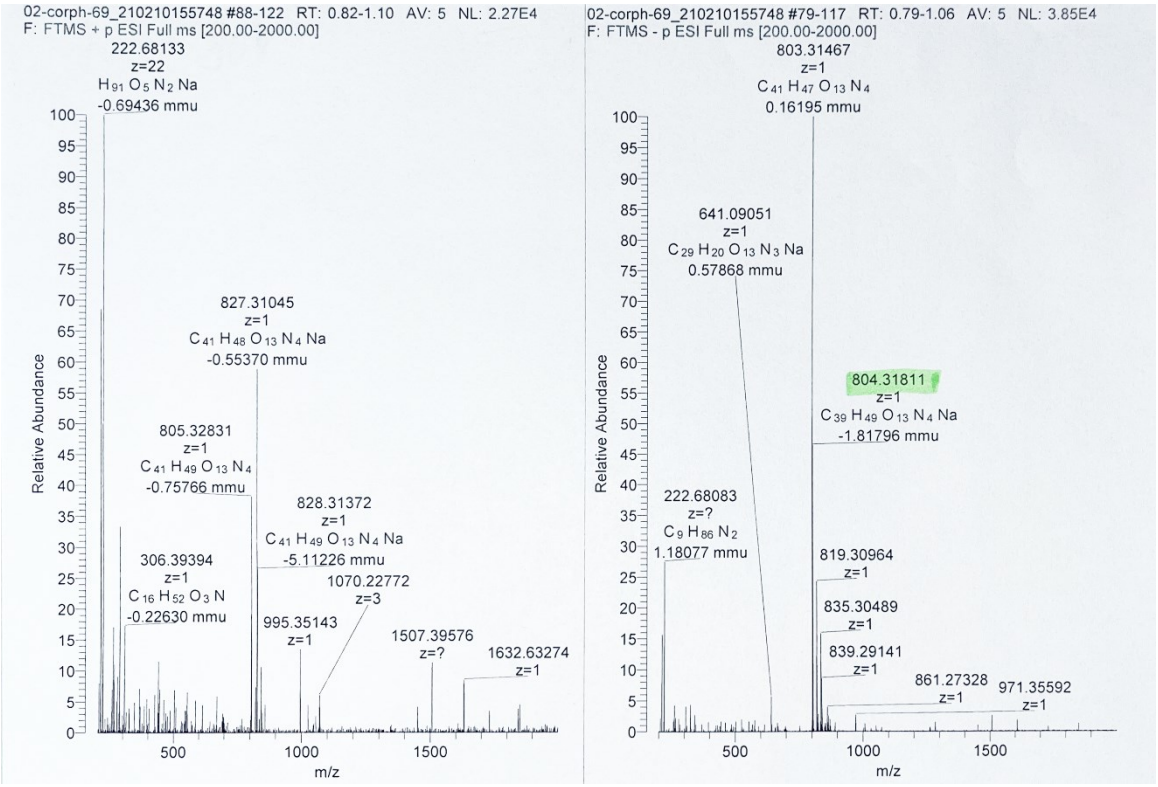

Supplementary Figure 1 HR-ESI-MS of *Ep*-PxB-5. Calculated exact mass for $C_{41}H_{48}O_{13}N_4$: 804,32179 g/mol. ESI-MS (m/z) for $C_{41}H_{48}O_{13}N_4$ $[M+H]^+$ found at 805,32831; $[M-H]^-$ found at 803,31467.

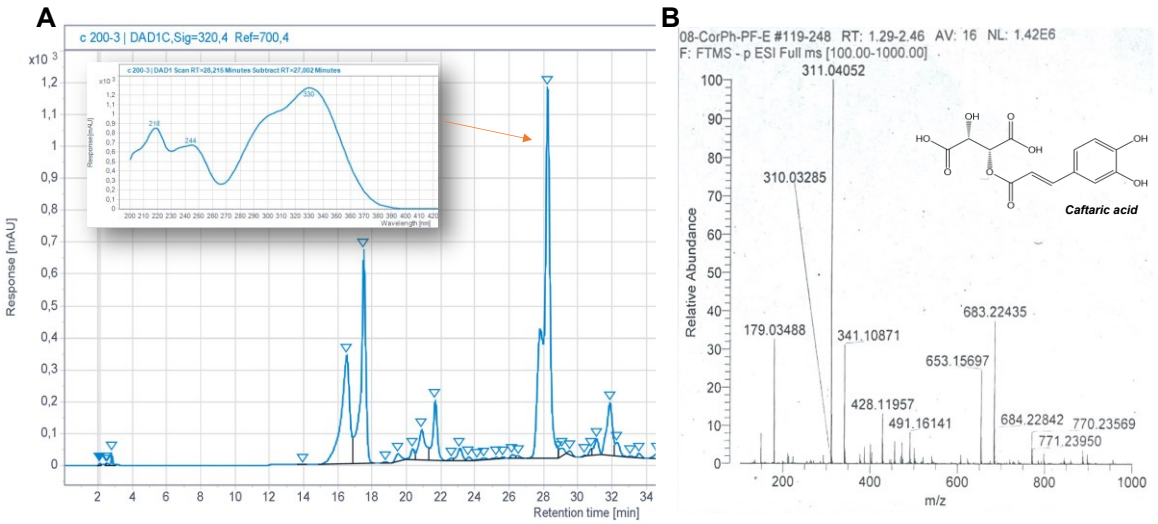

Supplementary Figure 2 (A) analytical HPL chromatogram of fresh Echinacea ratiopharm extract at day 0 and UV spectrum of highest peak. (320 nm, HPLC method Nr. 5) **(B) HR-ESI-MS** of collected substance corresponding to the peak at 28 min of **(A)**. Calculated exact mass for caftaric acid $C_{13}H_{12}O_9$: 312,23000 g/mol. ESI-MS (m/z) for $C_{13}H_{12}O_9$ $[M-H]^-$ found at 311.045042.

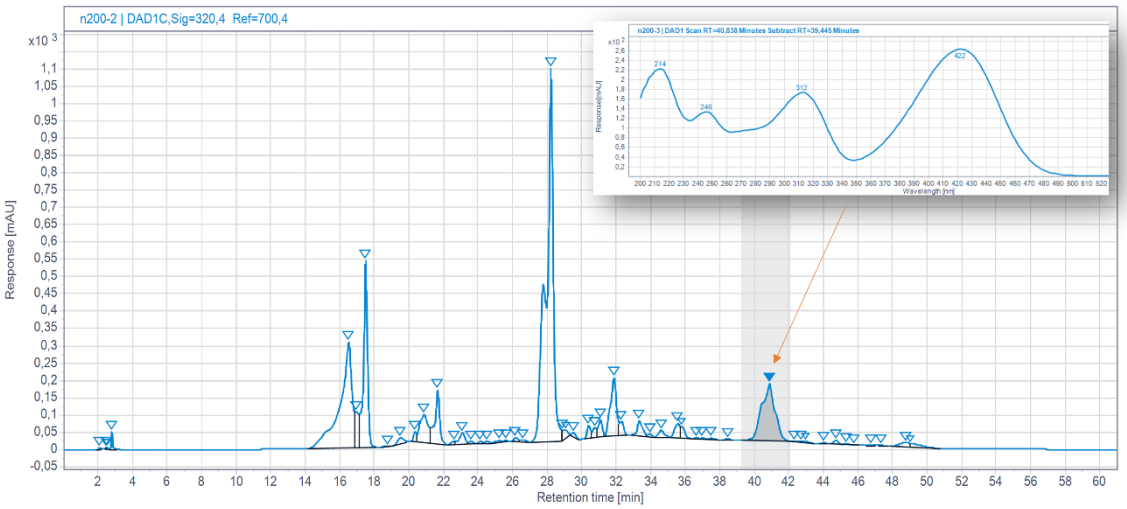

Supplementary Figure 3 analytical HPL chromatogram of fresh Echinacea ratiopharm extract with spiked *Ep*-PxB-5 at day 0 and UV spectrum of *Ep*-PxB-5. (320 nm, HPLC method Nr. 5)

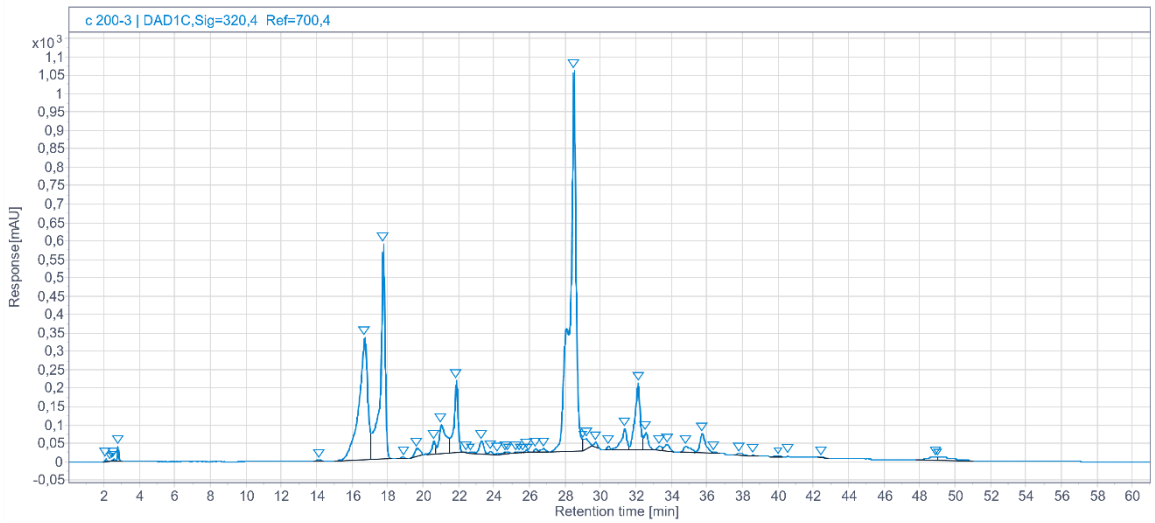

Supplementary Figure 4 analytical HPL chromatogram of Echinacea ratiopharm extract at day 0. (320 nm, HPLC method Nr. 5)

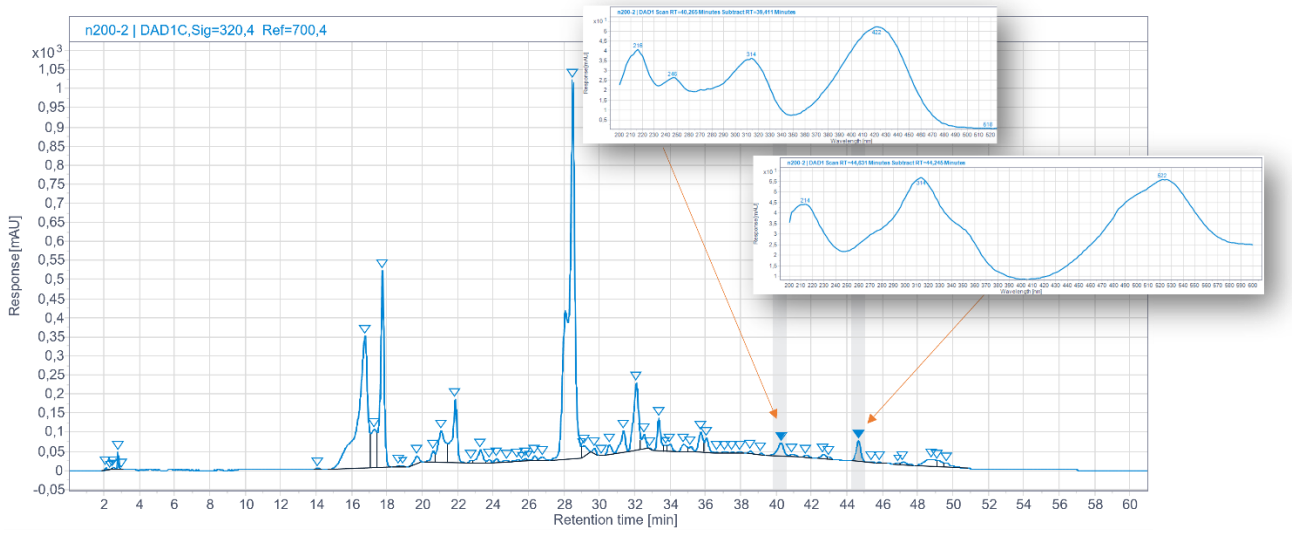

Supplementary Figure 5 analytical HPL chromatogram of Echinacea ratiopharm extract with spiked *Ep*-PxB-5 at day 10 and UV spectrum of *Ep*-PxB-5 and formed corresponding PrB. (320 nm, HPLC method Nr. 5)

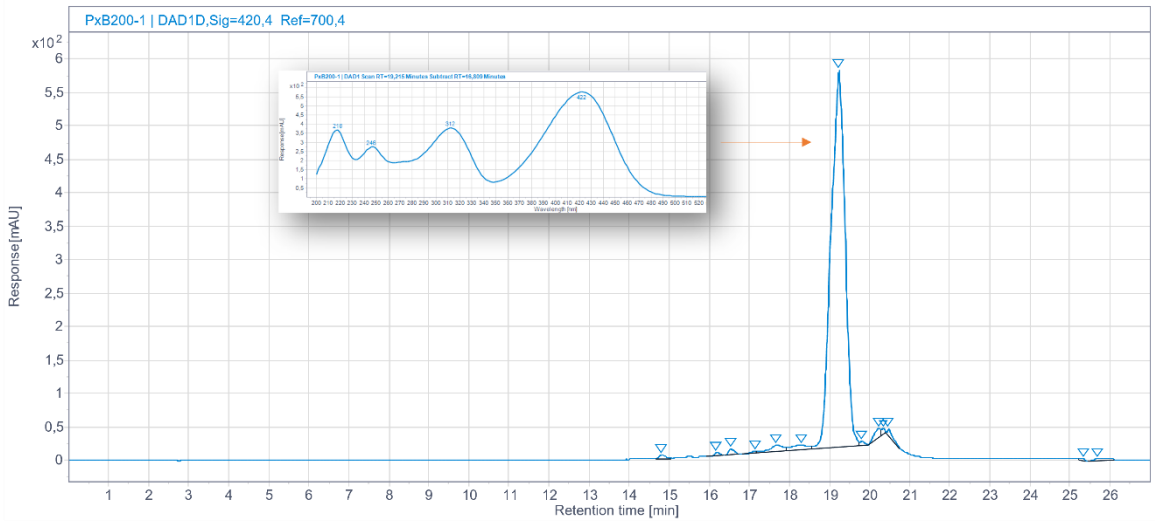

Supplementary Figure 6 analytical HPL chromatogram of Ep-PxB-5 in EtOH 22% at day 0. (420 nm, HPLC method Nr. 4)

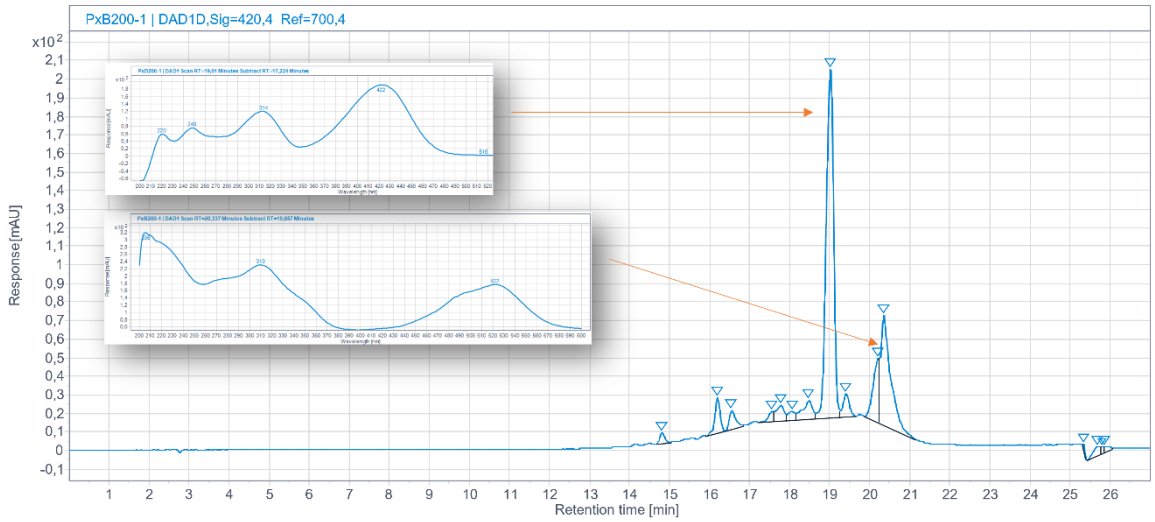

Supplementary Figure 7 analytical HPL chromatogram of *Ep*-PxB-5 in EtOH 22% at day 10 and UV spectra of *Ep*-PxB-5 and corresponding PrB. (420 nm, HPLC method Nr. 4)

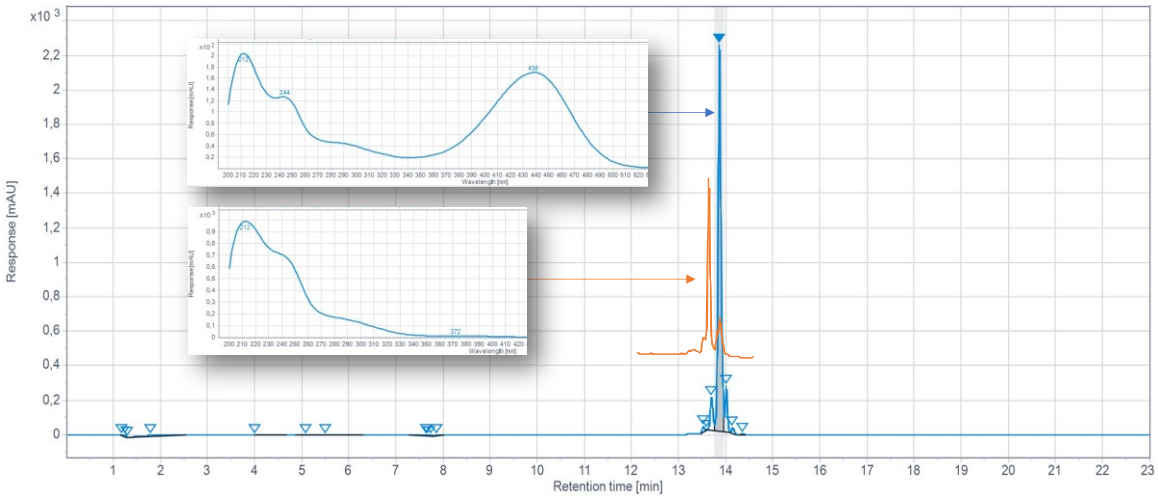

Supplementary Figure 8 HPLC trace overlay of isolated *Hl*-PleB (orange, 220 nm) and *Hl*-DPxB (blue, 420 nm) with characteristic UV spectra. Substances were provided by Christian Nadegger (University of Innsbruck). HPLC method Nr.1

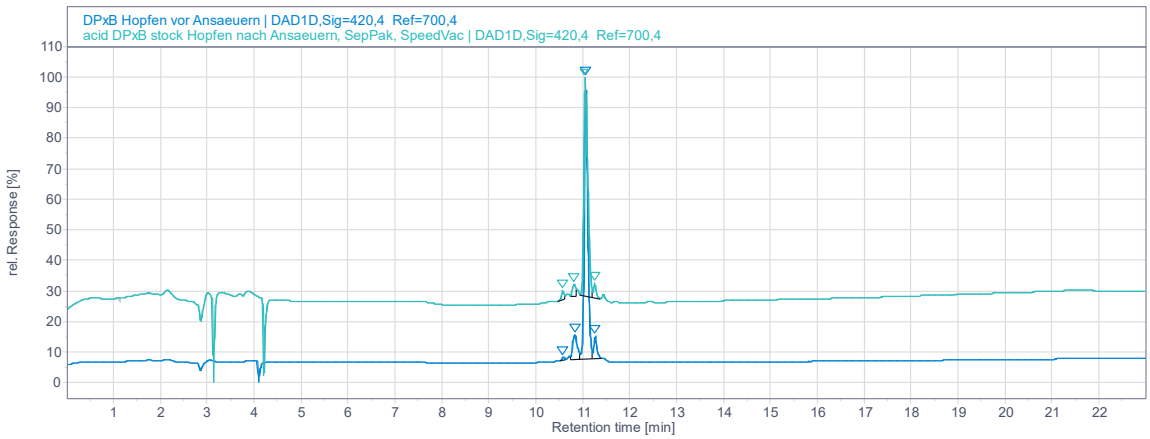

Supplementary Figure 9 Overlay of HPL chromatograms of *Hl*-DPxB before and after acidifying. (420 nm, HPLC method Nr. 1)

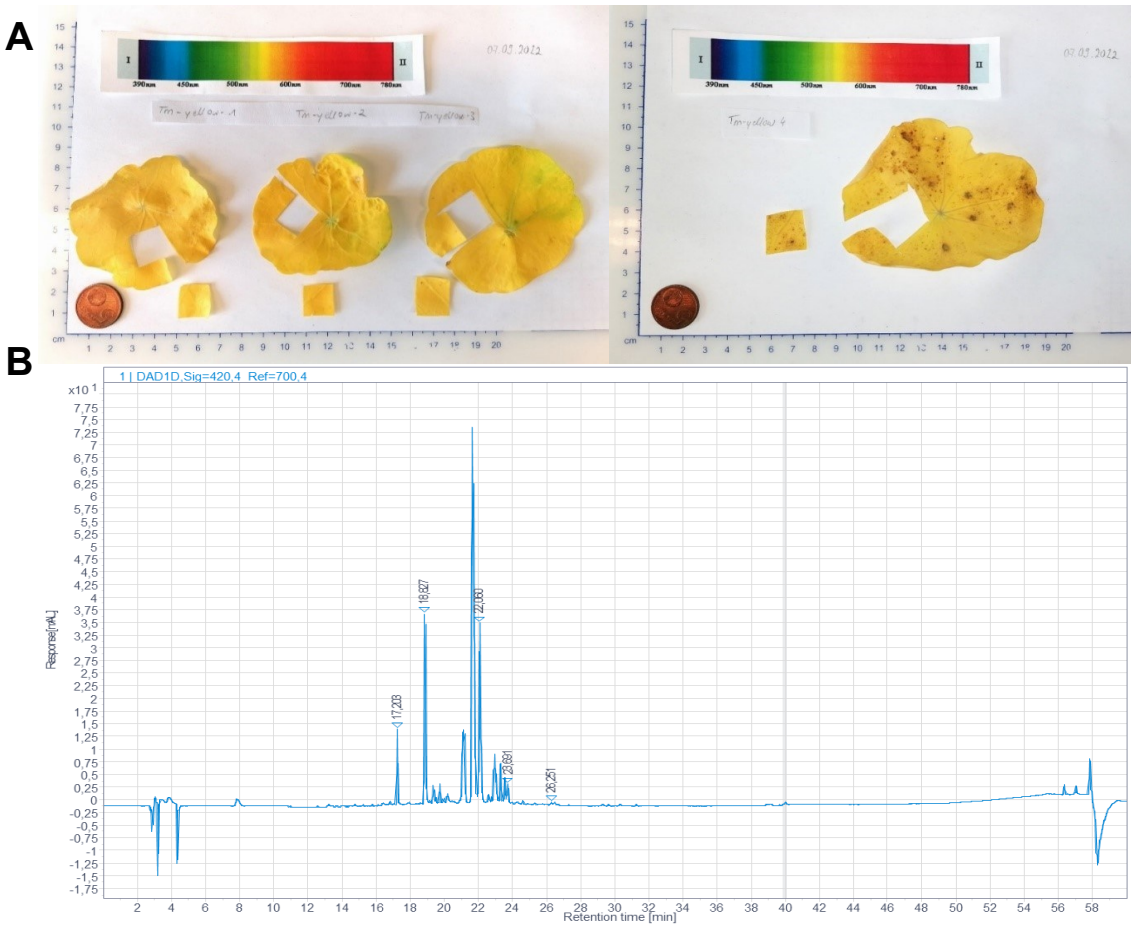

Supplementary Figure 10 Chemoprofiling of Tropaeolum majus leaves. (A) Leaf samples and areas of yellow nasturtium leaves used for extract preparation. **(B)** Analytical HPL chromatogram of sample *Tm*-yellow-1 from **(A)**. PxBs were identified by their characteristic UV spectra and retention times. Both, the E and Z isomer were identified[23a] at 17.2 min and 18.8 min, respectively (420 nm, HPLC method Nr. 3).

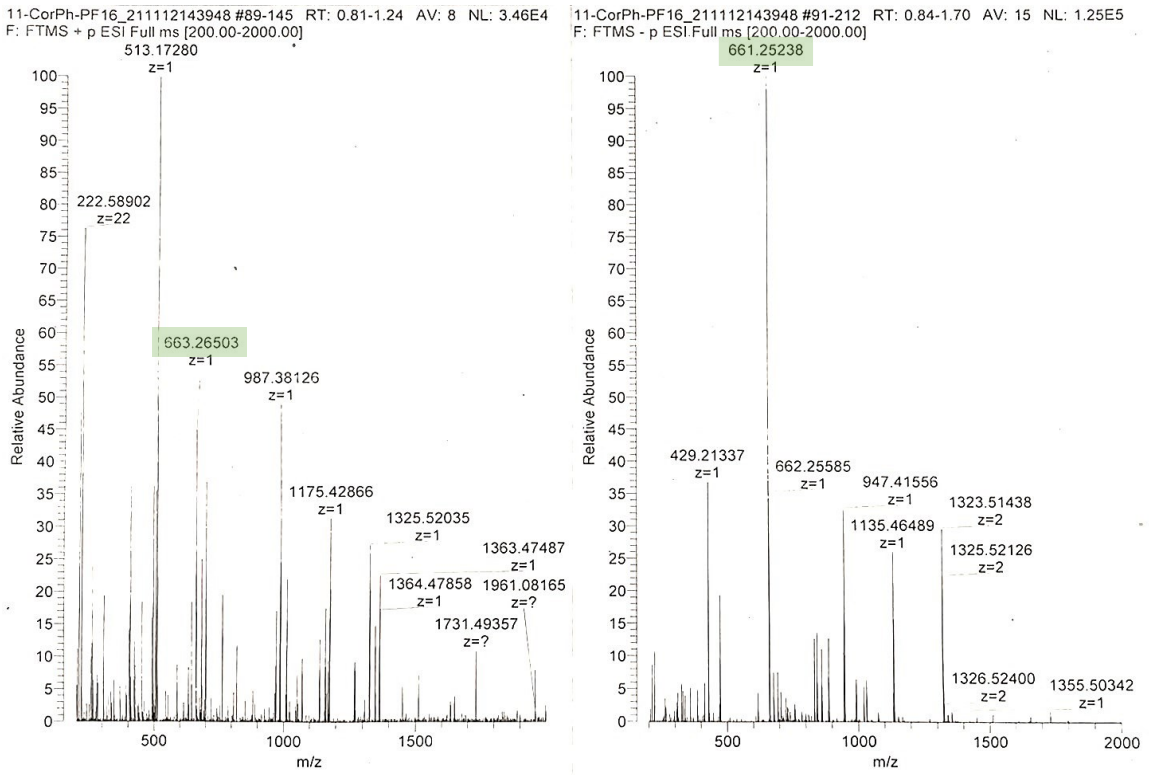

Supplementary Figure 11 HR-ESI-MS of *Tm*-PxB-1. m/z_{found} = 661.25238 $[M-H]^-$; $m/z_{calculated}$ ($C_{34}H_{37}N_4O_{10}$) = 661.251517 (Δ = 1.306 ppm)

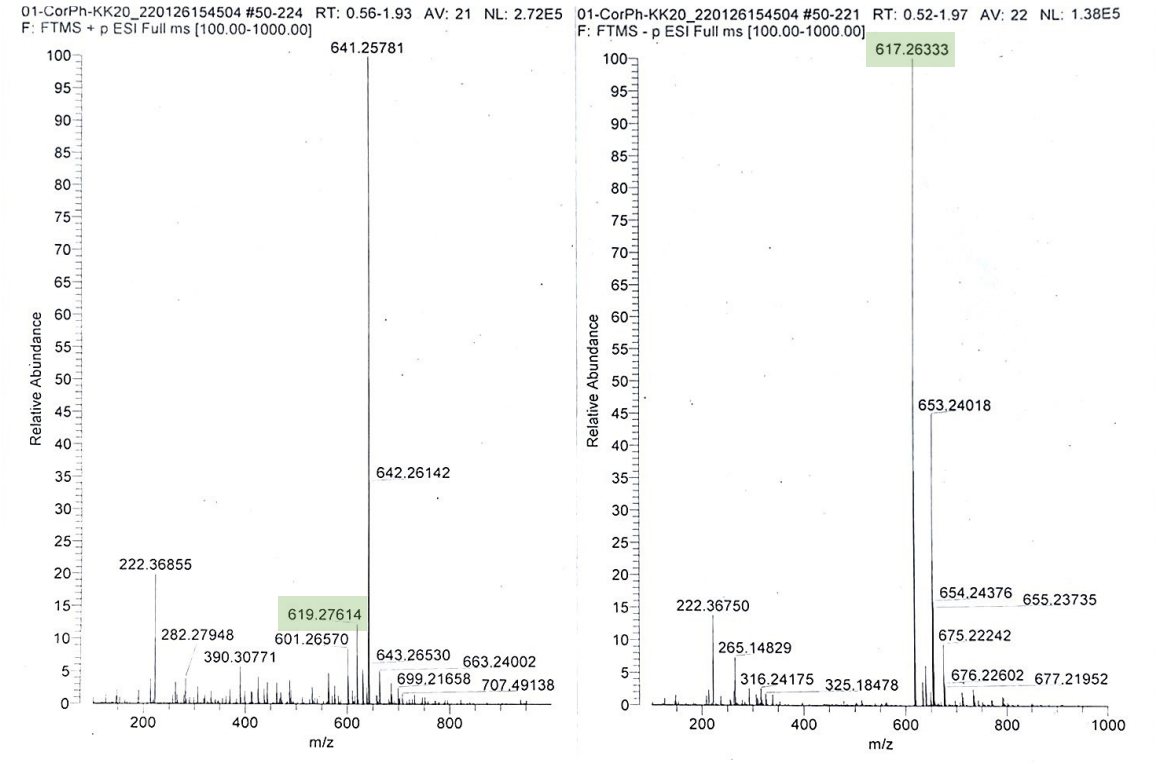

Supplementary Figure 12 HR-ESI-MS of *Tm*-PxB-2. m/z_{found} = 617.26333 $[M-H]^-$; $m/z_{calculated}$ ($C_{33}H_{37}N_4O_8$) = 617.261688 (Δ = 2.660 ppm).

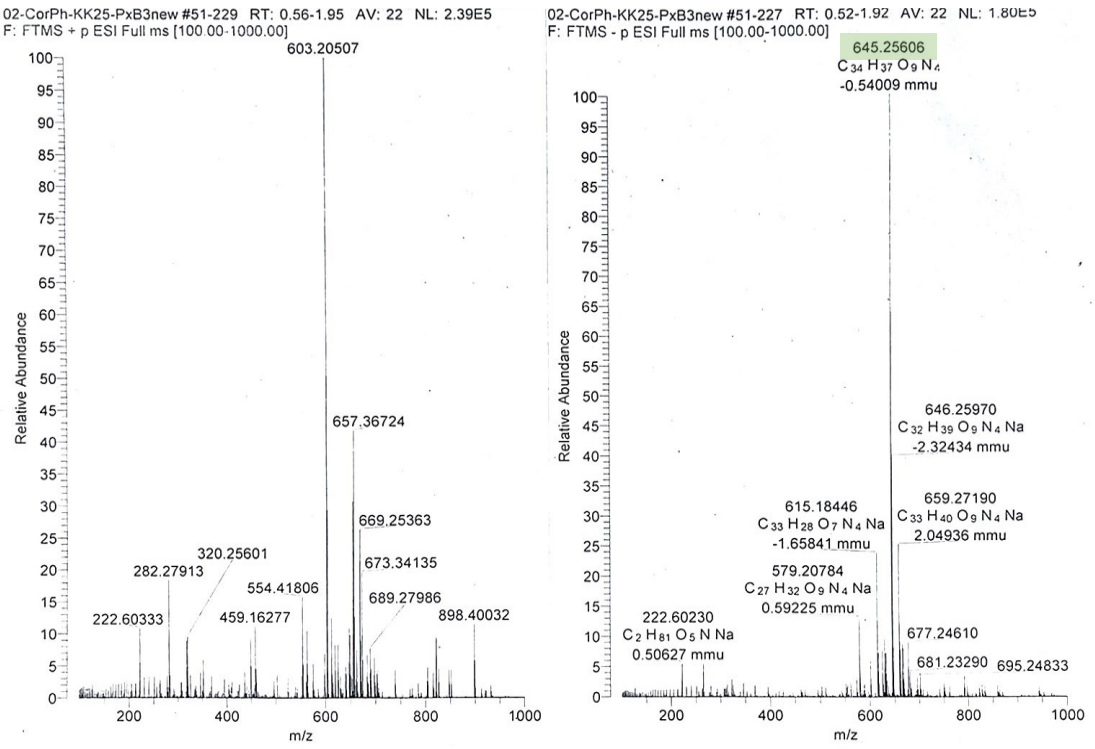

Supplementary Figure 13 HR-ESI-MS of *Tm*-PxB-3. m/z_{found} = 645.25606 $[M-H]^-$; $m/z_{calculated}$ ($C_{34}H_{37}N_4O_9$) = 645.256602 (Δ = -0.840 ppm).

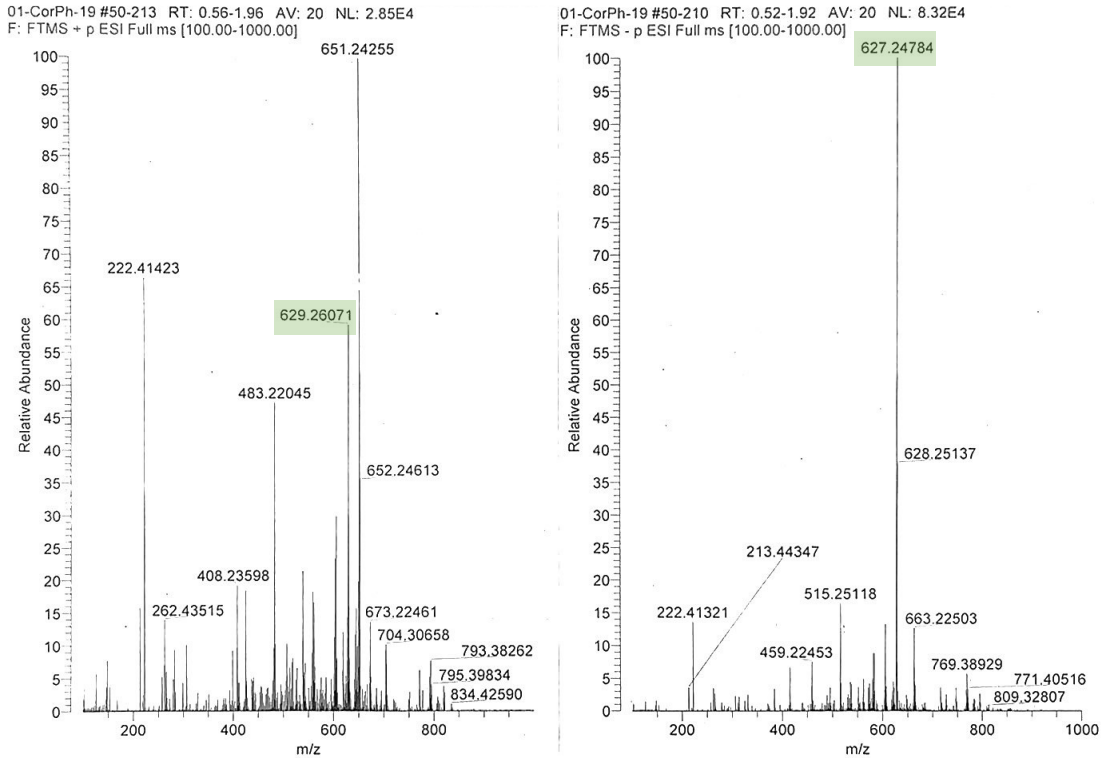

Supplementary Figure 14 HR-ESI-MS of *Tm*-PxB-4. m/z_{found} = 627.24784 [M-H]-; $m/zc_{alculated}$ (C34H35N4O8) = 627.246038 (Δ = 2.873 ppm).

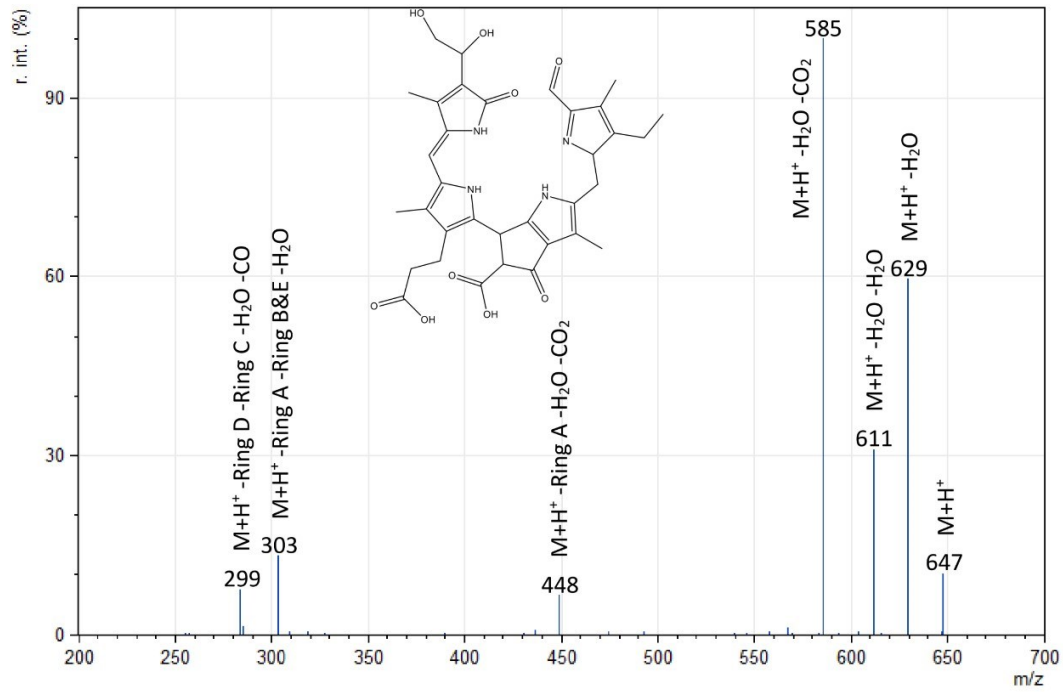

Supplementary Figure 15 MS² ESI mass spectrum of *Tm*-PxB-1. Fragmentation of $[M+H]^+$ at a normalized collision energy of 10.

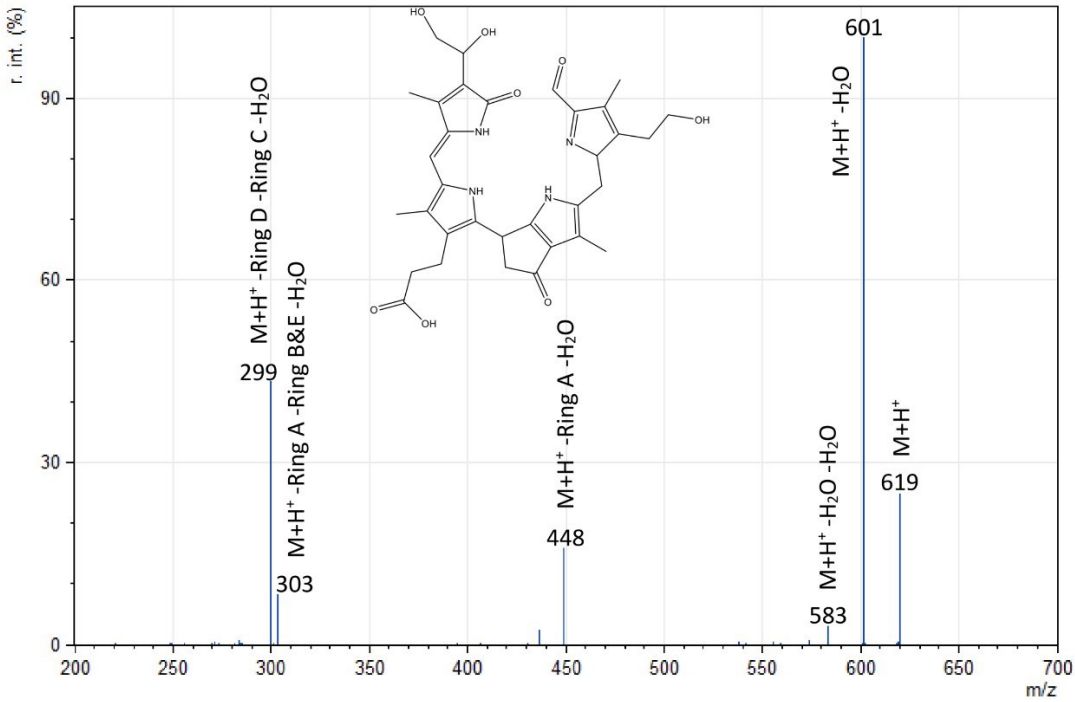

Supplementary Figure 16 MS² ESI mass spectrum of *Tm*-PxB-2. Fragmentation of $[M+H]^+$ at a normalized collision energy of 14.

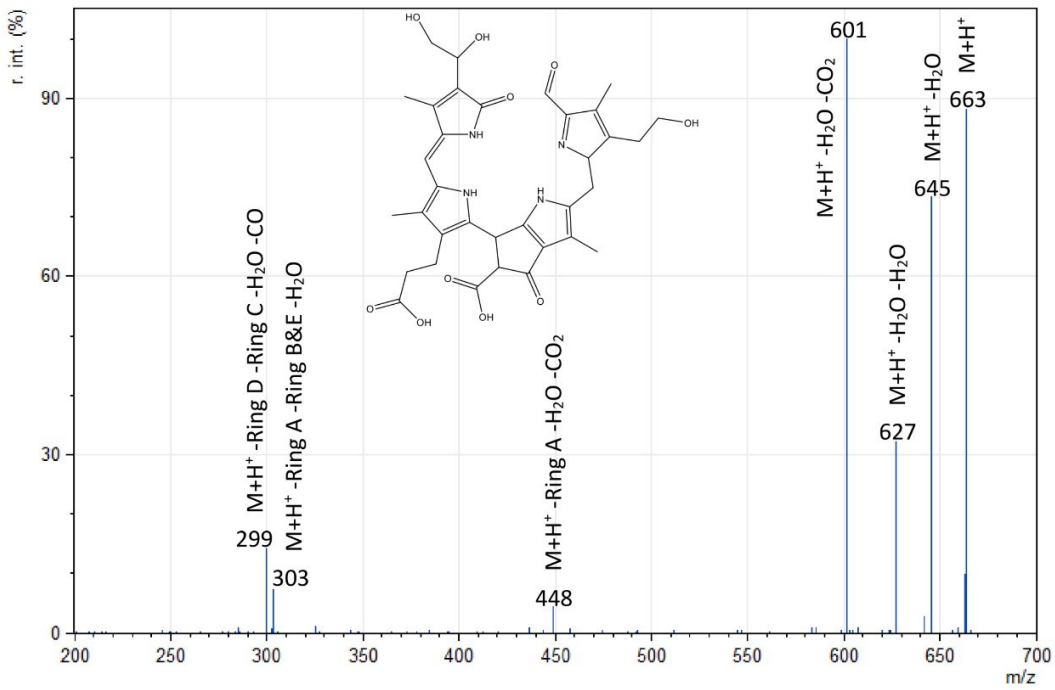

Supplementary Figure 17 MS² ESI mass spectrum of *Tm*-PxB-3. Fragmentation of $[M+H]^+$ at a normalized collision energy of 10.

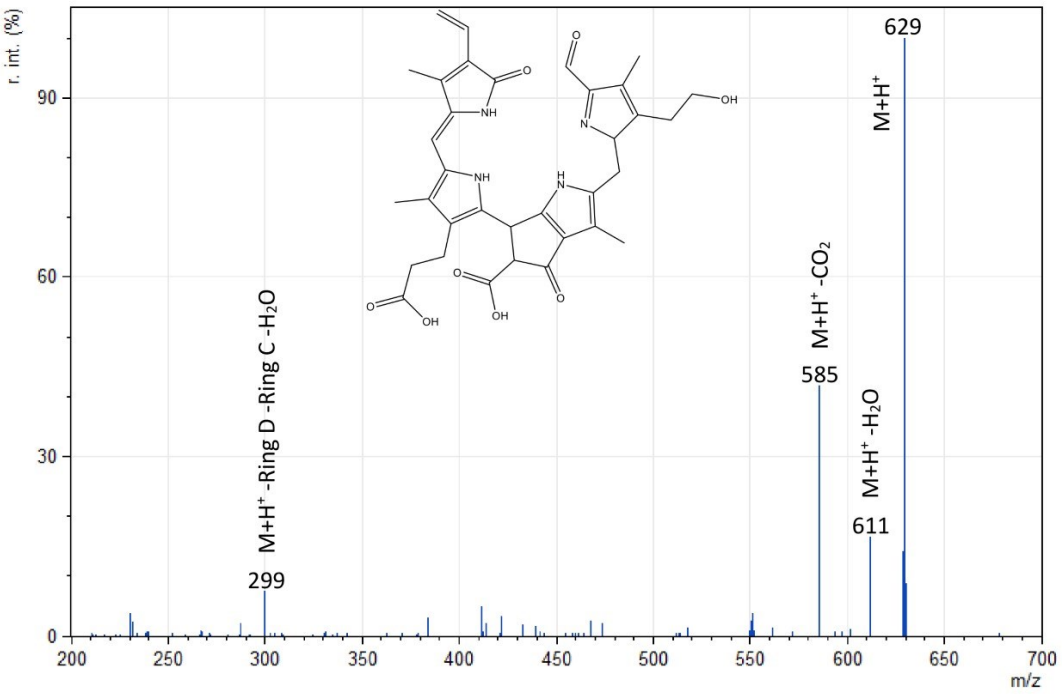

Supplementary Figure 18 MS² ESI mass spectrum of *Tm*-PxB-4. Fragmentation of $[M+H]^+$ at a normalized collision energy of 10.

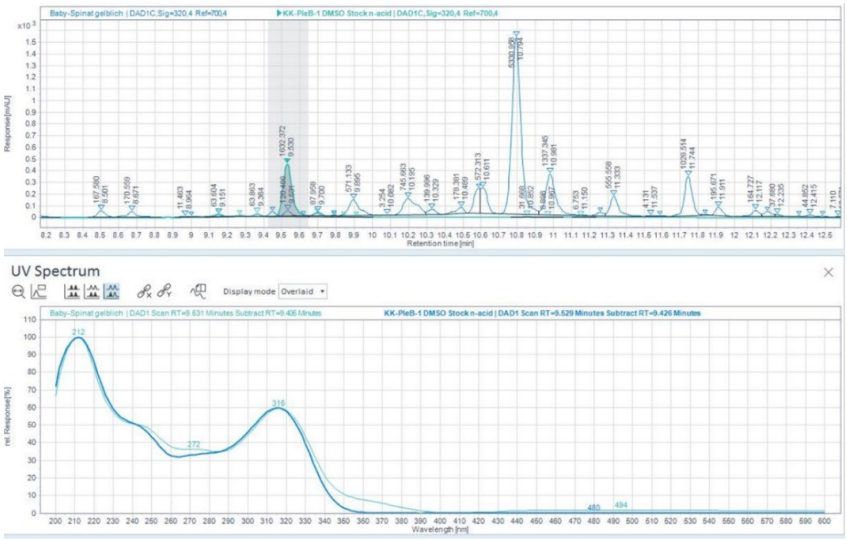

Supplementary Figure 19 Overlay of HPL chromatograms of spinach extract and isolated PleB for comparing retention times. (320 nm, HPLC Method Nr. 1)

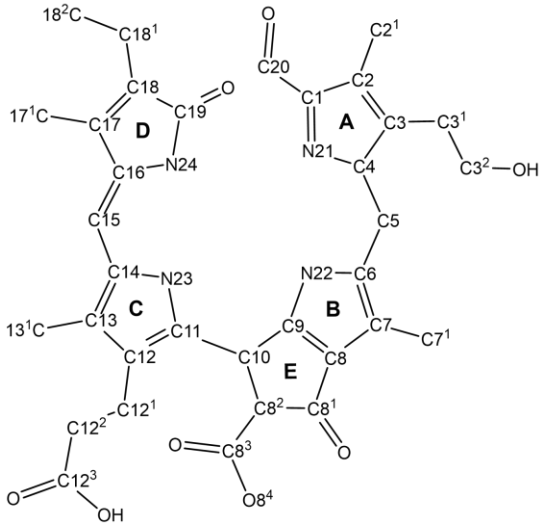

Supplementary Figure 20 Atom numbering used for PxB[7]

Supplementary Figure 21 500 MHz ^{1}H-NMR-spectrum of *Tm*-PxB-1 (25 °C, DMSO-D_6)

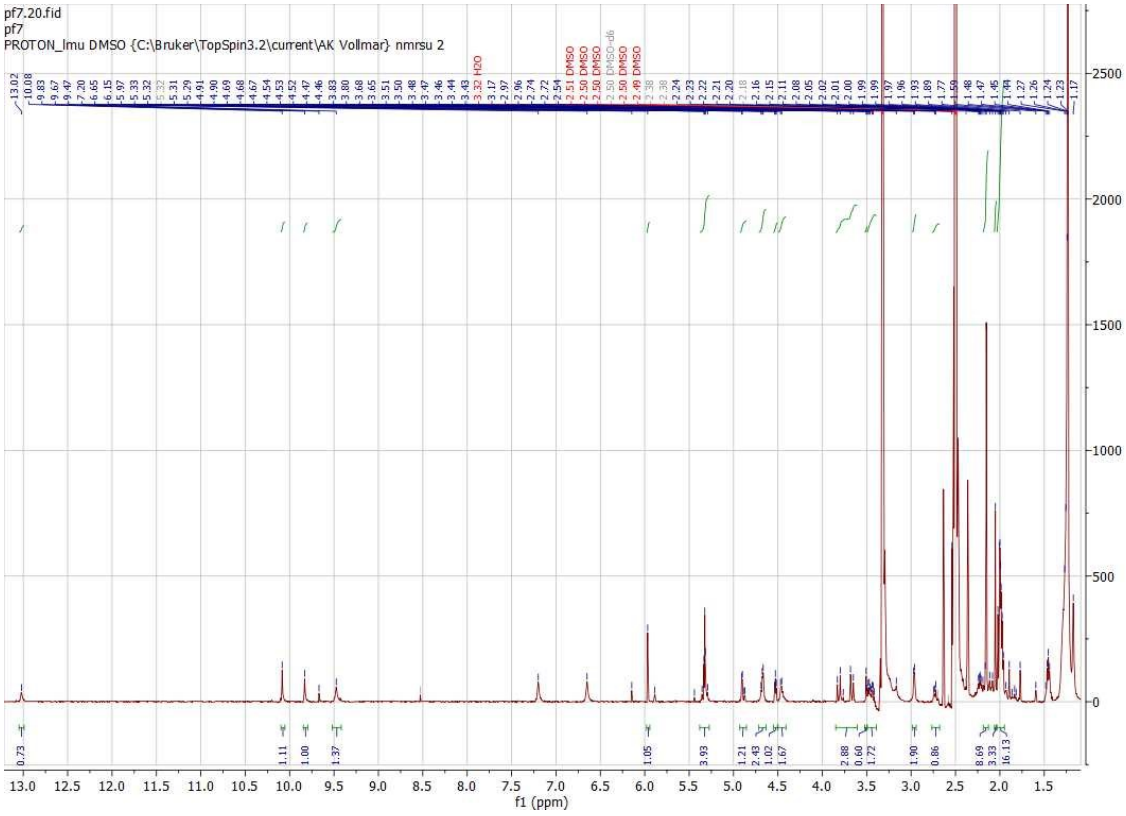

Supplementary Figure 22 500 MHz ^{1}H-NMR-spectrum of *Tm*-PxB-2 (25 °C, DMSO-D_6)

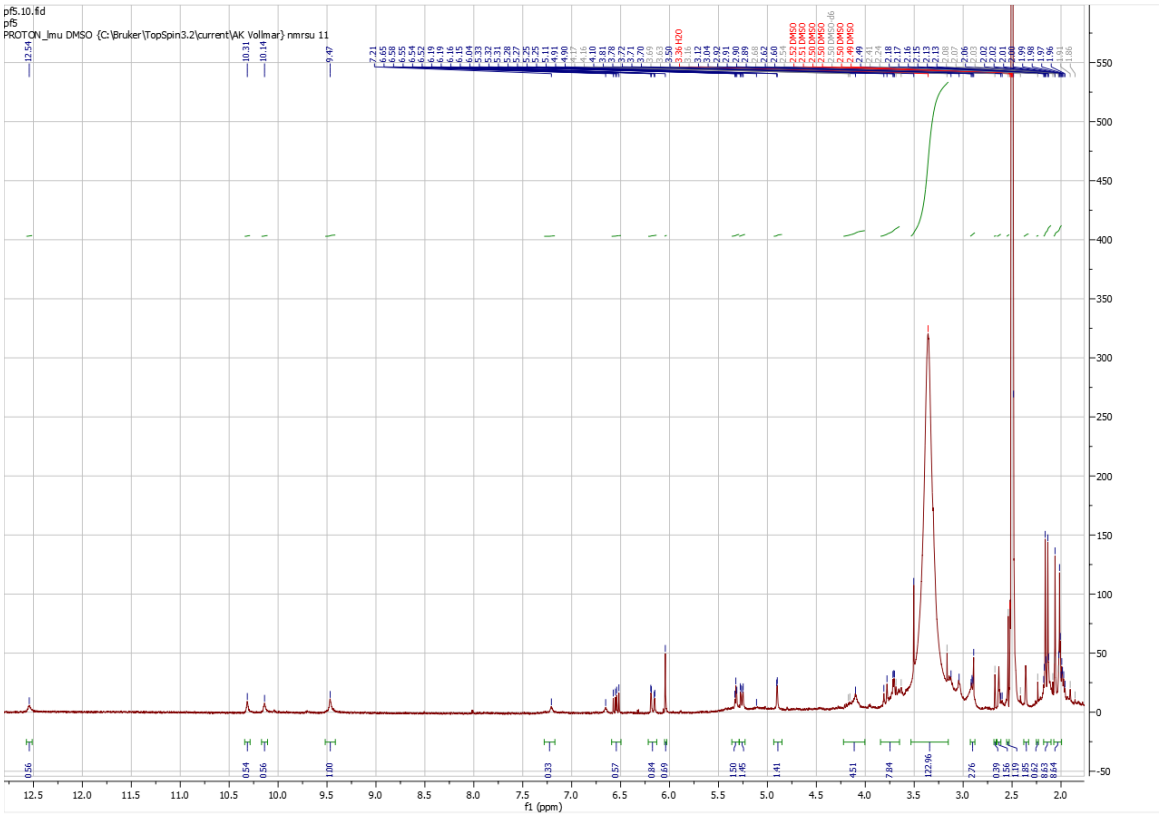

Supplementary Figure 23 500 MHz ^{1}H-NMR-spectrum of *Tm*-PxB-4 (25 °C, DMSO-D_6)

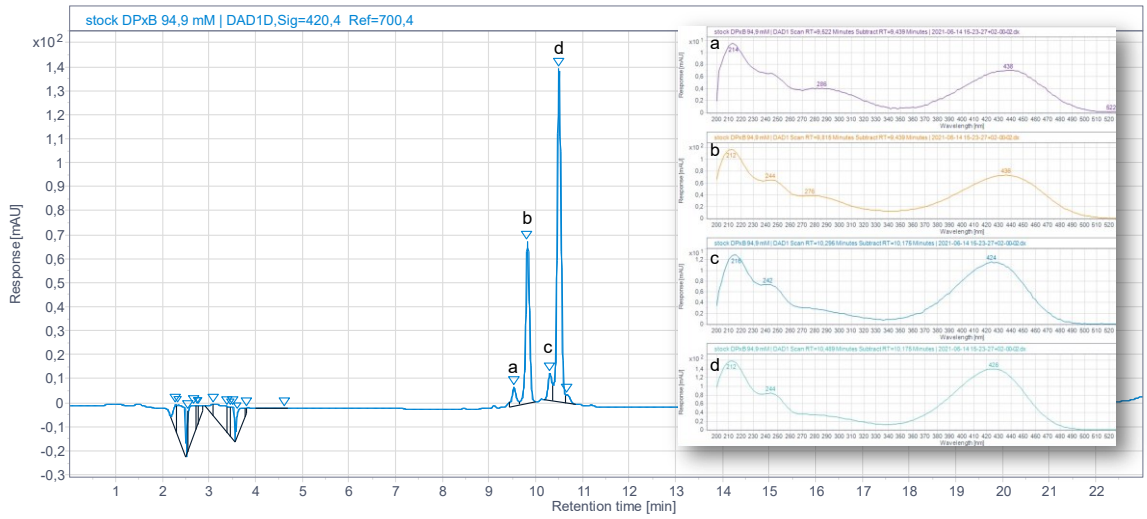

Supplementary Figure 24 HPL chromatogram of pure *Pp*-DPxB (*Vv*-DPxB) stock with characteristic UV spectra of all isomers.[20] (420 nm, HPLC method Nr. 1)

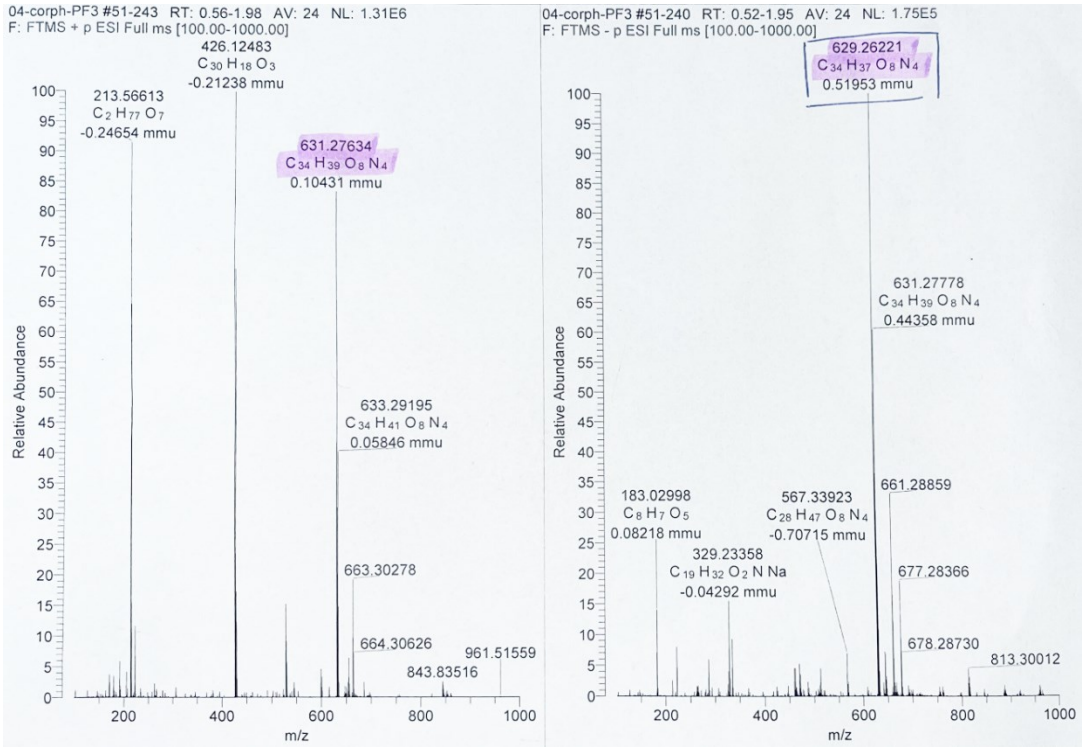

Supplementary Figure 25 HR-ESI-MS of *Pp*-DPxB (*Vv*-DPxB). m/z_{found} = 629.26221 $[M-H]^-$; $m/z_{calculated}$ ($C_{34}H_{37}N_4O_8$) = 629.26896.

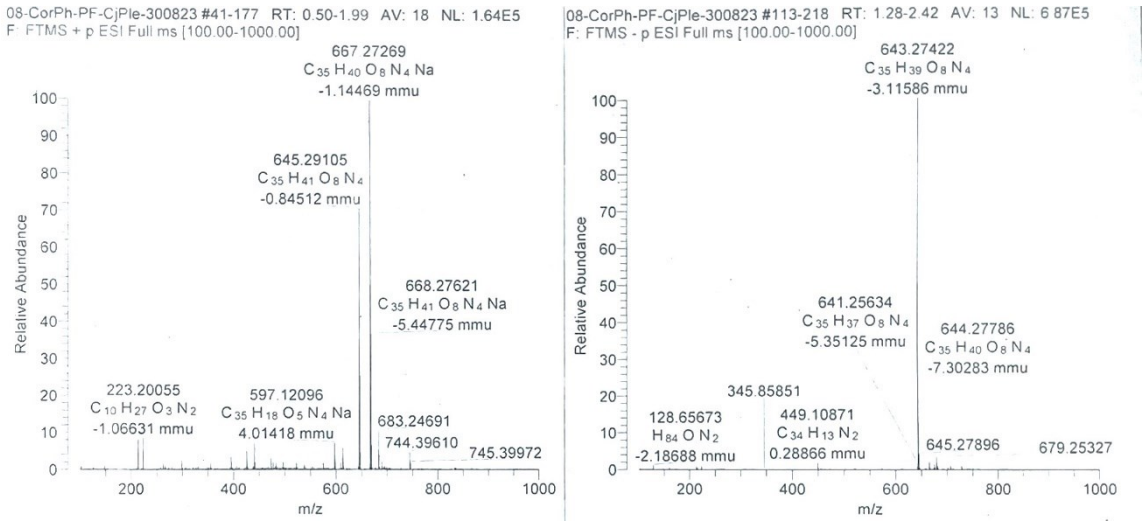

Supplementary Figure 26 HR-ESI-MS of *Cj*-PleB. m/z_{found} = 645.29105 $[M-H]^-$; $m/z_{calculated}$ ($C_{35}H_{41}N_4O_8$) = 645.28461.

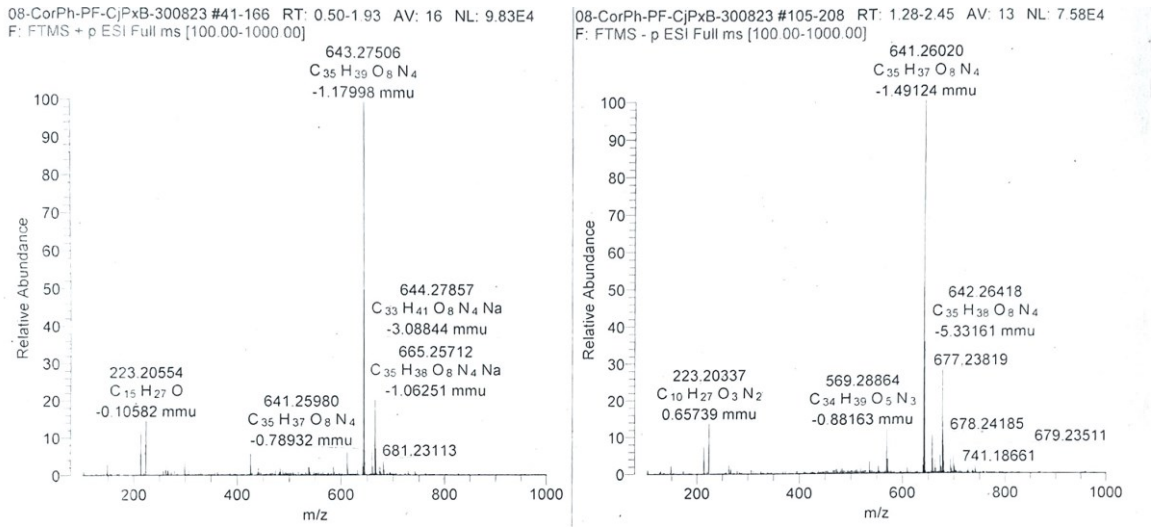

Supplementary Figure 27 HR-ESI-MS of *Cj*-PxB. m/z_{found} = 643.27506 $[M-H]^+$; $m/z_{calculated}$ ($C_{35}H_{39}N_4O_8$) = 642.26896.

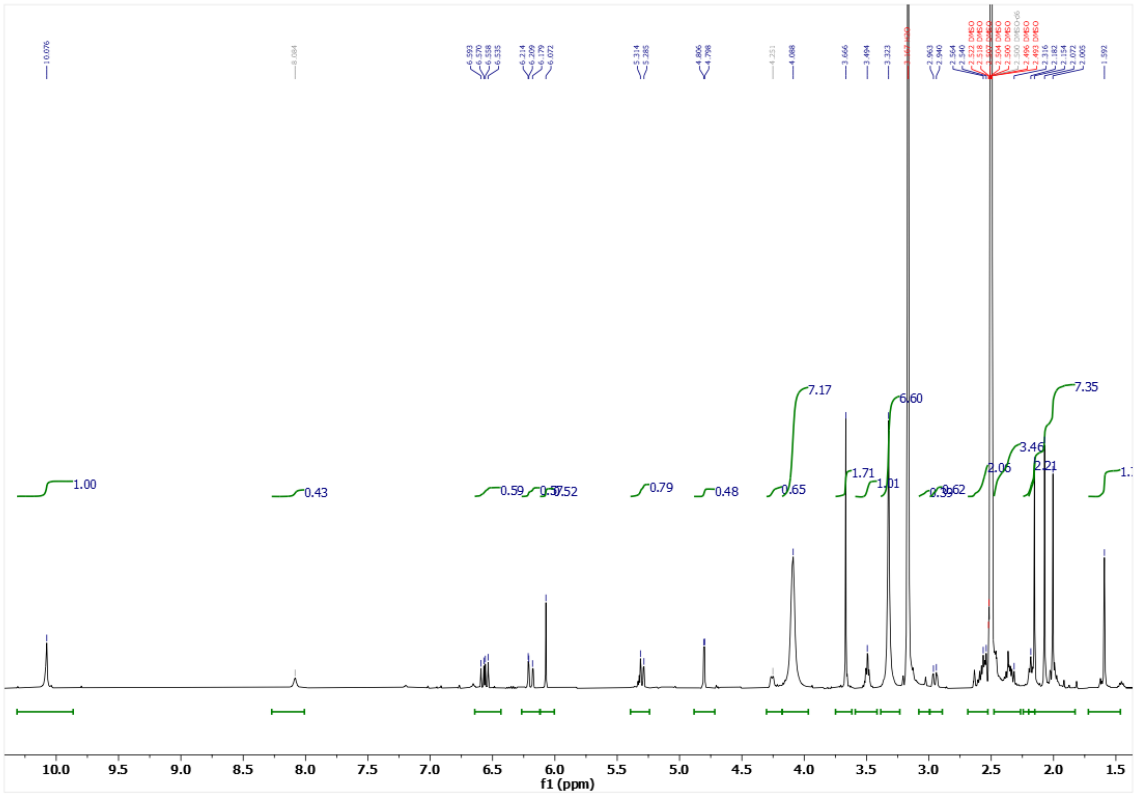

Supplementary Figure 28 500 MHz ^{1}H-NMR-spectrum of *Pp*-DPxB (*Vv*-DPxB) (25 °C, DMSO-D_6)

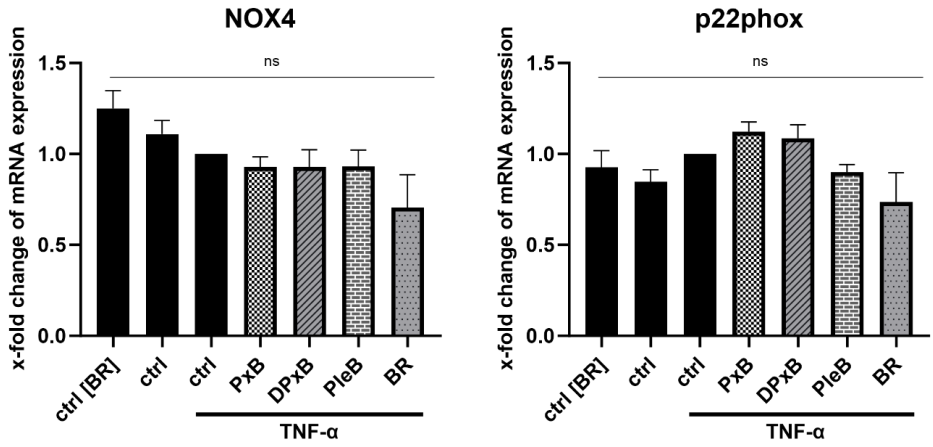

Supplementary Figure 29 Impact of PBs on NOX4 and p22phox mRNA levels of TNF-α activated HUVEC. Confluent cells were treated for 30 min with compound prior to the addition of TNF-α (50 ng/ml) for 24 h of incubation. Values represent mean ± SEM of three independent experiments ($p < 0.05$).

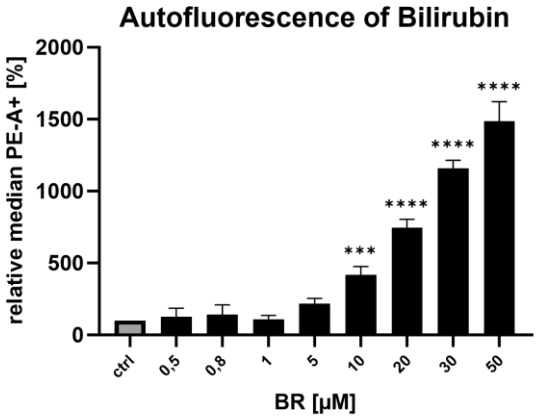

Supplementary Figure 30 Dose-dependent impact of with BR stimulated HUVEC cells on PE laser intensity. Values represent mean ± SD of three independent experiments ($p < 0.05$).

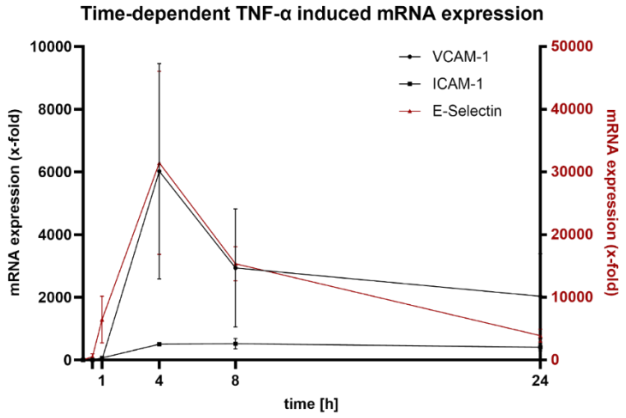

Supplementary Figure 31 Time course of VCAM-1, ICAM-1 and E-selectin mRNA expression of TNF-α stimulated HUVEC. Values represent mean ± SD of three independent experiments.

8.2 Abbreviations

Abbreviation	Term
°C	Degree celsius
ACN	Acetonitrile
ACS	Acute coronary syndrome
AcOH	Acetic acid
ANOVA	Analysis of variance between groups
BDE	Bond dissociation enthalpy
BR	Bilirubin
BSA	Bovine serum albumin
BV	Biliverdin
CAD	Coronary artery disease
cDNA	Complementary DNA
CGA	Chlorogenic acid
Ctrl	control
Chl	Chlorophyll
Cj	*Cercidiphyllum japonicum*
cm, cm^2	Centimeter, square centimeter
COX	Cyclooxygenase
DCF	2',7'-dichlorofluorescein
DCM	Dichloromethane
DMEM	Dulbecco's Modified Eagle Medium
DMSO	Dimethyl sulfoxide
DNA	Deoxyribonucleic acid
DPI	Diphenyleneiodonium chloride
DPPH	2,2-Diphenyl-1-picrylhydrazyl
DTT	1,4-dithiothreitol
DWML	Deep white matter lesions
DYCC	Dioxophylloxanthobilin
ECM	Extracellular matrix
EDTA	Ethylenediaminetetraacetic acid
em	Emission
ESI	Electrospray ionization
EtOH	Ethanol
ex	Excitation
FACS	Fluorescence-activated cell sorting
FCS	Fetal calf serum
FITC	Fluorescein isothiocyanate
FRAP	Ferric reducing antioxidant power
g	Gram
h	Hour
H_2O	Distilled water
H_2DCF-DA	2',7'-dichlorodihydrofluorescein diacetate
H_2O_2	Hydrogen peroxide

HAT	Hydrogen Atom Transfer
HCl	Hydrochloric acid
Hl	*Humulus lupulus*
HPLC	High Performance Liquid Chromatography
HR	High resolution
HUVECs	Human Umbilical Vein Endothelial Cells
IC_{50}	Half-maximal inhibitory concentration
ICAM	intercellular adhesion molecule
IQ	Isoquercitrin
kDA	Kilodalton
k	Kilo
M	Molar
m/z	Mass-to-charge ratio
MeOH	Methanol
mg, ml, mM, mm	Milligram, milliliter, millimolar, millimetre
$MgCl_2$	Magnesium chloride
min	Minute
MMP	Matrix metalloproteinase
mRNA	Messenger RNA
MS	Mass spectroscopy
M_w	Molecular weight
NADPH	Nicotinamide Adenine Dinucleotide Phosphate
NaOH	Sodium hydroxide
nd	Not determined
NH_4AcO	Ammonium acetate
NHMC	normal human mesangial cells
nM, nm	Nanomolar, nanometer
NMR	Nuclear magnetic resonance
NOX	NADPH oxidase
ns	Not significant
ORAC	Oxygen radical absorbance capacity
oxLDL	Oxidized Low-Density Lipoprotein
PAO	pheophorbide *a* oxygenase
PB	phyllobilin
PBMC	Peripheral Blood Mononuclear Cell
PBS	Phosphate-buffered saline
PCR	Polymerase chain reaction
pH	Potential of hydrogen
PleB	Phylloleucobilin
PluB	Phyllolumibilin
Po	*Platanus occidentalis*
Pp	*Parrotia persica*
PPH	pheophytinase
PrB	Phylloroseobilin
PxB	Phylloxanthobilin
py	Pyro

pyPxB	Pyro-phylloxanthobilin
PZN	Pharmazentralnummer
qPCR	Quantitative real-time PCR
QUE	Quercetin
RNA	Ribonucleic acid
ROS	Reactive oxygen species
rpm	Revolutions per minute
RT	Roomtemperature
R_t	Retention time
SD	Standard deviation
SDS	Sodium dodecyl sulfate
SEM	Standard error of the mean
SET	Single electron transfer
SGR	stay-green Mg-dechelatase
SMC	Smooth muscle cell
T/E	Trypsin/ethylenediaminetetraacetic acid
TIMP	Tissue inhibitor of metalloproteinase
Tm	Tropaeolum majus
TPTZ	2,4,6-Tri(2-pyridyl)-s-triazine
UV	Ultraviolet
VCAM	Vascular-cell adhesion molecule
VIS	Visible
VSMC	Vascular smooth muscle cell
v/v	Volume per volume
Vv	Vitis vinifera
ε	Extinction coefficient
µg, µl, µM, µm	Microgram, microliter, micromolar, micrometre

Table 17 List of abbreviations

8.3 Index of figures

Figure 1 Graphical abstract on phyllobilin sources and focus on Part I of the thesis..... 2

Figure 2 Schematic overview on chemical structures of BR and PB candidates and influences on early stages of atherosclerosis progression as found in Part II in this work. 4

Figure 3 Schematic overview of the first part of the PAO/pathway of chlorophyll breakdown in senescent leaves. 8

Figure 4 Second part of PAO/phallobilin pathway occurs in the cytosol and vacuoles and leads to the formation of Type-I and Type-II phyllobilins. 9

Figure 5 Graphical abstract on a naturally occurring pyPxB in yellow senescent *Tropaeolum majus* leaves 42

Figure 6 Chemical structure of *Ep*-PxB-5 44

Figure 7 Influence of *Ep*-PxB-5 on the peak area of a major constituent of a purchasable *Echinacea* extract over ten days. 45

Figure 8 Stability of *Ep*-PxB-5 in *Echinacea* extract compared to EtOH 22% over ten days. 46

Figure 9 Time-dependent influence of *Ep*-PxB-5 on the anti-oxidative potency of a standardized *Echinacea* extract. 47

Figure 10 *Hl*-PBs of senescent hop leaves. 48

Figure 11 Analytical HPL chromatograms of *Humulus lupulus* leaves of different colors. 49

Figure 12 *Hl*-DPxB is a potent antioxidant *in-vitro* and *in-cellulo* on HeLa cells. 50

Figure 13 *Hl*-PBs do not influence cell proliferation of HeLa cells in the tested concentrations. 50

Figure 14 Analytical HPLC trace of an acidified methanolic extract of senescent *Tropaeolum majus* leaves with UV/Vis spectra. 52

Figure 15 Chemical structure of *Tm*-PxB core and side chain modifications of the identified *Tm*-PxBs 54

Figure 16 Leaf spray mass spectrum of a freshly harvested senescent leaf of *Tropaeolum majus*. 55

Figure 17 *Tm*-PxBs possess strong anti-oxidative potential *in-vitro* and *in-cellulo*, as determined in a (A) FRAP and (B) in an intracellular ROS assay. 57

Figure 18 *In-vitro* dose-dependent inhibition of (A) COX-1 and (B) COX-2 activity by *Tm*-PxB-1, *Tm*-PxB-4, CGA, and IQ. 58

Figure 19 Molecular structures of Bilirubin (Br) and phyllobilin (PB) candidates DPxB, PleB and PxB. 65

Figure 20 Process of monocyte transmigration across endothelium involves adhesion protein expression and MMP-9 activation. 68

Figure 21 Fingerprint HPL chromatogram of a methanolic extract of a yellow *Parrotia persica* leaf and peak of a DPxB. 70

Figure 22 *Pp*-DPxB of senescent *Parrotia persica* leaves is identical to *Vv*-DPxB of fading *Vitis vinifera* leaves. 71

Figure 23 PBs differently influence proliferation of endothelial cells. 72

Figure 24 PBs are potent antioxidants *in-vitro* and *in-cellulo* on HUVEC cells. 73

Figure 25 PBs and BR decrease NADPH oxidases activity as assessed in a chemiluminescence assay. 74

Figure 26 Influence on NOX4 protein and mRNA levels and p22phox subunit mRNA expression. 75

Figure 27 PBs and BR inhibit THP-1 monocyte migration. 76

Figure 28 PBs influence THP-1 monocyte migration through a monolayer of HUVEC. . 77

Figure 29 PBs and BR do not influence VCAM-1 and ICAM-1 protein expression levels. 78

Figure 30 PBs and BR do not affect mRNA expression levels of VCAM-1, ICAM-1 and E-selectin after 4 h. 79

Figure 31 PBs and BR influence MMP-9 activity without affecting cellular protein expression levels *in-vitro* and *in-cellulo*. 81

Figure 33 Structures of the pyrogallol-derived polyphenol library. 91

Figure 34 Anti-oxidative potency of polyphenols *in-vitro* as assessed by (A) FRAP-assay and (B) ORAC assay. 92

8.4 Index of tables

Table 1 Compounds 13

Table 2 Reagents 15

Table 3 Primary antibodies 15

Table 4 Conjugated primary antibodies 16

Table 5 Secondary antibodies 16

Table 6 Technical devices and lab equipment 17

Table 7 Software 18

Table 8 Consumables 18

Table 9 analytical HPLC methods 19

Table 10 Assignment of ^{1}H-signals from 500 MHz ^{1}H-NMR spectra in DMSO-D_6; ^{13}C assignment HMQC und HMBC spectra. 23

Table 11 Extinction coefficients of PBs used for concentration determination by UV/VIS spectroscopy 25

Table 12 Cell culture buffers and solutions 27

Table 13 Composition of the Krebs-HEPES buffer 31

Table 14 Primers with nucleotide codes used for qPCR analysis 33

Table 15 Composition of buffers and solutions for Western Blot analysis 34

Table 16 Composition of gels for Western Blot analysis 35

Table 17 List of abbreviations 120

8.5 Acknowledgements

An erster Stelle möchte herzlich meiner Doktormutter Prof. Dr. Angelika Vollmar danken. Ihr Enthusiasmus und Ihre Frohnatur haben mich in den Achievements immer wieder aufs Neue inspiriert. Über die vielen Projekte, an welchen ich über die Jahre gearbeitet hatte, haben Sie nie den Überblick verloren. Durch Ihre scharfe Sichtweise konnten Sie mir in vielen Fragestellungen aus einer anderen Perspektive die Augen öffnen, um wichtige Kernaspekte nicht zu übersehen. Auch danke ich Ihnen, dass Sie in privaten Momenten des Verlusts aufrichtig Anteil genommen haben.

Ein großes Dankeschön geht an meine Betreuerin Prof. Dr. Simone Moser. Ich möchte mich über die fachlich kompetente Begleitung meines wissenschaftlichen Werdegangs und damit auch meiner persönlichen Weiterentwicklung danken. Sehr schätze ich, dass ich durch Dein großes Vertrauen selbstständig Ideen und Projekte einbringen und diese verfolgen konnte. Mit Deinen Ratschlägen hast du mich immer sehr motiviert. Ich bin sehr dankbar, dass Du mich in Dein Team geholt hast und mir dadurch, zusammen mit Prof. Vollmar, die Promotion überhaupt ermöglicht hast.

Der Prüfungskommission bestehend aus Frau Prof. Dr. Angelika M. Vollmar, Frau Prof. Dr. Simone Moser, Herrn Prof. Dr. Franz Paintner, Herrn Prof. Dr. Franz Bracher, Herrn Prof. Dr. Martin Biel und Herrn Prof. Dr. Gerhard Winter möchte ich ganz herzlich meinen Dank aussprechen für den aufgebrachten Zeitaufwand und die Bereitschaft zur Bewertung meiner Arbeit.

Mein besonderer Dank geht an die Firma Dr. Willmar Schwabe GmbH & Co. KG, insbesondere Dr. Dirk Bredenbröker, Dr. Martin Lehner und Dr. Andreas Rastetter für die spannende Kooperation und das Funding für das Atherosclerosis Projekt. Ich bin sehr dankbar für das Vertrauen in mich und das Projekt, sowie den gemeinsamen Austausch und den wissenschaftlichen Input in unseren Meilensteinmeetings. Die Möglichkeit meine Ergebnisse im Rahmen des Projektes am GA Congress 2023 in Dublin vorstellen zu dürfen, empfand ich als Geschenk und Privileg. Die Werksbesichtigung in Karlsruhe im

August 2023 hat mir wahnsinnige Freude gemacht und für die dabei entgegengebrachte Zeit möchte ich mich ausdrücklich bedanken.

Bedanken möchte ich mich ebenso bei meinen Kooperationspartnern Christian Nadegger und Prof. Thomas Müller (Organische Chemie, Innsbruck), Dr. Stefan Schwaiger (Pharmazie, Innsbruck) sowie Salavat Ashirbaev, Dr. Natercia Braz und Prof. Hendrik Zipse (Chemie, München) für die fruchtbare und unterstützende Zusammenarbeit, ohne welche wesentliche Kernaspekte der Arbeit nicht umsetzbar gewesen wären.

Des Weiteren möchte ich dem gesamten AK Vollmar danken für das schöne Miteinander und den herzlichen Umgang, der den Arbeitsalltag im Labor verschönert. Insbesondere möchte ich Dr. Maibritt Kretschmer danken für die hilfsbereite Unterstützung am Confocal, sowie Rita Socher, Jana Peliskova, Silvia Schnegg und Elke Bartusel für die technische Unterstützung meiner Arbeit und allen diejenigen, die für mich fleißig meine Kapuzinerkresse Pflanzen gegossen hatten. Auch möchte ich mich bei allen ehemaligen und aktuellen Doktoranden für die gemeinsame Zeit und die entstandene Freundschaft bedanken, die nicht nur im Basketball und Frisbee, sondern auch in gemeinsamen Unternehmungen gelebt wird. Dabei gilt ein großer Dank Dr. Cornelia Karg. Du hast mich in kritischen Momenten immer wieder bestärkt nicht aufzugeben. Nicht nur fachlich konnte ich immer mit einem fundierten Ratschlag rechnen, sondern auch im Privaten bin ich froh Dich hier kennengelernt zu haben.

Meinen Studenten Romy Busch und Mike (Mykhailo) Lytvynenko möchte ich danken für das Mitwirken an meinen Projekten und dem damit verbundenen fachlichen Austausch und der geleisteten Laborarbeit. Besonders hervorzuheben ist dabei der Einsatz von Mike.

Aus tiefstem Herzen möchte ich meinen Eltern Georg und Brigitte Frei und meinen Brüdern danken. Auch wenn Du, Papa, uns plötzlich dieses Jahr so früh verlassen musstest, möchte ich deine jahrelange aufopferungs- und liebevolle Unterstützung nicht ungeachtet lassen. Gleiches gilt meiner Mama. Wie kämpferisch Du dich gerade dem Leben stellt, dabei immer rücksichtvoll, hilfsbereit und voller Liebe bist, ist eine wahre Inspiration. Ich bin mir sicher, dass ich ohne Euren Rückhalt heute nicht dort wäre, wo ich jetzt bin. Ich möchte mich auch herzlich bei meinen Brüdern bedanken, insbesondere meinem Bruder Matthias, der mir die Pharmazie und die Promotion ans Herz gelegt hat und dabei immer ein zuverlässiger Zuhörer war.

Zu guter Letzt, danke ich meinem Freund Martin. Du bist mir in schwierigen Situationen eine wertvolle Hilfe und Zuflucht und ich bin so froh Dich hier kennengelernt zu haben.

8.6 List of publications and conference contributions

8.6.1 Research articles

i. Frei, P., Nadegger, C., Müller, T., Vollmar, A., Moser, S. (2023). Structural characterization, antioxidative-, and anti-inflammatory activities of phylloxanthobilins in *Tropaeolum majus* L., a plant with relevance in phytomedicine. Planta medica, in revision

ii. Nadegger, C.*, Frei, P.*, Vollmar, A., Müller, T., Moser, S. Structural characterization of phyllobilins in *Humulus lupulus* and probing their anti-oxidative bioactivities. Manuscript in preparation; *These authors contributed equally to the article.

iii. Ashirbaev, S., Brás, N., Frei, P., Liu, K., Moser, S. and Zipse, H. (2023). Redox-Mediated Amination of Pyrogallol-Based Polyphenols. Journal of the American Chemical Society, Manuscript in preparation.

8.6.2 Conference contributions

i. Frei P., Ran D., Vollmar A. M., Moser S.; **DPhG Annual Meeting 2021 - Trends and Perspectives in Pharmaceutical Sciences (September 2021) Virtual Meeting;** Phyllobilins as natural chlorophyll derived compounds with promising physiological bioactivities. Final Programme & Book of Abstracts.

ii. Frei, P; Vollmar A. M; Moser, S.; **DPhG Annual Meeting 2022 "From Behring to Biotechnology – moving Pharmaceutical Sciences towards One Health" (September 2022);** Establishing the overlooked natural product family of phyllobilins as important phytochemicals in phytotherapy. Final Programme & Book of Abstracts.

iii. Frei, P; Vollmar A. M; Moser, S.; **71st International Congress and Annual Meeting of the Society for Medicinal Plant and Natural Product Research (GA) (July 2023);** Phyllobilins as promising bilirubin-like compounds to counter atherosclerosis. Final Programme & Book of Abstracts